Study on Migration Behavior of Selenium for Safety Assessment of Radioactive Waste Disposal

Yoshihisa Iida

2012

Contents

1. General Introduction

1.1. Background

High-level radioactive waste (HLW) is planned to be vitrified, encapsulated in a metal container called overpack, surrounded by bentonite buffer materials, and emplaced in a repository constructed in stable rocks at a depth of 300 m or greater. After the emplacement of HLW, long-lived radionuclides may be leached from the vitrified waste and may subsequently be transported through the buffer material and surrounding rock masses to the biosphere. The migration of radionuclides is expected to be retarded by the following processes. (1) Most of the radionuclides are poorly soluble and precipitate near the vitrified waste under the disposal conditions. The concentrations of these radionuclides in the porewater of the buffer material are limited by the solubility of their compounds. (2) The bentonite buffer material provides a hydrological barrier. Because of its low permeability, the migration of radionuclides leached from the vitrified waste is dominated by slow diffusion through the buffer material. (3) The migration of radionuclides released from the buffer material in the geosphere is likely to be dominated by groundwater flow in rock fractures, limited by low groundwater velocities, and retarded by sorption onto rocks. In safety assessments of HLW disposal system, the migration of radionuclides is evaluated by considering these processes.[1)]

Safety assessment calculations for hypothetical HLW repositories[1)] show that selenium-79 (^{79}Se), a long-lived fission product with a half-life of 2.95×10^5 year,[2)] is one of the radionuclides that dominate the long-term radiological hazard (**Fig. 1-1**). The oxidation state of Se varies from selenide (Se(−II)) to selenite (Se(IV)) and selenate (Se(VI)) depending on redox conditions of groundwater,[3)] and aqueous species are usually anionic species such as hydrogen selenide (HSe^-), selenite (SeO_3^{2-}) and selenate (SeO_4^{2-}).[3)] Since the chemical conditions under deep underground environments are likely to be anoxic and reducing, Se is likely to be stable as Se(−II) under the disposal conditions. Hence, it is necessary to understand the migration behavior of Se(−II) species for the safety assessment of HLW disposal system.

1.2. Previous Studies on Migration Behavior of Selenium

1.2.1 Solubility of Selenium

Solubilities of radionuclides are determined from equilibrium constants of dissolution reactions (K^0) and activity coefficients of dissolved species (γ) in safety assessment calculations. The equilibrium constant is calculated from thermodynamic data (the standard molar free energies of formation ($\Delta_f G_m^0$)) of dissolved species and solubility limiting solids. For example, in the case of

the dissolution reaction

$$A(solid) + B(aqueous) = C(aqueous) + D(aqueous)\ , \qquad (1\text{-}1)$$

the standard energy of the reaction ($\Delta_r G^0$) is calculated from $\Delta_f G_m{}^0$ values of these species as

$$\Delta_r G^0 = \Sigma \Delta_f G_m{}^0{}_{(products)} - \Sigma \Delta_f G_m{}^0{}_{(reactants)}$$

$$= \Delta_f G_m{}^0{}_{(C)} + \Delta_f G_m{}^0{}_{(D)} - \Delta_f G_m{}^0{}_{(A)} - \Delta_f G_m{}^0{}_{(B)}, \qquad (1\text{-}2)$$

and the relationship between K^0 and $\Delta_r G^0$ is

$$\Delta_r G^0 = -RT \ln K^0 \qquad (1\text{-}3)$$

where R is gas constant and T is temperature.[3)] In calculations of solubilities, the reliability of the thermodynamic data and the selection of appropriate solubility limiting solid phases are of key importance. Thermodynamic data of Se species were recently compiled by OECD/NEA thermochemical database project.[3)] The values for $\Delta_f G_m{}^0$, standard molar enthalpy of formation ($\Delta_f H_m{}^0$), standard molar entropy ($S_m{}^0$), and standard molar heat capacity at constant pressure ($C_{p,m}{}^0$) of Se species are summarized in **Table 1-1**. In the literature,[3)] predominance areas in a pH-pe diagram for Se were presented (**Fig. 1-2**). Under the reducing conditions in deep subsurface environments, a Se(−II) species of HSe^- is considered to be dominant in neutral groundwater[1,3)] and polyselenide species of Se_n^{2-} (n = 1-4) is considered to be dominant in alkaline groundwater[3,4)] induced by cementitious materials in radioactive waste repositories (**Fig. 1-2**). The $\Delta_f G_m{}^0$ of HSe^- was reported to be 43.471±2.024 kJ mol^{-1},[3)] calculated from $\Delta_f G_m{}^0$ of $H_2Se(g)$ (15.217±2.003 kJ mol^{-1}), its solubility in water

$$H_2Se(g) = H_2Se(aq) \qquad \log K^0 = -1.10 \pm 0.01 \qquad (1\text{-}4)$$

and the first dissociation constant of $H_2Se(aq)$

$$H_2Se(aq) = HSe^- + H^+ \qquad \log K^0 = -3.85 \pm 0.05. \qquad (1\text{-}5)$$

The value for $\Delta_f G_m{}^0$ of Se^{2-} was reported to be 128.6±3.000 kJ mol^{-1} calculated from the second dissociation constant of $H_2Se(aq)$[3)]

$$HSe^- = Se^{2-} + H^+ \qquad \log K^0 = -14.91 \pm 0.20. \qquad (1\text{-}6)$$

The value for $\Delta_f G_m^0$ of Se_n^{2-} (n = 1-4) was determined from equilibrium constants for reactions between polyselenide species by spectrophotometric data,[4)]

$$1/2Se_2^{2-} + e^- = Se_2^{2-} \qquad \log K^0 = -11.97 \pm 0.10 \qquad (1\text{-}7)$$

$$1/3Se_3^{2-} + 4/3e^- = Se^{2-} \qquad \log K^0 = -15.74 \pm 0.14 \qquad (1\text{-}8)$$

$$1/4Se_4^{2-} + 3/2e^- = Se^{2-} \qquad \log K^0 = -17.24 \pm 0.15. \qquad (1\text{-}9)$$

The solubility limiting solids for Se are likely to be compounds with iron, copper or lead as can be observed from natural analogue systems.[5,6)] In the disposal environments, ferrous ion (Fe^{2+}) probably dissolves into groundwater from iron compounds such as pyrite (FeS_2) in bentonite buffer materials, carbon steel overpack, and its corrosion products. Therefore, the solubility of Se was expected to be limited by precipitation of ferroselite ($FeSe_2$)[1,5)] in the previous safety assessment calculations, based on geochemical calculations and the chemical analogy with sulfur. Azuma *et al*.[7)] showed that the aqueous concentration of Se was decreased by several orders of magnitude by precipitation of $FeSe_2$ compared to crystalline selenium (Se(cr)) in the disposal environments. Solubility limiting of Se by the precipitation of Fe-Se compounds has been investigated by several researchers. Shibutani *et al*.[8)] carried out dissolution experiments of Se under reducing conditions in the presence of Fe. The experiments were performed from both undersaturation and oversaturation directions at room temperature for 4 weeks. The precipitate formed in the oversaturation experiments was identified as only Se(cr) by powder X-ray diffraction (XRD), namely, the precipitation of Fe-Se compound was not observed and did not limit Se solubility. Tachikawa *et al*.[9)] carried out dissolution experiments of Se under reducing conditions in the presence of Fe from oversaturation direction. The samples were stored at 60°C for a month. The precipitates were identified as Se(cr), $FeSe_2$(cr), Fe_3O_4, and FeOOH. However, the concentrations of Fe or Se in almost samples were below the detection limit of the measurement by inductively coupled plasma mass spectrometry (ICP-MS), the equilibrium constant of dissolution reaction of Se could not be determined. Although the possibility of solubility limitation of Se by $FeSe_2$ was suggested from solid analysis, the solubility limiting solid could not be determined. Kitamura *et al*.[10)] carried out dissolution experiments of purified $FeSe_2$ reagent from undersaturation direction to obtain the equilibrium constant between $FeSe_2$(cr) and

SeO_3^{2-} under reducing conditions. The dependencies of solubility values on pH and redox potential were best interpreted that the solubility limiting solid was not $FeSe_2$(cr) but Se(cr). In this way, the solubility limiting of Se by Fe-Se compounds has not been observed in laboratory dissolution experiments till now. Therefore, uncertainties still remain in the determination of the solubility limiting solid of Se.

Activity coefficients (γ) of dissolved species are needed for a wide range of ionic strength (I_m) in case of possible intrusion of saline groundwater for coastal repositories. In the previous safety assessments, the Davies activity coefficient formula which does not depend on the type of soluble chemical species

$$\log \gamma = -0.5\left(\frac{\sqrt{I_m}}{1+\sqrt{I_m}} - 0.2\, I_m \right) \qquad (1\text{-}10)$$

was adopted.[1)] This formula is applicable up to an ionic strength of appropriately 0.1 mol kg^{-1} in general.[3)] At higher ionic strength, the more elaborate activity correction method, such as specific ion interaction theory (SIT),[3)] is necessary to applied. However, the activity correction parameters for Se species at high ionic strength are not available.

1.2.2 Diffusivity of Selenium through Bentonite Materials

Diffusivities of radionuclides were evaluated based on experimentally measured diffusion coefficients in the previous safety assessment calculations.[1)] The diffusion data for Se species through bentonite materials are scarce,[e.g. 11-16)], and data obtained under reducing conditions are limited (**Table 1-2**).[15, 16)] Sato *et al.*[15)] obtained apparent diffusion coefficients (D_a) for Se(−II) species in a compacted bentonite, Kunigel V1, for a range of dry densities from 800 - 1800 kg m^{-3} under reducing conditions. The dominant Se species in the porewater is predicted to be HSe^-. The D_a values were between 6.1×10^{-11} m^2 s^{-1} and 4.3×10^{-11} m^2 s^{-1}, and showed a tendency to slightly decrease with increasing dry density of bentonite. Sato *et al.*[16)] also obtained D_a values for Se in compacted bentonite/sand mixture at a dry density of 1600 kg m^{-3} as a function of silica sand content and temperature under reducing conditions, under which the dominant species of Se is predicted to be HSe^-. The obtained D_a values were compared with the values for SeO_3^{2-} obtained under anaerobic conditions. The D_a values for HSe^- were about one order of magnitude smaller than those for SeO_3^{2-}.

The effective diffusion coefficient (D_e) for Se obtained under reducing conditions, which is needed for safety assessment calculations, cannot be found. In the present safety assessments, the D_e value of iodide (I^-) is adopted for HSe^- (2×10^{-10} m^2 s^{-1} at 60°C) considering the charge of the species in the porewater.[1)]

In the long term, the diffusion behavior of radionuclides would change because the swelling characteristic of bentonite is likely to be deteriorated by contact with saline groundwater or alteration by alkaline groundwater originating from cementitious materials.[17)] For a long term safety assessment, it is necessary to evaluate the variation in diffusion of radionuclides. However, the systematic diffusion data, those are necessary for the evaluation of the variation, are not available. In addition, it is necessary to understand diffusion phenomena in bentonite porewater based on diffusion mechanisms for an interpretation of the variation in diffusion of Se species. Many researchers have developed mechanistic diffusion models, such as the pore diffusion model that is most widely used,[18, 19)] the model based on the electric double layer theory,[12,20,21)] and the model considering anion exclusion,[22,23)] surface diffusion,[23-25)] interlayer diffusion[25-27)] and Donnan equilibrium.[28)] However, diffusion models for evaluation of the variable D_e of anionic species depending on the bentonite content and porewater salinity are limited.[21,22,28)] Van Loon *et al*.[22)] modeled the diffusion behavior of Cl^- in compacted Volclay KWK bentonite as a function of the bulk dry density and the ionic strength of the external bulk solution. The effective diffusivity of Cl^-, $D_{e,Cl}$, is described as

$$D_{e,Cl} = D_{v,Cl}\,\phi_{Cl}^{n} \quad , \tag{1-11}$$

where $D_{v,Cl}$ is the diffusivity of Cl^- in free water (m^2 s^{-1}), n is an empirical parameter depending on the pore geometry of the porous medium, and ϕ_{Cl} is the diffusion-accessible porosity for Cl^-. Glaus *et al*.[29)] applied this model to the diffusion of Cl^- through Na-montmorillonite. The diffusion-accessible porosity for Cl^- which is a key parameter in this model is empirically determined. Therefore, it is not certain that this parameter can be applied to the evaluation of D_e of Se species through the other type of bentonite. Birgersson and Karnland[28)] developed a diffusion model based on the Donnan equilibrium as

$$D_e = \phi_c\,\Xi\,D_c \quad , \tag{1-12}$$

where ϕ_c is total clay porosity, D_c is the diffusivity in the clay and Ξ is a general ion equilibrium

constant derived from the Donnan potential of the charged surface of bentonite. They reported the estimation of the equilibrium constant for Cl^-, Ξ_{cl-}, from the cation exchange capacity of bentonite and electrolyte (NaCl) concentration in the external solution, but the Ξ_{cl-} cannot be applied directly to the evaluation of D_e of tracer Se species. Ochs *et al.*[21] developed a diffusion model based on the homogeneous pore structure and electrical double layer theory for bentonite materials, Kunigel V1, Kunipia F, and MX-80 as

$$D_e = \phi \frac{\delta_g \delta_{el}}{\tau^2} D_v \quad , \tag{1-13}$$

where ϕ is the porosity of the compacted bentonite, τ is the tortuosity of the diffusive pore, δ_g is the geometric constrictivity, and δ_{el} counts electrostatic effects. Predicted values consist with published D_e data for Cs^+, HTO, and TcO_4^-, and reproduced the trend of D_e values *vs*. dry density of the bentonite. Tachi *et al.*[30] modified Ochs *et al.*'s model and predicted the salinity dependence of D_e of Cs^+, HTO, and I^- reasonably well, but a relatively large discrepancy was observed for D_e of I^- at high salinity. This discrepancy was likely to be caused by a complicated pore structure of bentonite and consequent variation in anion diffusion, because the model does not take into account the variation of the pore structure depending on the porewater salinity.

1.2.3 Sorption of Selenium onto Rocks

Sorption behaviors of radionuclides were evaluated from experimentally measured sorption data in the previous safety assessment calculations.[1] A considerable amount of Se sorption data has been obtained under aerobic conditions,[*e.g.* 31-38] where SeO_3^{2-} and SeO_4^{2-} species are dominant. Shibutani *et al.*[31] performed butch sorption experiments of Se on granodiorite and tuff. Selenium scarcely sorbed on granodiorite, but the fraction of Se sorbed on tuff was above 90% in the pH range below 8. The sorption distribution coefficients (K_d) for tuff was 6×10^{-2} m^3 kg^{-1} at pH < 8, and 1×10^{-3} m^3 kg^{-1} at pH 12. Sorption behavior of Se was analyzed by a surface complexation model, assuming the dominant sorbent minerals are biotite, chlorite, and pyrite. Tachi *et al.*[32] performed butch sorption experiments and diffusion experiments of Se for tuff. The K_d values for tuff obtained by the batch sorption experiments were 2.3×10^{-2} m^3 kg^{-1} at pH 8 and 2.5×10^{-2} m^3 kg^{-1} at pH 11. The K_d values obtained by the diffusion experiments were lower than those by the batch experiments, and the differences were one order of magnitude. Comparison of pH dependencies of K_d values between tuff and its constituent minerals suggested that Fe minerals such as Fe-oxyhydroxide and pyrite contributed to Se sorption on tuff. Fujikawa *et al.*[34]

performed butch sorption experiments of SeO_3^{2-} and SeO_4^{2-} onto rocks (metamorphosed chert and shale, and granodiorite) and minerals (hematite, magnetite and calcite) in 0.001, 0.01, and 0.1 N solutions of Na_2SO_4 NaCl, Na_2CO_3, and $NaHCO_3$. The obtained K_d values were in the range of 1×10^{-3} - 3×10^{-1} m^3 kg^{-1} for each rocks. The K_d increased in the order $Na_2CO_3 < NaHCO_3 < NaCl < Na_2SO_4$, the difference in the pH of the solution is so large that the effect of ionic competition is outweighed by pH. In addition to these experimental studies, the sorption mechanisms of SeO_3^{2-} and SeO_4^{2-} species onto minerals were almost clarified from modeling studies.[33,39)]

On the other hand, data obtained under reducing conditions are limited.[36-38)] Igarashi *et al.*[36)] performed butch sorption experiments of Se onto mudstone and sandstone under aerobic conditions with 0.01 mol dm^{-3} sodium hydrosulfite ($Na_2S_2O_4$) as a reducing agent. The obtained K_d values were 1×10^{-2} - 5×10^{-1} m^3 kg^{-1} (pH 3.5 - 6.2) for each rocks, and showed negative dependence on pH. These values were higher than those without the reducing agent, 1×10^{-3} - 1×10^{-2} m^3 kg^{-1} (pH 8.2 - 8.7). Ticknor *et al.*[36)] performed butch sorption experiments of Se onto granite, gabbro, and basalt under reducing conditions with 0.08 mol dm^{-3} hydrazine (N_2H_4) as a reducing agent, at pH 10 and *E*h −370 to −260 mV. The obtained K_d values were within a range of 3.7×10^{-3} - 7.9×10^{-3} m^3 kg^{-1}, and lower than the values under aerobic conditions (1.1×10^{-2} - 1.6×10^{-2} m^3 kg^{-1}). Xia *et al.*[40)] carried out sorption experiments of Se on sedimentary rock samples containing pyrite under reducing conditions. Selenium(IV) in a test solution was reduced to Se(−II)/Se(0) by mixed gas (H_2 (4.9 %) + N_2) in the presence of platinum (Pt) catalyst. The obtained K_d values were 6×10^{-3} - 8×10^{-2} m^3 kg^{-1}, and showed negative dependence on pH. These values were higher than those without the reducing agent, 1×10^{-3} - 1×10^{-2} m^3 kg^{-1} (pH 8.2 - 8.7). Most of the Se sorbed on the sedimentary rocks was determined to be Se(0) by X-ray absorption near-edge structure (XANES), and the sorption mechanism was explained as incorporation into pyrite. Barney *et al.*[37)] investigated the sorption of Se onto sandstone and tuff at pH 8.5 - 9.5 under reducing conditions (0.05 mol dm^{-3} N_2H_4). The obtained K_d values were 8.7×10^{-4} - 1.25×10^{-2} m^3 kg^{-1} for sandstone, and 1.5×10^{-3} - 1.2×10^{-2} m^3 kg^{-1} for tuff at 23°C. They reported that hydrazine failed to reduce SeO_3^{2-}, the obtained K_d data are not reliable. As stated above, sorption data of Se under reducing condition are limited and the sorption mechanisms have not been clarified.

In the previous safety assessments, the K_d values of Se on granite and sand stone under reducing conditions were evaluated from limited data obtained by Ticknor *et al.*[36)] to be 0.01 and 0.001 m^3 kg^{-1}, respectively. (**Table 1-3**).[41)] The data for basalt, tuff, and mudstone were not available, therefore, the K_d values for these rocks were evaluated as the same values as those for granite. The validity of these evaluations of K_d have not been confirmed.

1.3. Outline of the Thesis

As mentioned above, the reliability and validity of the evaluation of the migration behavior of Se under the disposal conditions of HLW are not enough. The purpose of this study is to obtain the geochemical information on the migration of Se with laboratory experiments to improve reliability of the safety assessment of HLW disposal system. For the purpose, this thesis consists of 6 chapters as follows. Chapter 1 describes background of this study, previous studies on migration behavior of Se, and the objective of this study.

The solubility of Se under the disposal conditions of HLW is discussed in Chapter 2 and 3. The solubility limiting solid of Se near the vitrified waste and overpack is determined by dissolution experiments in the presence of Fe under anoxic conditions in chapter 2. In addition, the equilibrium constants for the dissolution reactions of Se are directly measured and activity coefficients for Se(−II) species are obtained, to confirm the validity of the solubility evaluations by using existing thermodynamic data in chapter 3.

The diffusivities of Se(−II) species in the porewater of bentonite buffer materials are discussed in Chapter 4. Systematic D_e data of Se(−II) species through compacted bentonite materials are obtained under variable bentonite content and porewater salinity. Diffusion behaviors of Se(−II) species are modeled to quantitatively explain the variations in diffusivity of Se(−II).

The sorption characteristics of Se(−II) species onto rocks are discussed in Chapter 5. Systematic sorption data of Se(−II) species onto rocks are obtained under variable pH and salinity. The sorption data for major constituent minerals and accessory minerals of rocks are also obtained to identify which minerals are the most sorbent for Se(−II) species and to discuss the sorption mechanisms.

In chapter 6, finally, a summary of this thesis was provided and the contributions of this study to the safety assessment of HLW disposal system are described.

References

1) Japan Nuclear Cycle Development Institute (JNC), *H12: Project to establish the scientific and technical basis for HLW disposal in Japan - Second progress report on research and development for the geological disposal of HLW in Japan*, JNC TN 1410 2000-001, JNC (2000).

2) S. S. Jiang, M. He, L. J. Diao, J. R. Guo, S. Y. Wu, "Remeasurement of the half-life of ^{79}Se with the projectile X-ray detection method," *Chin. Phys. Lett*., **18**, 746-749 (2001).

3) A. Olin, B. Nolang, E. G. Osadchii, L.- O. Ohman, E. Rosen, *Chemical thermodynamics of selenium*, Elsevier, Amsterdam (2005).

4) L. Lyons, T. Young, "Alkaline selenide, polyselenide electrolytes: concentrations, absorption-spectra and formal potentials," *Aust. J. Chem*., **39[3]**, 511-527, (1986).

5) J. Bruno, E. Cera, J. de Pablo, L. Duro, S. Jordana, D. Savage, "Determination of radionuclide solubility limits to be used in SR 97. Uncertainties associated to calculated solubilities," SKB TR-97-33 (1997).

6) E. M. Elkin, *Selenium and selenium compounds*, In Kirk-Othmer Encyclopedia of chemical technology, 3rd edition, vol. 20, John Wiley & Sons, New York (1982).

7) J. Azuma, M. Shibata, , M. Yui, T. Shibutani, S. Notoya, Y. Yoshida, *Solubility and speciation of radioactive elements of high-level radioactive waste disposal system*, JNC TN8400 99-071, JNC (1999), [in Japanese].

8) S. Shibutani, H. Yoshikawa, M. Yui, *Solubility measurement of Se in Se-H_2O system under reducing condition*, PNC TN8410 94-204, Power Reactor and Nuclear Fuel Development Corporation (1995) , [in Japanese].

9) H. Tachikawa, H. Kitao, K. Katsurai, I. Yanagisawa, M. Shibata, T. Suyama, M. Yui, *Experimental study on the solubility of selenium under simulated disposal conditions*, JNC TN8400 99-068, , JNC (1999), [in Japanese].

10) A. Kitamura, M. Shibata, H. Kitao, "Solubility measurement of iron-selenium compounds under reducing conditions," *Mater. Res. Soc. Symp. Proc.,* **807**, 609-614 (2004).

11) M. García-Gutiérrez, T. Missana, M. Mingarro, J. Samper, Z. Dai, J. Molinero, "Solute transport properties of compacted Ca-bentonite used in FEBEX Project," *J. Contam. Hydrol*. **47**, 127–137 (2001).

12) H. Sato, M. Yui, H. Yoshikawa, "Diffusion behavior for Se and Zr in sodium bentonite," *Mater. Res. Soc. Symp. Proc.,* **353**, 269–276 (1995).

13) H. Sato, *Measurements of Apparent Diffusion Coefficients (Da) for Cs(I), Ni(II) and Se(IV) in Bentonite with Silica Sand*, JNC TN8400 99–060, JNC (1999).

14) H. Sato, *Acquisitions of Effective Diffusion Coefficients (De) for Ni(II), Am(III), Sm(III) and Se(IV) in Bentonite by Through-Diffusion Method*, JNC TN8400 99–062, JNC (1999).
15) H. Sato, "Diffusion behaviour of Se(−II) and Sm(III) in compacted sodium bentonite," *Radiochim. Acta*, **82**, 173–178 (1998).
16) H. Sato, S. Miyamoto, "Diffusion behaviour of selenite and hydroselenide in compacted bentonite," *Appl. Clay Sci*. **26**, 47–55 (2004).
17) Japan Atomic Energy Agency (JAEA) and Federation of Electric Power Companies of Japan (FEPC), *Second Progress Report on Research and Development for TRU Waste Disposal in Japan –Repository Design, Safety Assessment and Means of Implementation in the Generic Phase*-, JAEA-Review 2007–010, FEPC TRU–TR2–2007–01, JAEA and FEPC (2007).
18) J. V. Brakel, P. M. Heertjes, "Analysis of diffusion in macroporous media in terms of a porosity, a tortuosity and a constrictivity factor," *Int. J. Heat Mass Transfer*, **17**, 1093–1103 (1974).
19) I. Neretnieks, "Diffusivities of some constituents in compacted wet bentonite clay and the impact on radionuclide migration in the buffer," *Nucl. Technol*., **71**, 458–470 (1985).
20) H. Kato, M. Muroi, N. Yamada, H. Ishida, H. Sato, "Estimation of effective diffusivity in compacted bentonite," *Mater. Res. Soc. Symp. Proc.*, **353**, 277–284 (1995).
21) M. Ochs, B. Lothenbach, H. Wanner, H. Sato, M. Yui, "An integrated sorption-diffusion model for the calculation of consistent distribution and diffusion coefficients in compacted bentonite," *J. Contam. Hydrol*., **47**, 283–296 (2001).
22) L. R. Van Loon, M. A. Glaus, W. Müller, "Anion exclusion effects in compacted bentonites: towards a better understanding of anion diffusion," *Appl. Geochem.* 2536–2552 (2007).
23) J. Lehikoinen, A. Muurinen, M. Valkiainen, "A consistent model for anion exclusion and surface diffusion," *Mater. Res. Soc. Symp. Proc.,* **556**, 663–670 (1999).
24) M. Molera, T. Eriksen, "Diffusion of $^{22}Na^{+}$, $^{85}Sr^{2+}$, $^{134}Cs^{+}$ and $^{57}Co^{2+}$ in bentonite clay compacted to different densities: experiments and modeling," *Radiochim. Acta*, **90**, 753–760 (2002).
25) T. Kozaki, J. Liu, S. Sato, "Diffusion mechanism of sodium ions in compacted montmorillonite under different NaCl concentration," *Phys. Chem. Earth.*, **33**, 957–961 (2008).
26) I. C. Bourg, G. Sposito, A. C. M. Bourg, "Tracer diffusion in compacted, water–saturated bentonite," *Clays Clay Miner*., **54**, 363–374 (2006).
27) M. A. Glaus, B. Baeyens, M. H. Bradbury, A. Jakob, L. R. VanLoon, A. Yaroshchuk, "Diffusion of ^{22}Na and ^{85}Sr in montmorillonite: Evidence of interlayer diffusion being the dominant pathway at high compaction," *Environ. Sci. Technol.*, **41**[2], 478–485 (2007).

28) M. Birgersson, O. Karnland, "Ion equilibrium between montmorillonite interlayer space and an external source – Consequences for diffusional transport," *Geochim. Cosmochim. Acta*, **73**, 1908–1923 (2009).

29) M.A. Glaus, S. Frick, R. Rossé, L.R. Van Loon, "Comparative study of tracer diffusion of HTO, $^{22}Na^{+}$ and $^{36}Cl^{-}$ in compacted kaolinite, illite and montmorillonite," *Geochim. Cosmochim. Acta*, **74**, 1999–2010 (2010).

30) Y. Tachi, K. Yotsuji, Y. Seida, M. Yui, "Diffusion of cesium and iodine in compacted montmorillonite under different saline conditions," *Mater. Res. Soc. Symp. Proc.*, **1193**, 545–552 (2009).

31) T. Shibutani, Y. Nishikawa, S. Inui, N. Uchidate, M. Yui, *Study on Sorption Behavior of Se on Rocks and Minerals*, PNC TN8410 94-395, Power Reactor and Nuclear Fuel Development Corporation (1994), [in Japanese].

32) Y. Tachi, T. Shibutani, H. Sato, M. Yui, "Sorption and diffusion behavior of selenium in tuff," *J. Contam. Hydrol*., **35**, 77– 89 (1998).

33) K. F. Hayes, C. Papelis, J. O. Leckie, "Modeling ionic strength effects on anion adsorption at hydrous oxide/solution interfaces," *J. Colloid Interface Sci.*, **125**[2], 717–726 (1988).

34) Y. Fujikawa, M. Fukui, "Radionuclide sorption to rocks and minerals: Effect of pH and inorganic anion. Part. 2. Sorption and speciation of selenium," *Radiochim. Acta*, **76**, 163–172 (1997).

35) K. V. Ticknor, J. McMurry, "A study of selenium and tin sorption on granite and goethite," *Radiochim. Acta*, **73**, 149–156 (1996).

36) K. V. Ticknor, D. R. Harris, T. T. Vandergraaf, *Sorption/Desorption Studies of Selenium on Fracture-Filling Minerals under Aerobic and Anaerobic Conditions*, AECL TR-453, Atomic Energy of Canada Limited (1988).

37) G. S. Barney, *Radionuclide Sorption on Basalt-Interbed Materials*, FY 1981 Annual Report, RHO-BW-ST-35P (1982)

38) T. Igarashi, T. Nakazawa, S. Ueda, *Redox Potential and its Effects to Distribution Coefficients*, KURRI KR-44, 177–182 (2000), [in Japanese].

39) K. Fukushi, D. A. Sverjensky, "A surface complexation model for sulfate and selenate on iron oxides consistent with spectroscopic and theoretical molecular evidence," *Geochim. Cosmochim. Acta,* **71**, 1–24 (2007).

40) X. Xia, G. Kamei, K. Iijima, M. Shibata, T. Ohnuki, N. Kozai, "Selenium sorption in a sedimentary rock/saline groundwater system and spectroscopic evidence," *Mater. Res. Soc. Symp. Proc*., **932,** 933–942 (2006).

41) T. Shibutani, T. Suyama, M. Shibata, *Distribution Coefficient of Radionuclides on Rocks for*

Performance Assessment of High-level Radioactive waste Repository, JNC TN8410 99-051, JNC (1999), [in Japanese].

Table 1-1 A part of the available thermodynamic data of Se species compiled in Ref. 3)

Compound	$\Delta_f G_m^0$ (kJ mol^{-1})	$\Delta_f H_m^0$ (kJ mol^{-1})	S_m^0 (J K^{-1} mol^{-1})	$C_{p,m}^0$ (J K^{-1} mol^{-1})
Se(cr) (= trigonal)	0.000	0.000	42.090	25.090
			± 0.330	± 0.300
Se(cr) (= monoclinic)	1.281	2.140	44.970	25.090
	± 0.184	± 0.100	± 0.400	± 0.800
Se^{2-}	128.600	-	-	-
	± 3.000			
Se_2^{2-}	112.670	-	-	-
	± 6.294			
Se_3^{2-}	100.590	-	-	-
	± 9.198			
Se_4^{2-}	97.580	-	-	-
	± 12.149			
SeO_2(cr)	–171.797	–225.390	67.490	58.230
	± 0.620	± 0.600	± 0.400	± 0.180
SeO_3(cr)	–86.154	–163.100	91.740	77.240
	± 2.222	± 2.200	± 1.000	± 0.790
SeO_3^{2-}	–362.392	–507.160	–5.055	-
	± 1.756	± 1.130	± 7.011	
SeO_4^{2-}	–439.485	–603.5	32.965	-
	± 1.431	± 3.500	± 12.687	
HSe^-	43.471	-	-	-
	± 2.024			
H_2Se(g)	15.217	29.000	219.000	34.700
	± 2.003	± 2.000	± 0.100	± 0.100
H_2Se(aq)	21.495	14.300	148.637	-
	± 2.003	± 2.022	± 1.029	
$HSeO_3^-$	–410.112	–512.330	137.656	-
	± 1.166	± 1.010	± 5.184	
$HSeO_4^-$	–449.474	–582.700	136.232	-
	± 1.312	± 4.700	± 16.370	
H_2SeO_3(aq)	–425.181	–505.320	211.710	-
	± 0.849	± 0.650	± 3.601	
$FeSe_2$(cr) *	–101.300	–108.700	86.800	72.900
	± 15.000	± 15.000	± 1.000	± 1.000
β-$Fe_{1.04}Se$*	–70.100	–69.600	72.100	57.100
	± 4.000	± 4.000	± 0.800	± 0.700
γ-Fe_3Se_4*	–244.000	–235.000	279.800	220.100
	± 30.000	± 30.000	± 3.000	± 2.000
α-Fe_7Se_8*	–489.000	–463.500	613.800	442.100
	± 20.000	± 20.000	± 5.000	± 4.000

* : provisional value

Table 1-2 Experimentally measured diffusion data of Se through bentonite materials

Bentonite	Dry density ($kg\ m^{-3}$)	Bentonite content (wt%)	Solution	Condition	Temperature (°C)	D_e ($m^2\ s^{-1}$)	D_a ($m^2\ s^{-1}$)	Method	Reference
Kunigel V1	400	100	Distilled water	N_2	20.0	-	4.3×10^{-10}	In-diffusion	Sato (1995)
	400	100			20.0	-	4.6×10^{-10}		
	800	100			20.0	-	1.4×10^{-10}		
	800	100			20.0	-	1.7×10^{-10}		
	1400	100			20.0	-	6.8×10^{-11}		
	1400	100			20.0	-	8.0×10^{-11}		
	1800	100			20.0	-	3.2×10^{-11}		
	800	85	Bentonite water	Reducing (N_2 + $Na_2S_2O_4$)	23.6	-	1.7×10^{-10}	In-diffusion	Sato (1998)
	800	85			23.6	-	4.3×10^{-10}		
	1400	85			23.6	-	2.2×10^{-10}		
	1400	85			23.6	-	1.6×10^{-10}		
	1800	85			23.7	-	6.1×10^{-11}		
	1800	85			23.7	-	2.3×10^{-10}		
	1800	100	Fresh type groundwater	Ar	22.9	8.1×10^{-12}	-	Through-diffusion	Sato (1999a)
	1800	100			22.5	6.1×10^{-12}	-		
	1800	70	Bentonite water	Ar	23.0	-	1.1×10^{-11}	In-diffusion	Sato (1999b)
	1800	70			23.0	-	1.2×10^{-11}		
	1600	100	Bentonite water	Reducing (N_2 + $Na_2S_2O_4$)	22.5	-	5.0×10^{-12}	In-diffusion	Sato (2004)
	1600	100			22.5	-	4.0×10^{-12}		
	1600	100			60.0	-	1.0×10^{-11}		
	1600	100			60.0	-	1.0×10^{-11}		
	1600	70			22.5	-	5.0×10^{-12}		
	1600	70			22.5	-	1.0×10^{-11}		
	1600	70			60.0	-	3.0×10^{-11}		
	1600	70			60.0	-	3.0×10^{-11}		
	1600	50			22.5	-	2.5×10^{-11}		
	1600	50			22.5	-	2.5×10^{-11}		
	1600	50			60.0	-	8.0×10^{-11}		
	1600	50			60.0	-	8.0×10^{-11}		

Table 1-3 Distribution coefficients of Se onto rocks evaluated in the present safety assessment quoted from Ref. 41). FRHP: fresh-reducing-high pH, FRLP: fresh-reducing-low pH, SRLP : saline-reducing-low pH, SRHP: saline-reducing-high pH, and MRNP: mixing-saline-reducing-neutral pH.

		Groundwater type				
		FRHP	FRLP	SRHP	SRLP	MRNP
Distribution coefficient (m^3 kg^{-1})	Granite	0.01	0.01	0.01	0.01	0.01
	Basalt	0.01	0.01	0.01	0.01	0.01
	Sandstone	0.001	0.001	0.001	0.001	0.001
	Tuff	0.01	0.01	0.01	0.01	0.01
	Mudstone	0.01	0.01	0.01	0.01	0.01
Water composition	pH	8.47	5.70	7.98	5.91	7.01
	pe	–4.75	–2.64	–5.12	–2.69	–4.12
	Ionic strength (mol dm^{-3})	0.004	0.004	0.632	0.654	0.389

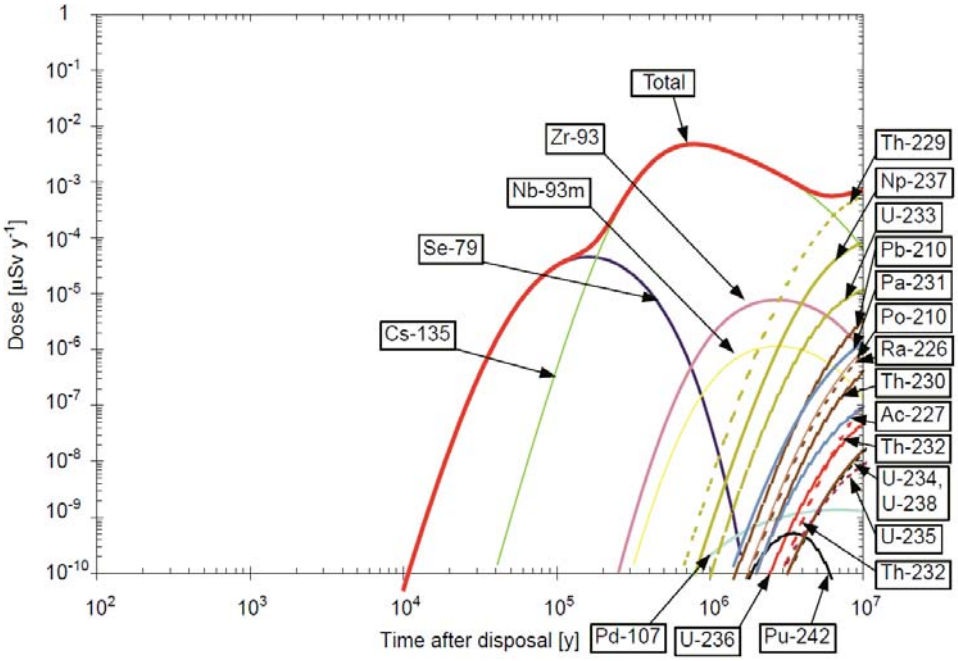

Fig. 1-1 A case of the results of safety assessment calculations for HLW repositories (doses corresponding to release rates from the waste packages to the biosphere), quoted from Ref. 1).

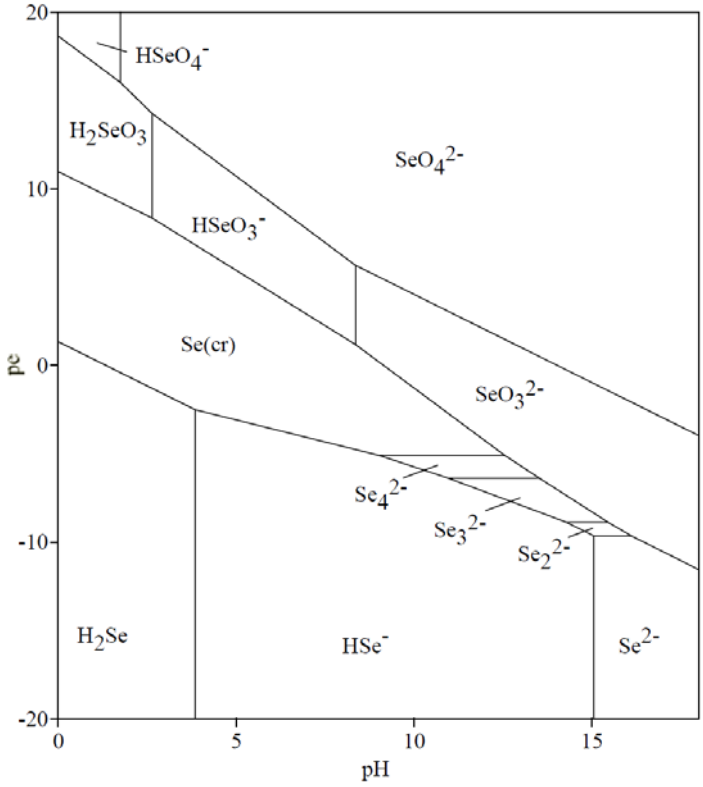

Fig.1-2 Predominance areas in a pH-pe diagram for the H-O-Se system at standard conditions, quoted from Ref. 3). The total concentration of selenium is 10^{-6} mol dm^{-3}.

2. Solubility Limiting Solid of Selenium

2.1. Introduction

The solubility of Se is expected to be limited by ferroselite ($FeSe_2$) in the previous safety assessment calculations.[1,2] The aqueous concentration of Se is considered to be decreased by several orders of magnitude by $FeSe_2$ compared to crystalline Se (Se(cr)) in the disposal environments. However, the low concentrations of Se limited by Fe-Se compounds have not been observed in laboratory dissolution experiments till now.[3-5] Therefore, there is a possibility of underestimation of the solubility of Se.

In this chapter, dissolution experiments of Se in the presence of Fe under reducing conditions were performed to determine the solubility limiting solid of Se in the disposal environments. The experiments were carried out under the conditions under which $FeSe_2$ was thermodynamically stable, to examine if $FeSe_2$ limits the concentration of Se.

2.2. Experimental

2.2.1. Stock Solutions

Stock solutions were prepared in a controlled atmosphere glove box ($p_{O2} < 10^{-6}$ atm) under argon (Ar). Selenium(−II) stock solution was prepared by the following procedure. An appropriate amount of powdered solid elemental Se (Wako Pure Chemical Ind. Ltd.) was soaked in a sodium hydroxide solution (NaOH, 0.01 mol dm^{-3}) for 7 days in a polypropylene test tube to remove soluble impurities such as SeO_2. Three grams of washed powdered Se was dissolved in a 1 cm^3 volume of 98 % hydrazine monohydrate ($N_2H_4 \cdot H_2O$) and diluting it with a 39 cm^3 volume of 1mol dm^{-3} NaOH solution.[6] The pH of the Se solution was adjusted to 6 with hydrochloric acid (HCl). The Se solution was filtered through 0.45μm filter (Millipore) to remove the precipitate of Se and diluted with distilled deionized water (WT-100U, Yamato Scientific Co., Ltd) to adjust the ionic strength to 0.1 mol dm^{-3}.

Fe(II) stock solution was prepared by using powdered metallic Fe (Rare Metallic Co., Ltd) without using a reagent of iron dichloride ($FeCl_2$) to prevent a contamination of ferric ion (Fe^{3+}) in the solution. Three grams of powdered metallic Fe were dissolved in 39 cm^3 of 2 mol dm^{-3} HCl solutions. After a day, the color of the solution turned blue by the formation of ferrous ion (Fe^{2+}), the solution was filtered through 0.45μm filter to remove the unreacted powered Fe. One cm^3 of 98 % $N_2H_4 \cdot H_2O$ was added to the solution and the pH was adjusted to the same value as the Se(−II) stock solution with a NaOH solution, to prevent precipitation of Se solid (Se(s)) by

change of pH or *E*h when Se(−II) and Fe(II) stock solutions were mixed. The solution was filtered through 0.45μm filter to remove the white precipitate of ferrous hydroxide ($Fe(OH)_2$)[7] and diluted with distilled deionized water to adjust the ionic strength to 0.1 mol dm^{-3}.

2.2.2. Dissolution Experiments

Dissolution experiments of Se were performed from both undersaturation and oversaturation directions at 25°C, 45°C, and 60°C. The temperatures at 45°C and 60°C were set to simulate temperature in the disposal environments[1] and to promote generation of Fe-Se compounds. [4] Sodium chloride (NaCl) was used as ionic strength adjuster and $N_2H_4 \cdot H_2O$ was used as a reducing agent. All the experiments were performed in 50 cm^3 polypropylene centrifuge tubes in the controlled atmosphere glove box under Ar, and the tubes were agitated once a day. The sample tubes for the experiments at 45°C and 60°C were placed in constant temperature ovens. The equilibration period was 240 days.

The oversaturation experiments were carried out by mixing 10 cm^3 volume of Fe(II) and Se(−II) stock solutions which had been maintained at desired temperature of 25°C, 45°C, or 60°C. After a week, a part of the precipitate was removed for analysis by powder X-ray diffraction with cobalt tube (XRD, Rigaku Co., Ltd).

Two types of solids were used in the undersaturation experiments, one was a precipitate formed by the oversaturation method at 60°C (self-assembled precipitate) and the other was a commercial reagent of $FeSe_x$ (Mitsuwa Chemical Co., Ltd) (purchased reagent). Prior to the start of the experiments, 1 gram of above mentioned solids were washed with 0.1 mol dm^{-3} $N_2H_4 \cdot H_2O$ solution and a part of the solid was removed for XRD analysis. The $N_2H_4 \cdot H_2O$ solution was then replaced by 40 cm^3 of a solution consisting of 0.1 mol dm^{-3} NaCl and 0.05 mol dm^{-3} $N_2H_4 \cdot H_2O$.

2.2.3. Analyses

After 240-day, the pH and *E*h of the sample suspensions were measured at room temperature. The pH was measured with a combination glass electrode (ROSS 8172BNWP, Thermo Fisher Scientific Inc.) calibrated with standard pH buffer solutions of 4, 7, and 10, and the *E*h was measured with a platinum electrode (ROSS 9180BNMD, Thermo Fisher Scientific Inc.) after checking with saturated quinhydrone solutions. A 2 cm^3 aliquot was sampled from the suspensions and ultrafiltered through 10,000 nominal molecular weight limit (NMWL) regenerated cellulose filter (Millipore Co.) after filtering a small amount of sample solution for preconditioning. The filtration was performed at room temperature, since the available filters were not applicable for filtrations at 45°C and 60°C. One cm^3 was taken out of the grove box and oxidized by adding a 2 or 3 cm^3 volume of 30 % hydrogen peroxide (H_2O_2) to prevent

precipitation and volatilization of Se. After diluting the solution with 10 cm^3 3% nitric acid, the concentrations of Se and Fe were determined by inductively coupled plasma mass spectrometry (ICP-MS, JMS-PLASMAX2, JEOL Ltd.). The detection limit was 10^{-9} mol dm^{-3} for Se and 10^{-7} mol dm^{-3} for Fe. The remaining solution was used to analyze aqueous Se species by UV-Vis spectrometry (JASCO, V-570). At the end of the equilibration period, part of the solid phase was taken and dried at 60°C in the controlled atmosphere glove box, taken out of the glove box, and analyzed by XRD in atmospheric conditions.

2.3. Results and Discussion

Figure 2-1 shows the XRD patterns of the solid phases obtained from the oversaturation experiments after 7 days and 240 days of aging. The solid phases after 7 days of aging were identified as ferroselite ($FeSe_2$), magnetite (Fe_3O_4), and goethite (FeOOH) at all temperatures. Goethite would have been generated by oxidation of $Fe(OH)_2$ soon after taking the solid phase out of the glove box. After 240-day equilibration, the peaks of $FeSe_2$ grew at 60°C, Se(cr) was identified in addition to the above mentioned solid phases at 45°C, and the peaks of only Fe_3O_4 were observed at 25°C. Therefore, $FeSe_2$ and Se(cr) were recognized as candidates of the solubility limiting solid. The difference in the solid phases with temperature might be caused by slow crystallization kinetics of Se(s) and $FeSe_2$.

Figure 2-2 shows the XRD patterns of the solid phases obtained from the undersaturation experiments before and after the experimental period at 25°C. The same patterns were observed in the solids at 45°C and 60°C. In the systems using the self-assembled precipitates as the initial solids, the solid phases were identified as $FeSe_2$, Fe_3O_4, and FeOOH before and after the experimental period. In the systems using the purchased reagents as the initial solids, peaks of $FeSe_2$, Fe_7Se_8, FeSe, and Se(cr) were observed in the solid before the experimental period. After 240-day equilibration, the peaks of Se(cr) disappeared, the peaks of Fe_7Se_8 weakened, and the peaks of $FeSe_2$ grew. The change of these peaks indicates that Se(cr) and Fe_7Se_8 would change to thermodynamically stable $FeSe_2$, by the reaction of $6Se(cr) + Fe_7Se_8 = 7FeSe_2$. From these results, $FeSe_2$ was recognized as candidates of the solubility limiting solid.

Experimental data of the sample solutions are summarized in **Table 2-1**. Low pe values of the sample solutions show that the reducing agent was effective enough to prevent oxidation during the experimental period. The experimental conditions are plotted on pH-pe diagrams for the system H-O-Se and H-O-Se-Fe shown in **Fig. 2-3**. The experimental conditions thermodynamically prefer the formation of $FeSe_2$ (**Fig. 2-3(b)**). UV-Vis spectra of the sample solutions from undersaturation direction exhibit absorption bands at 247 nm and 377 nm as

shown in **Fig. 2-4**. These peaks were assigned to HSe^- and Se_4^{2-}, respectively.[8,9] Peaks assigned to any Se species were not detected in spectra of the sample solutions from oversaturation direction because of low Se concentration.

The dissolution reaction of $FeSe_2$ which was identified in the solids by XRD can be described as

$$0.5FeSe_2 + H^+ + e^- = 0.5Fe^{2+} + HSe^- \qquad K_1^0. \tag{2-1}$$

The ion activity product (Q) for the dissolution reaction of $FeSe_2$

$$Q = a_{Fe2+}{}^{0.5}\, a_{HSe-}\, a_{H+}{}^{-1}\, a_{e-}{}^{-1} \tag{2-2}$$

was estimated from experimental data. The activities of Fe^{2+} and HSe^-, a_{Fe2+} and a_{HSe-}, were determined from the total concentrations of these elements and the equilibrium constants between major species by using following equations.

$$[Fe]_{tot} = [Fe^{2+}] + [Fe(OH)^+] = (a_{Fe2+}) / (\gamma_{Fe2+}) + (a_{Fe(OH)+}) / (\gamma_{Fe(OH)+}) \tag{2-3}$$

$$Fe^{2+} + H_2O = Fe(OH)^+ + H^+ \qquad K_2^0 = 10^{-9.5}\ ^{10)} \tag{2-4}$$

$$[Se]_{tot} = [HSe^-] + 4[Se_4^{2-}] = (a_{HSe-}) / (\gamma_{HSe-}) + 4(a_{Se_4 2-}) / (\gamma_{Se_4 2-}) \tag{2-5}$$

$$Se_4^{2-} + 4H^+ + 6e^- = 4HSe^- \qquad K_3^0 = 10^{-13.4}\ ^{11)} \tag{2-6}$$

The activity coefficient (γ) was calculated by using the extended Debye-Hückel limiting law.[12] The values of the ion activity product shown as equation (2-2) obtained from the experiments at 25°C were calculated to be ranging between $10^{-5.4}$ and $10^{-4.3}$ (**Table 2-1**). These values were 3 to 4 orders of magnitude higher than the value of $K_1^0 = 10^{-8.6}$ calculated from the existing thermodynamic data of $\Delta_f G_m^0(FeSe_2) = -101.3$ kJ mol^{-1},[11] $\Delta_f G_m^0(Fe^{2+}) = -90.5$ kJ mol^{-1},[10] and $\Delta_f G_m^0(HSe^-) = 43.471$ kJ mol^{-1}.[11] This disagreement indicates that $FeSe_2$ with a solubility product of $10^{-8.6}$ did not limit the solubility of Se under the experimental conditions. The Q values could not be accurately calculated at 45°C and 60°C, because the data of pH, Eh, and the Se and Fe concentrations were obtained at room temperature, and because the data for temperature correction of the activities of HSe^- and Se_4^{2-} were not available. It is, however, not likely that the concentrations of Se and Fe limited by $FeSe_2$ in the sample tubes increase remarkably during the

cooling to room temperature, thus the Q values at 45°C and 60°C estimated from the data measured at room temperature are possible to compare with the value of K_1^0 calculated from the existing thermodynamic data. Since the Q values at 45°C and 60°C were similar to that at 25°C, it was not probable that $FeSe_2$ limit the solubility of Se at also 45°C and 60°C.

To determine the solubility limiting solid of Se, a slope analysis was performed for dissolution reactions of Fe_nSe. The dissolution reaction can be described as

$$Fe_nSe + H^+ + (2-2n)e^- = nFe^{2+} + HSe^- \qquad K_4^0, \qquad (2\text{-}7)$$

where solids with the n value of 0, 0.5, 0.75, 0.875, and 1.04 are known.[11] The relationship of a_{HSe^-}, a_{Fe2+}, pH and pe can be described as

$$(\log a_{HSe^-} + pH + 2pe) = -n\,(\log a_{Fe2+} - 2pe) + \log K_4^0. \qquad (2\text{-}8)$$

Figure 2-5 shows the correlation between ($\log a_{HSe^-}$ + pH +2pe) and ($\log a_{Fe2+}$ − 2pe). Using the least squares method, the slope was determined to be −0.05±0.07 for 25°C, which virtually indicates $n = 0$. Then,

$$Se(s) + H^+ + 2e^- = HSe^- \qquad K_5^0 \qquad (2\text{-}9)$$

is probably the predominant dissolution reaction. The plot of the data obtained from both the oversaturation and undersaturation experiments are identical, which assures the attainment of the equilibrium within 240 days.

Applying a least-squares fitting on the experimental data obtained at 25°C to the Eq. (2-9) yields the equilibrium constants of $\log K_5^0 = -7.46 \pm 0.11$. This value agrees with the value of $\log K^0 = -7.62 \pm 0.06$ for the reaction of $Se(cr) + H^+ + 2e^- = HSe^-$ calculated from the existing thermodynamic data of $\Delta_f G_m^0(Se(cr)) = 0$ kJ mol^{-1} and $\Delta_f G_m^0(HSe^-) = 43.471$ kJ mol^{-1} [11] within errors. From the results, the solubility limiting solid of Se is determined to be Se(cr), although Se(cr) was not be detected by XRD in most samples. Formed Se(cr) was likely to be blow the detection limit of XRD which is in the order of a few %.

The plots of the data obtained at 45°C and 60°C showed similar tendency to those at 25°C, as shown in **Fig. 2-5**. The equilibrium constants were not strictly calculated at 45°C and 60°C, but the solution data suggests that the solubility limiting solid is Se(cr) at also 45°C and 60°C.

2.4. Conclusion

The solubility limiting solid of Se in the disposal environments was determined by dissolution experiments in the presence of Fe under reducing conditions. Ferroselite which was the most thermodynamically stable solid phase under the experimental condition was identified in the solids by XRD. However, the values of ion activity product for the reaction of $0.5FeSe_2 + H^+ + e^- = 0.5Fe^{2+} + HSe^-$ obtained from both undersaturation and oversaturation directions were 3 to 4 orders of magnitude higher than the equilibrium constants calculated from existing thermodynamic data. The dominant dissolution reaction of Se was determined as $Se(s) + H^+ + 2e^- = HSe^-$ and its equilibrium constant was determined to be $\log K^0 = -7.46 \pm 0.11$. This value agrees with the value of $\log K^0 = -7.62 \pm 0.06$ calculated from existing thermodynamic data of Se(cr) within errors. We concluded that the solubility limiting solid is Se(cr) in the disposal environments even if the Fe-Se compounds are formed.

References

1) Japan Nuclear Cycle Development Institute (JNC), *H12: Project to establish the scientific and technical basis for HLW disposal in Japan - Second progress report on research and development for the geological disposal of HLW in Japan*, JNC TN 1410 2000-001, JNC (2000).

2) J. Bruno, E. Cera, J. de Pablo, L. Duro, S. Jordana, D. Savage, "Determination of radionuclide solubility limits to be used in SR 97. Uncertainties associated to calculated solubilities," SKB TR-97-33 (1997).

3) S. Shibutani, H. Yoshikawa, M. Yui, *Solubility measurement of Se in Se-H_2O system under reducing condition*, PNC TN8410 94-204, Power Reactor and Nuclear Fuel Development Corporation (1995), [in Japanese].

4) H. Tachikawa, H. Kitao, K. Katsurai, I. Yanagisawa, M. Shibata, T. Suyama, M. Yui, *Experimental study on the solubility of selenium under simulated disposal conditions*, JNC TN8400 99-068 , JNC (1999), [in Japanese].

5) A. Kitamura, M. Shibata, H. Kitao, "Solubility measurement of iron-selenium compounds under reducing conditions," *Mater. Res. Soc. Symp. Proc.,* **807**, 609–614 (2004).

6) L. Syper, J. Mlochowski, "The convenient syntheses of organoselenium reagents," *Synthesis*, **5**, 439–442 (1984).

7) D. L. Leussing, I. M. Kolthoff, "The solubility product of ferrous hydroxide and the ionization of the aquo-ferrous ion," *J. Am. Chem. Soc*, **75**, 2476–2479 (1953).

8) L. Lyons, T. Young, "Alkaline selenide, polyselenide electrolytes: concentrations, absorption-spectra and formal potentials," *Aust. J. Chem*., **39[3]**, 511–527, (1986).

9) S. Licht, F. Forouzan, "Speciation analysis of aqueous polyselenide solutions," *J. Electrochem. Soc*., **142[5]**, 1546–1551 (1995).

10) I. Otuka, H. Taki, Y. Yamaguchi, Y. Iida, F. Yamada, D. Inada, T. Tanaka, *Effects of Overpack Corrosion on Redox Potential of Bentonite Pore Water under. Geological Disposal Environment. –Important Parameter Acquisition and a Preliminary Eh Analysis–*, JAEA-Research 2008-043, Japan Atomic Energy Agency (2008), [in Japanese].

11) A. Olin, B. Nolang, E. G. Osadchii, L.- O. Ohman, E. Rosen, *Chemical thermodynamics of selenium*, Elsevier, Amsterdam (2005).

12) W. Stumm, J. J. Morgan, *Aquatic Chemistry, 3rd edition*, John Wiley & Sons, Inc., New York (1996).

Table 2-1 Measured Se and Fe concentration from under- and oversaturation directions after 240-day equilibration in 0.1 mol dm^{-3} NaCl / 0.05 mol dm^{-3} N_2H_4 solutions, and the ion activity product (Q) for the reaction (2-1)

Sample		Temp. (°C)	pH	pe	[Se] (mol dm^{-3})	[Fe] (mol dm^{-3})	log$Q$
Stock solution	Fe(II)		5.96	–5.1	–	2.36×10^{-1}	
	Se(-II)		6.57	–6.3	5.38×10^{-3}	–	
Undersatulation	Purchased reagent	25	9.17	–5.3	4.68×10^{-5}	1.54×10^{-5}	–4.7
			9.61	–6.1	2.34×10^{-4}	9.43×10^{-6}	–4.3
		45	9.30	–6.8	3.81×10^{-3}	2.81×10^{-6}	–3.9
			9.41	–5.2	3.45×10^{-5}	1.12×10^{-5}	–4.9
		60	9.21	–5.2	7.09×10^{-5}	6.15×10^{-5}	–4.4
			9.11	–5.2	2.44×10^{-5}	4.64×10^{-5}	–4.6
	Self-assembled precipitate	25	9.52	–5.1	1.18×10^{-5}	9.83×10^{-5}	–4.6
			9.54	–5.2	1.38×10^{-5}	2.39×10^{-6}	–5.4
		45	9.40	–5.1	7.62×10^{-6}	1.18×10^{-6}	–5.6
			9.45	–5.1	1.12×10^{-4}	8.32×10^{-5}	–4.4
		60	9.15	–4.9	2.88×10^{-5}	4.58×10^{-6}	–5.3
			9.16	–4.9	1.90×10^{-5}	3.09×10^{-5}	–4.9
Oversatulation		25	5.29	–3.7	3.55×10^{-6}	9.88×10^{-3}	–5.2
			6.08	–4.0	5.47×10^{-6}	7.54×10^{-4}	–5.1
		45	5.53	–4.1	3.89×10^{-6}	9.12×10^{-3}	–5.3
			4.06	–3.1	5.21×10^{-6}	1.10×10^{-2}	–5.7
		60	5.31	–3.8	1.76×10^{-5}	7.23×10^{-3}	–4.7
			4.62	–3.3	8.91×10^{-6}	1.74×10^{-2}	–5.0

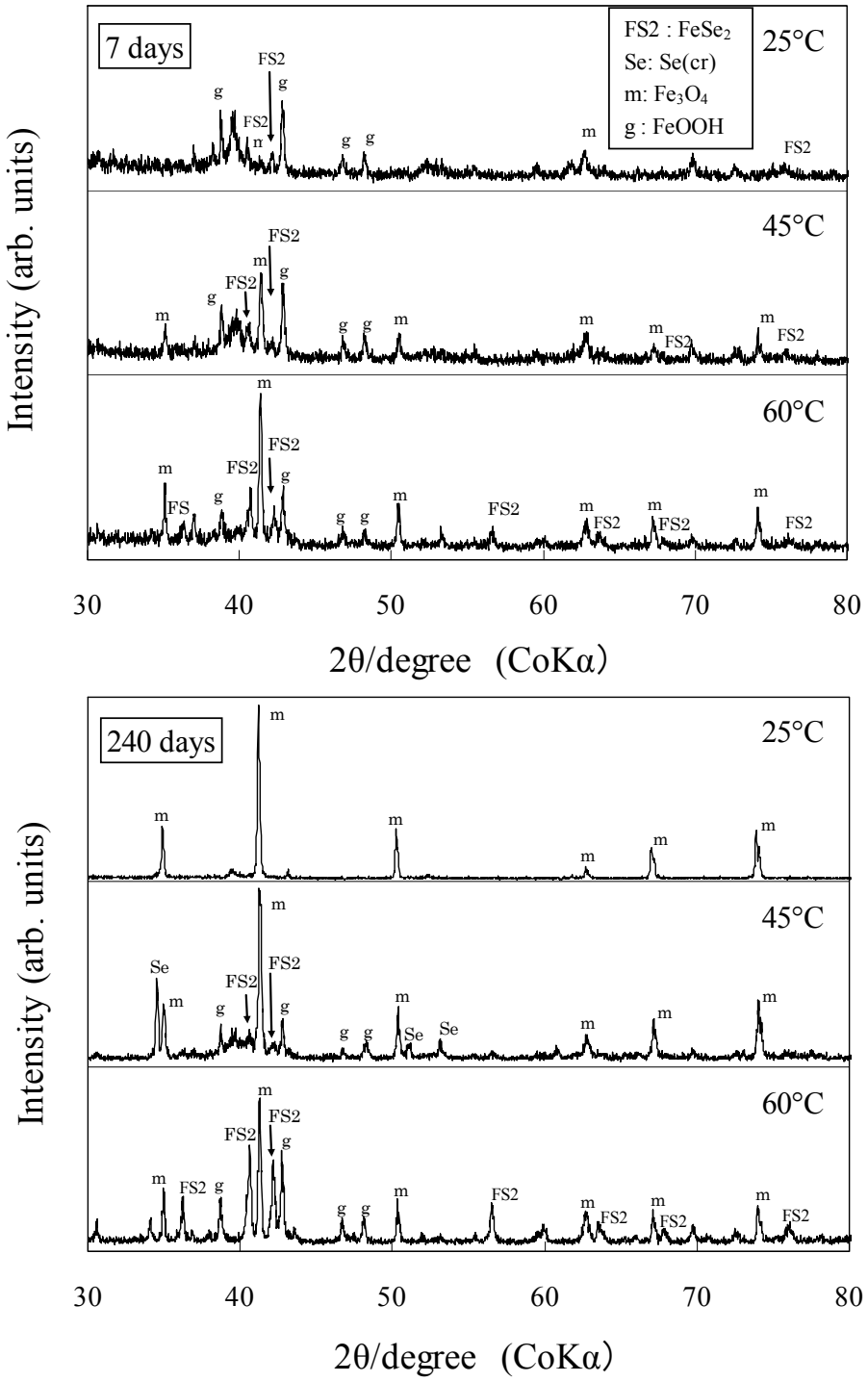

Fig. 2-1 XRD patterns of the solid phases obtained from oversaturation experiments after 7 days (upper) and 240 days aging (lower). The solid phases after 7 days aging were identified as ferroselite (FS2: $FeSe_2$), magnetite (m: Fe_3O_4) and goethite (g: FeOOH) at all temperatures. After 240-day equilibration, the peaks of $FeSe_2$ grew at 60°C, Se(cr) was identified in addition to the above mentioned solid phases at 45°C, and the peaks of only Fe_3O_4 were observed at 25°C.

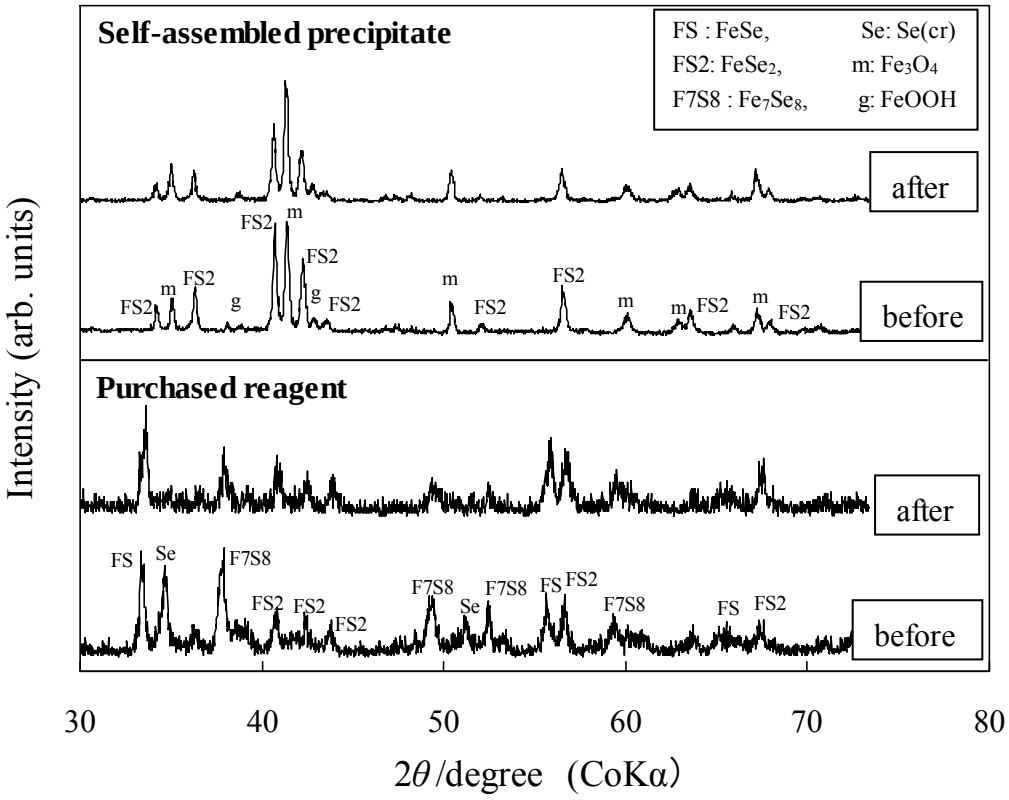

Fig. 2-2 XRD patterns of the solid phases obtained from undersaturation experiments before and after equilibration. In the system using the self-assembled precipitates (upper), $FeSe_2$, Fe_3O_4 and FeOOH were identified before and after equilibration. In the system using the purchased reagents (lower), the peaks of $FeSe_2$, Fe_7Se_8, FeSe, and Se(cr) were observed before equilibration, but the peaks of Se(cr) disappeared after 240-day equilibration.

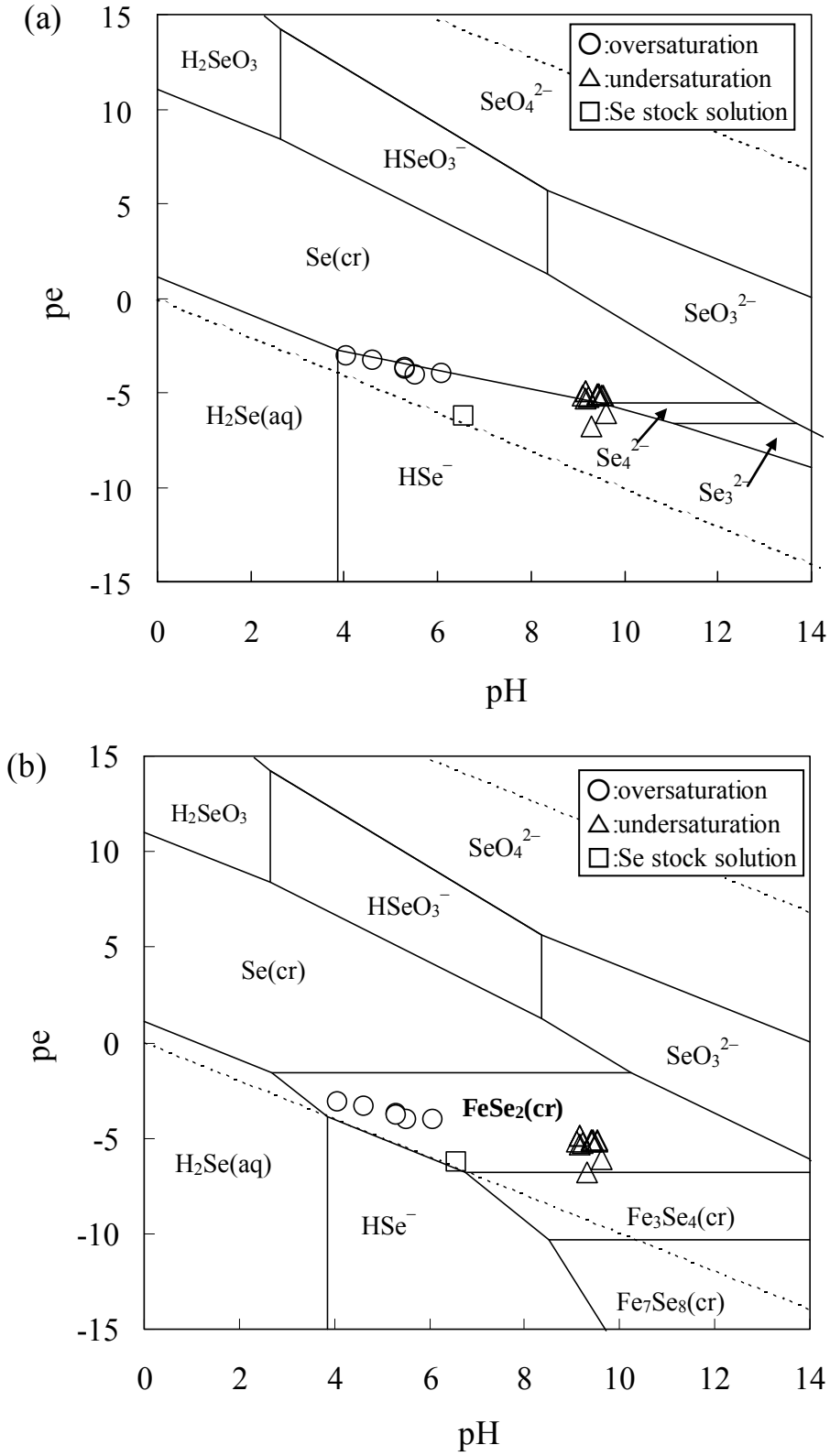

Fig. 2-3 pH-pe diagrams for the system H-O-Se (a) and H-O-Se-Fe (b). The activities for dissolved species are Se = 10^{-6} ((a), (b)) and Fe^{2+} = 10^{-5} (b).

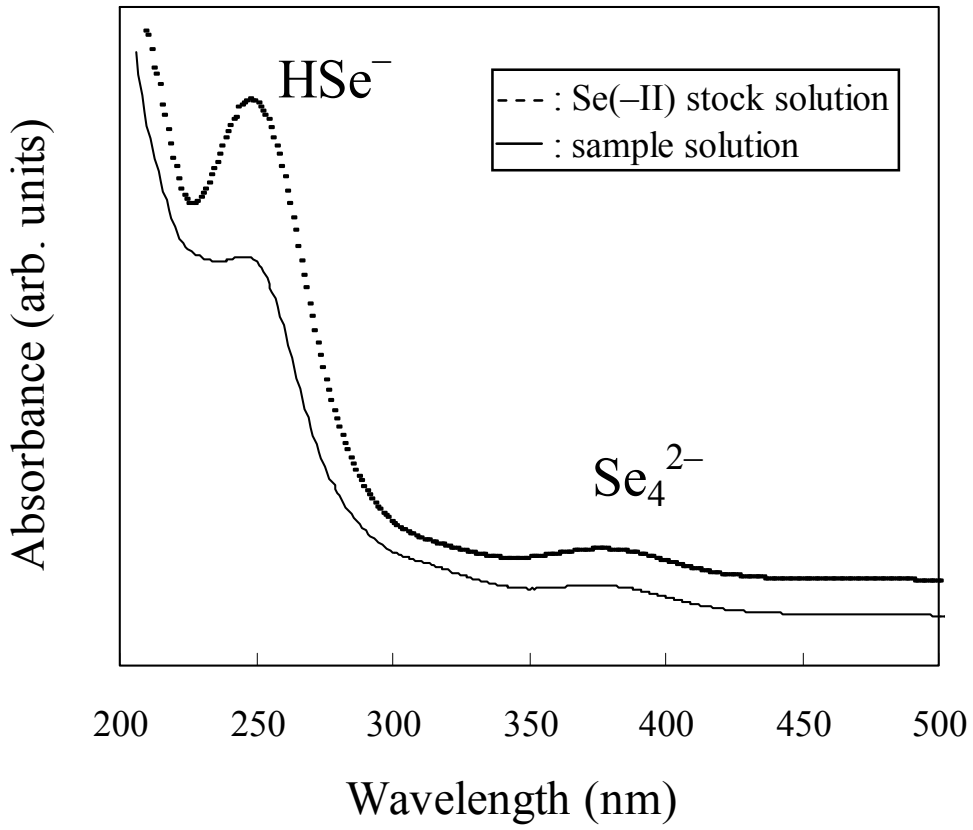

Fig. 2-4 UV-Vis spectra of the Se(−II) stock solution and sample solutions from the undersaturation direction after 240-day equilibration. The absorption band at 247 nm was assigned to HSe^- anion and the one at 377 nm to Se_4^{2-}

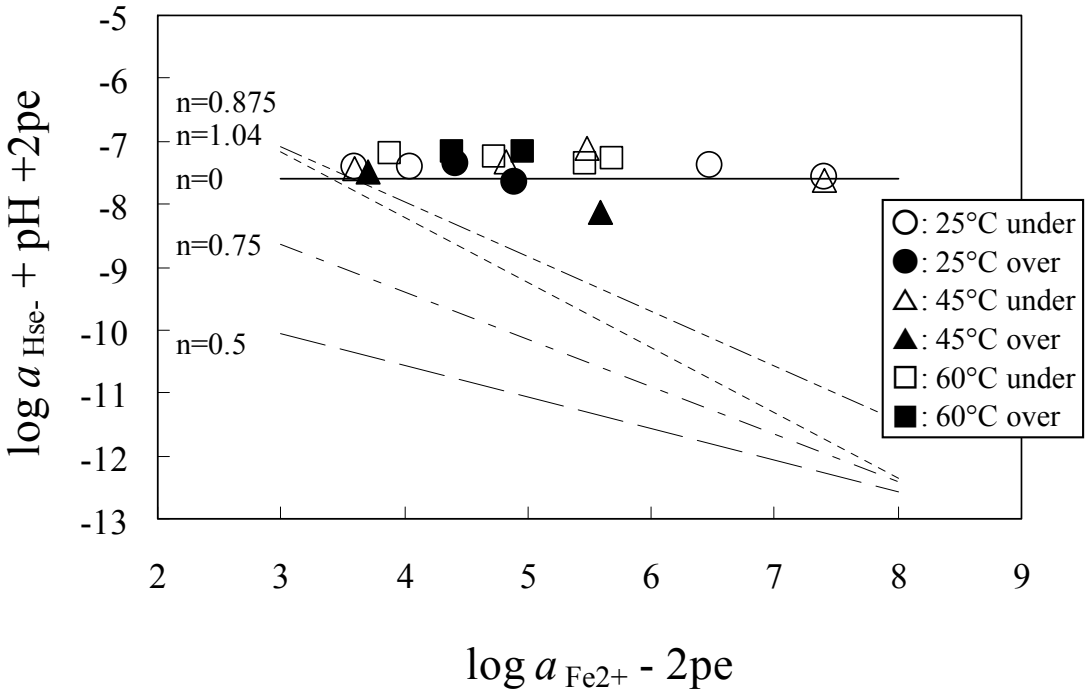

Fig. 2-5 A plot of (log a_{HSe^-} + pH +2pe) versus (log a_{Fe2+} − 2pe). The circles (○, ●), triangles (△, ▲) and squares (□, ■) represent the data obtained at 25°C, 45°C and 60°C, respectively. Open marks and closed marks represent the data obtained from the undersaturation and the oversaturation experiments, respectively. The lines represent the values for dissolution reactions calculated from existing thermodynamic data.

3. Thermodynamic Data and Activity Coefficients of Selenium Species

3.1. Introduction

The solubility of Se is expected to be limited by Se(cr) in the disposal environments (chapter 2). Under the disposal condition of HLW, dominant Se species are considered to be HSe^- in neutral groundwater[1)], and polyselenide species of Se_n^{2-} (n = 1-4) in alkaline groundwater[1-3)] induced by cementitious materials. Therefore, the equilibrium constants of the reactions

$$Se(cr) + H^+ + 2e^- = HSe^- \quad (3\text{-}1)$$

and

$$nSe(cr) + 2e^- = Se_n^{2-} \quad (3\text{-}2)$$

are critical for evaluating the solubility of Se. To confirm the validity of the equilibrium constants of dissolution reactions (3-1) and (3-2) calculated from existing thermodynamic data, and to obtain activity coefficients of Se species at high ionic strength in the case of possible intrusion of saline groundwater for coastal repositories, dissolution experiments of Se were performed as a function of pH and ionic strength under reducing conditions.

3.2. Experimental

3.2.1. Dissolution Experiments

Dissolution experiments of Se were performed from both undersaturation and oversaturation directions. A mixture of NaCl and $N_2H_4 \cdot H_2O$ was used. The ionic strength of the solution was adjusted to 0.1, 1.0, or 2.0 mol dm^{-3} using NaCl, and $N_2H_4 \cdot H_2O$ (0.05 mol dm^{-3}) was used to maintain chemically reducing conditions. Prior to the start of the dissolution experiments from the undersaturation direction, 2 grams of powdered solid elemental Se were soaked in 30 cm^3 of 0.01 mol dm^{-3} NaOH solution for 7 days in a polypropylene test tube to remove soluble impurities such as SeO_2. After removing a small amount of the solid phase for analysis by XRD, the NaOH solution was replaced by the same volume of the fresh mixture solution. The pH of the solution was adjusted to a desired value between 5 and 13 with NaOH or HCl.

The Se stock solution used in the oversaturation experiments was prepared in a controlled atmosphere glove box under Ar by the following procedure. An appropriate amount of powdered

Se was soaked in a 0.01 mol dm^{-3} NaOH solution for 7 days in a polypropylene test tube to remove soluble impurities. Ten grams of washed powdered Se was dissolved in a 2 cm^3 volume of 98% $N_2H_4 \cdot H_2O$ solution and diluted with a 48 cm^3 volume of 1.5 mol dm^{-3} NaOH solution.[4)] A 2 cm^3 volume of the Se stock solution was mixed with a 2 cm^3 volume of 1.5 mol dm^{-3} HCl and diluted to 30 cm^3 with NaCl solution to adjust the ionic strength. The pH of the sample solutions was adjusted to a desired value between 5 and 13 with HCl. The ionic strength of the sample solutions was 0.1, 1.0, or 2.0 mol dm^{-3} and the concentration of $N_2H_4 \cdot H_2O$ was 0.05 mol dm^{-3} in all the sample solutions.

The sample solutions were stored in the controlled atmosphere glove box at 25.0±1.0 °C and agitated once a day. After a 40-day equilibration, the pH and *E*h of the solutions were measured. The pH was measured with a combination glass electrode (ROSS 8172BNWP, Thermo Fisher Scientific Inc.) which is suitable for the measurement of high-ionic-strength samples, calibrated with standard pH buffer solutions of 4.01, 7.00, and 10.01. The *E*h was determined in relation to a normal hydrogen electrode (NHE) using a platinum electrode combined with a Ag/AgCl reference electrode (ROSS 9180BNMD, Thermo Fisher Scientific Inc.) after checking its accuracy with saturated quinhydrone solutions. A small amount of the solid phase was removed for analysis by XRD. A 5 cm^3 aliquot was sampled and filtered through a 10,000 NMWL regenerated cellulose filter (Amicon Ultra, Millipore), which is available for alkaline samples (< 0.5 mol dm^{-3} NaOH), after preconditioning with a small amount of the sample solution. One cm^3 of filtered sample solution was removed from the glove box and oxidized by adding a 2 or 3 cm^3 volume of 30 % H_2O_2 to prevent the precipitation and volatilization of the Se. After diluting the solution with 3% nitric acid, the concentration of Se was determined by ICP-MS. The remaining solution was used to determine the aqueous Se species by UV-Vis spectrometry.

3.2.2. Determination of pH

Due to the difference in activity coefficients between the calibration buffers and those of the high-ionic-strength solutions, the observed pH (pH_{obs}) can be shifted from pH(= $-\log a_{H+}$) as given by

$$pH_{obs} = pH + \Delta pH. \quad (3\text{-}3)$$

The ΔpH value was determined by measuring the pH_{obs} of NaCl/HCl and NaCl/NaOH solutions of known H^+ and OH^- concentrations in the controlled atmosphere glove box under Ar to avoid the effect of CO_2. The pH of the solution was estimated using the following relationships:

$$pH = -\log [H^+] - \log \gamma_{H+} \quad \text{(acid solutions)} \quad (3\text{-}4)$$

$$pH = -\log K_w + \log [OH^-] + \log \gamma_{OH-} - \log a_{H2O} \quad \text{(basic solutions)} \quad (3\text{-}5)$$

where K_w is the ion product of water (1.01×10^{-14}), [5] and a_{H2O} is the activity of water (0.9966, 0.9661, and 0.9284 for the ionic strengths of 0.1, 1.0, and 2.0 mol dm^{-3},[1] respectively). The activity coefficients of H^+ and OH^-, γ_{H+} and γ_{OH-}, were estimated with the specific ion interaction theory (SIT)[1] as

$$\log \gamma_{H+} = -D + \varepsilon(H^+, Cl^-)\, I_m \quad (3\text{-}6)$$

$$\log \gamma_{OH-} = -D + \varepsilon(Na^+, OH^-)\, I_m \quad (3\text{-}7)$$

where $\varepsilon(H^+, Cl^-)$ and $\varepsilon(Na^+, OH^-)$ are ion interaction coefficients, 0.12±0.01 and 0.04±0.01,[1] respectively, I_m is the molal ionic strength (0.10046, 1.0215, and 2.0858 mol kg^{-1} for the ionic strength of 0.1, 1.0, and 2.0 mol dm^{-3},[1] respectively), and D is the Debye-Hückel term,

$$D = \frac{0.509\sqrt{I_m}}{1+1.5\sqrt{I_m}} \quad (3\text{-}8)$$

The ΔpH value was determined from the difference between pH and pH_{obs} by least-squares fitting on the measured pH_{obs} (**Fig. 3-1**) as

$\Delta pH = 0.00\pm0.02$ at $I = 0.1$ mol dm^{-3},

$\Delta pH = -0.19\pm0.02$ at $I = 1.0$ mol dm^{-3},

$\Delta pH = -0.30\pm0.03$ at $I = 2.0$ mol dm^{-3}.

The correct pH value corresponding to the H^+ ion activity is then given by

$$pH = pH_{obs} - \Delta pH. \quad (3\text{-}9)$$

3.3. Results and Discussion

Experimental data from the solubility determinations are summarized in **Table 3-1**. Only crystalline Se (trigonal) could be identified by XRD in the washed purchased solid elemental Se employed for the undersaturation experiments. The solid phase, formed by precipitation in the oversaturation experiments, was initially red but turned black in a few days. The XRD pattern of the red solid phase was broad (**Fig. 3-2**), indicating the absence of an appreciable crystal phase and the formation of overall amorphous Se. After equilibration for all the experiments, all the XRD peaks of the solid phase were assigned to crystalline trigonal Se as shown in **Fig. 3-3**. Therefore, amorphous and crystalline Se were recognized as candidates of the solubility limiting solid.

UV-Vis spectra of the sample solutions at the pH range between 5 and 8 show an absorption band at 245 nm. This peak was assigned to HSe^-.[2,3,6] At pH between 9 and 13, the sample solutions were reddish and showed absorption bands at 220, 282, and 377 nm. These results are indicative of the formation of Se_4^{2-}.[2,3] The UV-Vis spectra of the 1.0 mol dm^{-3} NaCl sample solutions at pH 7 and pH 10 are shown in **Fig. 3-3** as representative examples. The same patterns were observed at samples with ionic strengths of 0.1 and 2.0 mol dm^{-3}. The governing dissolving reactions of Se can then be described as

$$Se(s) + H^+ + 2e^- = HSe^- \qquad K_1 \quad (5 < pH < 8) \text{ and} \tag{3-10}$$

$$4Se(s) + 2e^- = Se_4^{2-} \qquad K_2 \quad (9 < pH < 13). \tag{3-11}$$

At pH between 8 and 9, the chemical potentials of HSe^- and Se_4^{2-} are approximately the same. Reaction (3-10), involving the reduction of Se(0) to Se(−II) and participation of a proton, is represented by a straight line with a slope of (–1) on the plot of (log [total Se concentration] + 2pe) versus pH, and reaction (3-11) shows the line with a slope of 0 (**Fig. 3-4**). The plots of the data obtained under various pe conditions show good agreement with Eqs. (3-10) and (3-11). In addition, the plots of the data obtained from both oversaturation and undersaturation directions are identical, confirming that equilibrium was attained during the experimental periods. The large difference in the concentrations of Se between the oversaturation and the undersaturation experiments at similar pH (**Table 3-1**) is caused by the difference in pe values.

The conditional equilibrium constants for K_1 and K_2 for reactions (3-10) and (3-11) are described as

$$K_1 = [HSe^-]\,(a_{H+})^{-1}\,(a_{e-})^{-2} \quad \text{and} \tag{3-12}$$

$$K_2 = [Se_4^{2-}]\,(a_{e-})^{-2}, \tag{3-13}$$

where (a_M) is the activity of species M. The total Se concentration, $[Se]_{tot}$, is given as

$$[Se]_{tot} = [HSe^-] + 4[Se_4^{2-}] = K_1\,(a_{H+})\,(a_{e-})^2 + 4K_2\,(a_{e-})^2. \tag{3-14}$$

Applying the least-squares fitting on the measured total Se concentrations to the Eq. (3-14) yields the conditional equilibrium constants of reactions (3-10) and (3-11), $\log K_{1(0.1\ \text{mol dm}-3)} = -6.53\pm0.09$ and $\log K_{2(0.1\ \text{mol dm}-3)} = -16.24\pm0.09$ in the 0.1 mol dm^{-3} NaCl solutions, $\log K_{1(1\ \text{mol dm}-3)} = -6.23\pm0.12$ and $\log K_{2(1\ \text{mol dm}-3)} = -15.79\pm0.12$ in the 1.0 mol dm^{-3} NaCl solutions, and $\log K_{1(2\ \text{mol dm}-3)} = -6.38\pm0.10$ and $\log K_{2(2\ \text{mol dm}-3)} = -15.68\pm0.10$ in the 2.0 mol dm^{-3} NaCl solutions (**Table 3-2**). The regression line shows a good fit to the experimental data as shown in **Fig. 3-4**. The uncertainty associated with the log K values are associated with the uncertainty in the least-squares fitting.

The equilibrium constants at zero ionic strength ($\log K^0$) were also estimated with SIT.[1)] The equilibrium constant determined in a solution of the non zero ionic strength is related to the corresponding value at zero ionic strength,

$$\log K_1^0 = \log K_1 + \log \gamma_{HSe-} \tag{3-15}$$

$$\log K_2^0 = \log K_2 + \log \gamma_{Se42-} \quad . \tag{3-16}$$

The activity coefficient, γ_i, can be described as

$$\log \gamma_i = -z_i^2 D + \Sigma\varepsilon_{ij}\, m_j\,, \tag{3-17}$$

where z_i is the charge of species, D is the Debye-Hückel term, ε_{ij} is the ion interaction coefficient for ion i and oppositely charged electrolyte ion j, and m_j (mol kg^{-1}) is the molal concentration of ion j.[1)] The value of m_j is equal to the molal ionic strength, I_m (mol kg^{-1}), for a 1:1 electrolyte solution. By plotting ($\log K - z^2 D$) versus I_m, a straight line with the slope ε_{ij} and intercept $\log K^0$ can be obtained as

$$\log K_1 - D = -\varepsilon(HSe^-, Na^+)\, I_m + \log K_1^0 \tag{3-18}$$

$$\log K_2 - 4D = -\varepsilon(\mathrm{Se_4^{2-}}, \mathrm{Na^+})\, I_\mathrm{m} + \log K_2^{\,0}\,. \tag{3-19}$$

The equilibrium constants for reactions (3-10) and (3-11) were found to be $\log K_1^{\,0} = -6.57\pm0.15$ and $\log K_2^{\,0} = -16.67\pm0.03$, respectively (**Fig. 3-5**). The plot of $\log K_1$ data do not show clear tendency (**Fig. 3-5(a)**) due to the variation in the measured data, and thus, the $\log K_1^{\,0}$ has comparatively large uncertainty. The corresponding ion interaction coefficients were $\varepsilon(\mathrm{HSe^-}, \mathrm{Na^+}) = -0.01\pm0.10$ and $\varepsilon(\mathrm{Se_4^{2-}}, \mathrm{Na^+}) = -0.03\pm0.02$, as determined from the plot in **Fig. 3-5**. These values are nearly 0, indicating that most of the interactions of these Se species with $\mathrm{Na^+}$ are coulomb attractions, which are considered in the Debye-Hückel theory. The value of $\varepsilon(\mathrm{HSe^-}, \mathrm{Na^+})$ is within the range of the variations of the previously reported values for monovalent anions (−0.18 to 0.08),[1)] and that of $\varepsilon(\mathrm{Se_4^{2-}}, \mathrm{Na^+})$ within the range of the values for divalent anions (−0.30 to −0.02). [1)] The activity coefficients for $\mathrm{HSe^-}$ and $\mathrm{Se_4^{2-}}$ in Na-rich solution can be described with Eq. (3-8) and (3-17) as

$$\log \gamma_{(\mathrm{HSe^-}, \mathrm{Na^+})} = -\frac{0.509\sqrt{I_\mathrm{m}}}{1+1.5\sqrt{I_\mathrm{m}}} - 0.01\, I_\mathrm{m} \tag{3-20}$$

$$\log \gamma_{(\mathrm{Se_4^{2-}}, \mathrm{Na^+})} = -4\times\frac{0.509\sqrt{I_\mathrm{m}}}{1+1.5\sqrt{I_\mathrm{m}}} - 0.03\, I_\mathrm{m}\,. \tag{3-21}$$

The value obtained for $\log K_1^{\,0} = -6.57\pm0.15$ is higher than the value of $\log K^0 = -7.62\pm0.06$ for reaction (3-10) calculated from the existing thermodynamic data of $\Delta_\mathrm{f}G_\mathrm{m}^{\,0}(\mathrm{Se(cr)}) = 0$ kJ mol^{-1} and $\Delta_\mathrm{f}G_\mathrm{m}^{\,0}(\mathrm{HSe^-}) = 43.471\pm2.024$ kJ mol^{-1}.[1)] Shibutani *et al*. also reported a higher equilibrium constant of $\log K^0 = -6.48\pm0.01$, obtained from aqueous dissolution experiments, than that calculated from the existing thermodynamic data.[7)] This inconsistency between the equilibrium constants is not due to the overestimation of the existing data of $\Delta_\mathrm{f}G_\mathrm{m}^{\,0}(\mathrm{HSe^-})$, but likely to the low crystallinity of the solubility-limiting solid in the aqueous experiments. Maes *et al*.[8)] reported that the solubility of Se under Boom Clay conditions was dependent on the respective solid phase formed. In that case, the solubility limited by amorphous Se (2.2×10^{-8} mol dm^{-3}) was about one order of magnitude higher than that by crystalline Se (1.5×10^{-9} mol dm^{-3}). In this experiment, the solid phase after equilibration was identified as crystalline Se by XRD; however, the solubility of Se was not limited by crystalline Se probably due to the rapid precipitation and slow crystallization kinetics of amorphous Se. For this reason, Eq. (3-10) is applicable to an amorphous

form of Se, Se(am), with a log K_1^0 value of −6.57±0.15,

$$Se(am) + H^+ + 2e^- = HSe^- \qquad \log K_1^0 = -6.57 \pm 0.15. \tag{3-22}$$

The standard molar free energy of formation of Se(am) can be determined as $\Delta_f G_m^0(Se(am)) = 6.0 \pm 2.2$ kJ mol^{-1}, from the obtained equilibrium constant K_1^0 and the existing thermodynamic data of $\Delta_f G_m^0(HSe^-)$. This value is higher than that of glassy Se (2.7 kJ mol^{-1}).[9)]

On the other hand, the value obtained for log K_2^0 = −16.67±0.03 agrees with that for log K^0 = −17.1±2.1, as calculated from existing thermodynamic data of $\Delta_f G_m^0(Se(cr)) = 0$ kJ mol^{-1} and $\Delta_f G_m^0(Se_4^{2-}) = 97.580 \pm 12.149$ kJ mol^{-1}.[1)] Assuming that the solubility-limiting solid for the reaction (3-11) was crystalline Se which was identified by XRD after equilibration, the standard molar free energy of formation of Se_4^{2-} was determined to be $\Delta_f G_m^0(Se_4^{2-}) = 95.14 \pm 0.17$ kJ mol^{-1}. Licht and Forouzan[2)] determined the equilibrium constants for reactions between polyselenide species using spectrophotometric data,

$$Se_3^{2-} + Se^{2-} = 2Se_2^{2-}, \qquad \log K_3^0 = 0.7 \pm 0.1 \tag{3-23}$$

$$2Se_4^{2-} + Se^{2-} = 3Se_3^{2-}, \qquad \log K_4^0 = 4.0 \pm 0.1 \tag{3-24}$$

which were found to be independent of the ionic medium employed and agree with the value of log K_3^0 = 0.67±2.30 and log K_4^0 = 3.85±4.13 calculated from existing thermodynamic data.[1)] The standard molar free energies of formation of Se_2^{2-} and Se_3^{2-} were calculated to be $\Delta_f G_m^0(Se_2^{2-}) = 111.64 \pm 1.61$ kJ mol^{-1} and $\Delta_f G_m^0(Se_3^{2-}) = 98.68 \pm 1.02$ kJ mol^{-1} from the equilibrium constants of reactions (3-23) and (3-24), and the standard molar free energies of formation, $\Delta_f G_m^0(Se^{2-}) = 128.600 \pm 3.000$ kJ mol^{-1} [1)] and $\Delta_f G_m^0(Se_4^{2-}) = 95.14 \pm 0.17$ kJ mol^{-1}. Meanwhile, assuming that the solubility-limiting solid for the reaction (3-11), as well as for the reaction (3-22), was amorphous Se, the standard molar free energy of formation of Se_4^{2-} is calculated to be $\Delta_f G_m^0(Se_4^{2-}) = 119.1 \pm 4.4$ kJ mol^{-1} from log K_2^0 = −16.67±0.03 and $\Delta_f G_m^0(Se(am)) = 6.0 \pm 2.2$ kJ mol^{-1}. Using this value, the standard molar free energies of formation of Se_2^{2-} and Se_3^{2-} were calculated to be $\Delta_f G_m^0(Se_2^{2-}) = 119.6 \pm 1.9$ kJ mol^{-1} and $\Delta_f G_m^0(Se_3^{2-}) = 114.7 \pm 2.3$ kJ mol^{-1}, respectively. Based on these values for polyselenide species, Se_4^{2-} is less stable than Se_3^{2-} under any pH-pe condition because the value of $\Delta_f G_m^0(Se_4^{2-})$ is larger than that of $\Delta_f G_m^0(Se_3^{2-})$. This inconsistency is not due to the equilibrium constants for the reactions between polyselenide species, but due to overestimated $\Delta_f G_m^0(Se_4^{2-})$. Therefore, the solubility limiting solid of reaction (3-11) was likely to be crystalline Se. Harañczyk *et al.*[10)] have

investigated the morphology of precipitated Se compounds by reduction of aqueous selenite solution. The redox reaction proceeds fast at the low pH region and the solid phase formed was amorphous red Se. The redox reaction at the high pH region (pH > 8) proceeds slowly and black crystalline Se appeared directly from the solution. In the same manner, the crystallization of Se was presumed to be promoted by a slow redox reaction at the high-pH region in this study. In addition, this phenomenon can be inferred from the difference in the structure between crystalline Se and amorphous Se. The crystalline Se (trigonal) is known to consist of polymeric Se_n chains,[11,12] while amorphous Se consists of closed Se_8 rings at room temperature[13]. Kawarada and Nishina[14] reported that the crystal transformation of Se is attributed to the polymerization of short chains in solution. Since the structure of Se_4^{2-} is a straight chain,[15,16] the crystallization of Se was presumed to occur through polymerization and homogeneous nucleation[17] of Se_4^{2-} at the high-pH region. For this reason, Eq. (3-11) is applicable to a crystalline form of Se with a log K_2^0 value of −16.67±0.03,

$$4Se(cr) + 2e^- = Se_4^{2-} \qquad \log K_2^0 = -16.67 \pm 0.03. \tag{3-25}$$

The datasets of the standard molar free energies of formation of amorphous Se, hydrogen selenide, and polyselenide species are tabulated in **Table 3-3**. The standard molar free energies of formation of polyselenide species agree with the existing thermodynamic data[1] and have a smaller uncertainty, especially for Se_4^{2-} .

3.4. Conclusion

The equilibrium constants of the dissolution reaction of Se under reducing conditions and ion interaction coefficients for Se species were obtained by dissolution experiments. The solubility limiting solid and the dominant dissolved species were determined as Se(am) and HSe^- at pH between 5 and 8. The equilibrium constant of dissolution reaction was obtained as,

$$Se(am) + H^+ + 2e^- = HSe^- \qquad \log K_1^0 = -6.57 \pm 0.15.$$

The solubility of Se limited by Se(am) can be about 1 order of magnitude higher than that limited by Se(cr). However, the solubility of Se will be limited by Se(cr) near overpacks in the disposal environments, because the concentration of HSe^- was likely to be limited by Se(cr) in the presence of Fe (chapter 2). The standard molar free energy of formation of Se(am) was obtained as $\Delta_f G_m^0(\text{Se(am)}) = 6.0 \pm 2.2$ kJ mol^{-1}, from the obtained equilibrium constant K_1^0 and the

existing thermodynamic data of $\Delta_f G_m^0(HSe^-)$.

The solubility limiting solid and the dominant dissolved species were determined as Se(cr) and Se_4^{2-} at pH between 9 and 13. The equilibrium constant of dissolution reaction was obtained as

$$4Se(cr) + 2e^- = Se_4^{2-} \qquad \log K_2^0 = -16.67 \pm 0.03.$$

This value agrees with the value calculated from existing thermodynamic data. The validity of the equilibrium constants of dissolution reactions calculated from existing thermodynamic data was confirmed. The standard molar free energy of formation of Se_4^{2-} was determined to be $\Delta_f G_m^0(Se_4^{2-}) = 95.14 \pm 0.17$ kJ mol^{-1}. By using this value and the existing equilibrium constants of reactions between polyselenide species, the standard molar free energies of formation of other polyselenide species, $\Delta_f G_m^0(Se_2^{2-}) = 111.64 \pm 1.61$ kJ mol^{-1} and $\Delta_f G_m^0(Se_3^{2-}) = 98.68 \pm 1.02$ kJ mol^{-1} were determined. These values also agree with the existing thermodynamic data and have smaller uncertainty.

The ion interaction coefficients for HSe^- and Se_4^{2-} versus Na^+, $\varepsilon(HSe^-, Na^+) = -0.01 \pm 0.10$ and $\varepsilon(Se_4^{2-}, Na^+) = -0.03 \pm 0.02$, were also determined. These values were within the range of the variations of the existing values for mono- or divalent anions. The solubility of Se in Na-rich saline groundwater can be evaluated by using these obtained ion interaction coefficients.

References

1) A. Olin, B. Nolang, E. G. Osadchii, L.- O. Ohman, E. Rosen, *Chemical thermodynamics of selenium*, Elsevier, Amsterdam (2005).

2) S. Licht, F. Forouzan, "Speciation analysis of aqueous polyselenide solutions," *J. Electrochem. Soc*., **142[5]**, 1546–1551 (1995).

3) L. Lyons, T. Young, "Alkaline selenide, polyselenide electrolytes: concentrations, absorption-spectra and formal potentials," *Aust. J. Chem*., **39[3]**, 511–527, (1986).

4) L. Syper, J. Mlochowski, "The convenient syntheses of organoselenium reagents," *Synthesis*, **5**, 439–442 (1984).

5) W. Stumm, J. J. Morgan, *Aquatic Chemistry, 3rd edition*, John Wiley & Sons, Inc., New York (1996).

6) D. E. Levy, R. Myers, "Spectroscopic determination of the second dissociation constant of hydrogen selenide and the activity coefficients and spectral shifts of its ions," *J. Phys. Chem*., **94**, 7842–7847 (1990).

7) S. Shibutani, H. Yoshikawa, M. Yui, *Solubility measurement of Se in Se-H_2O system under reducing condition*, PNC TN8410 94-204, Power Reactor and Nuclear Fuel Development Corporation (1995). [in Japanese]

8) A. Maes, C. Bruggeman, J. Vancluysen, "Reduction and solubility behaviour of selenium under Boom Clay conditions," *Proc. the Euradwaste-2004 Conference*, Luxembourg, March 29–31, 2004 (2004).

9) A. J. Bard, R. Parsons, J. Jordan, *Standard Potentials in Aqueous Solution*, Marcel Dekker, Inc., New York (1985).

10) I. Harañczyk, B. Szafirska, K. Fitzner, "The influence of the rate of selenium crystallization from aqueous solutions on its morphology," *Journal of Mining and Metallurgy*, B, **38** (1-2), 33–48 (2002).

11) B. Wunderlich, H. C. Shu, "The crystallization and melting of selenium," *J. Crystal Growth*, **48**, 227–239, (1980).

12) Y. Ding, Q. Li, Y. Jia, L. Chen, J. Xing, Y. Qian, "Growth of single crystal selenium with different morphologies via a solvothermal method," *J. Crystal Growth*, **241** [4], 489–497 (2002).

13) U. Köster, "Crystallization and decomposition of amorphous semiconductors," *Adv. Colloid Interface Sci.*, **10**, 129–172 (1979).

14) M. Kawarada, Y. Nishina, *Far-infrared investigation on structure of amorphous selenium,* Science reports of the Research Institutes, Tohoku University. Ser. A, Phys. Chem. Metal., **26**,

101–106 (1976)

15) A. Goldbach, J. Johnson, D. Meisel, L. A. Curtiss, M. L. Saboungi, "On the constituents of aqueous polyselenide electrolyte : a combined theoretical and Raman spectroscopic study," *J. Am. Chem. Soc.*, **121**[18], 4461–4467 (1999).

16) A.Goldbach, J. Johnson, M. L. Saboungi, J. A. Johnson, A. R. Cook, D. Meisel, "Oxidation of aqueous polyselenide solutions. a mechanistic pulse radiolysis study," *J. Phys. Chem. A*, **104**[17], 4011–4016 (2000)

17) I. Sunagawa, *Kessho* (Crystal), Kyoritsu Shuppan Co., Tokyo (2003) [in Japanese].

Table 3-1 Measured selenium solubilities from under- and oversaturation directions after 40-day equilibration in sample solutions adjusted to different pH values and ionic strength (1/3)

Ionic strength (mol dm^{-3})	Undersaturation			Oversaturation		
	pH	pe	Concentration of Se (mol dm^{-3})	pH	pe	Concentration of Se (mol dm^{-3})
0.1	5.11	–3.1	3.26×10^{-6}	6.16	–5.5	9.04×10^{-3}
	5.31	–3.1	1.08×10^{-6}	6.38	–5.6	8.68×10^{-3}
	5.73	–3.5	5.73×10^{-6}	6.43	–5.7	9.32×10^{-3}
	5.84	–3.5	4.21×10^{-6}	6.66	–5.8	1.17×10^{-2}
	6.75	–3.6	2.81×10^{-6}	6.75	–5.8	1.36×10^{-2}
	7.18	–4.1	6.98×10^{-6}	7.53	–6.2	1.67×10^{-2}
	7.87	–4.4	1.03×10^{-5}	7.60	–6.2	1.93×10^{-2}
	8.27	–4.4	1.63×10^{-6}	8.18	–6.5	2.55×10^{-2}
	8.96	–5.2	4.63×10^{-5}	8.31	–6.5	2.37×10^{-2}
	9.05	–5.1	3.39×10^{-5}	8.53	–6.6	1.53×10^{-2}
	9.79	–6.1	2.73×10^{-4}	9.11	–6.0	2.53×10^{-4}
	10.40	–6.4	1.02×10^{-3}	9.16	–6.3	8.02×10^{-4}
	11.46	–6.5	2.72×10^{-3}	9.19	–6.9	4.13×10^{-2}
	12.68	–6.7	9.83×10^{-3}	9.29	–6.9	4.36×10^{-2}
				9.32	–6.1	3.80×10^{-4}
				9.77	–6.9	2.10×10^{-2}
				10.26	–7.0	2.78×10^{-2}
				10.30	–6.3	9.36×10^{-4}
				10.48	–6.9	1.45×10^{-2}
				11.16	–6.1	4.90×10^{-4}
				11.36	–6.4	8.41×10^{-4}
				11.43	–6.9	1.44×10^{-2}
				12.30	–6.5	6.28×10^{-4}
				12.37	–6.5	8.16×10^{-4}
				12.45	–6.9	1.53×10^{-2}
				13.03	–7.1	5.00×10^{-2}

Table 3-1 continued (2/3)

Ionic strength (mol dm^{-3})	Undersaturation			Oversaturation		
	pH	pe	Concentration of Se (mol dm^{-3})	pH	pe	Concentration of Se (mol dm^{-3})
1.0	4.94	–2.8	8.42×10^{-6}	6.48	–5.7	2.79×10^{-2}
	5.55	–3.2	1.11×10^{-5}	6.52	–5.8	2.65×10^{-2}
	6.06	–3.4	2.81×10^{-6}	6.80	–6.0	3.07×10^{-2}
	6.19	–3.5	1.17×10^{-5}	6.93	–6.2	3.04×10^{-2}
	6.65	–3.8	3.40×10^{-6}	7.36	–6.2	3.53×10^{-2}
	7.61	–4.3	9.62×10^{-6}	7.43	–6.3	3.50×10^{-2}
	7.89	–4.4	8.67×10^{-5}	7.49	–5.9	2.15×10^{-2}
	8.81	–4.9	3.43×10^{-6}	7.76	–6.0	2.70×10^{-2}
	9.88	–5.9	2.69×10^{-4}	7.88	–6.5	2.94×10^{-2}
	10.66	–5.9	1.87×10^{-3}	7.92	–6.2	3.51×10^{-2}
	10.71	–6.4	2.98×10^{-3}	8.31	–6.6	4.94×10^{-2}
	11.04	–6.7	1.72×10^{-2}	8.56	–6.5	4.77×10^{-2}
	11.89	–6.5	1.02×10^{-2}	8.69	–6.8	5.38×10^{-2}
	12.74	–7.0	2.90×10^{-2}	9.68	–7.1	8.68×10^{-2}
				9.98	–6.8	5.75×10^{-2}
				10.27	–7.0	1.20×10^{-1}
				10.52	–6.8	1.74×10^{-2}
				10.52	–7.1	4.95×10^{-2}
				11.20	–7.2	1.23×10^{-1}
				11.39	–6.7	2.93×10^{-2}
				11.73	–7.3	1.26×10^{-1}
				11.87	–6.7	1.96×10^{-2}
				12.14	–7.1	1.48×10^{-1}
				12.15	–7.1	1.43×10^{-1}
				12.27	–7.3	1.27×10^{-1}
				12.92	–7.0	5.31×10^{-2}

Table 3-1 continued (3/3)

Ionic strength (mol dm^{-3})	Undersaturation			Oversaturation		
	pH	pe	Concentration of Se (mol dm^{-3})	pH	pe	Concentration of Se (mol dm^{-3})
2.0	4.44	–2.7	5.39×10^{-6}	6.64	–5.9	2.60×10^{-2}
	4.61	–2.9	6.10×10^{-6}	6.67	–5.9	2.56×10^{-2}
	4.96	–2.6	2.52×10^{-6}	7.18	–6.1	3.01×10^{-2}
	6.20	–3.5	5.93×10^{-6}	7.27	–6.1	3.16×10^{-2}
	6.25	–3.5	6.03×10^{-6}	7.49	–6.4	3.29×10^{-2}
	7.03	–3.9	4.02×10^{-6}	7.56	–6.3	3.54×10^{-2}
	8.31	–4.6	1.54×10^{-5}	7.57	–6.3	3.41×10^{-2}
	9.32	–5.2	1.09×10^{-4}	7.59	–6.5	3.67×10^{-2}
	10.32	–6.3	9.69×10^{-4}	7.75	–6.5	3.41×10^{-2}
	10.63	–6.1	2.69×10^{-3}	7.78	–6.5	3.83×10^{-2}
	10.91	–6.5	3.71×10^{-3}	8.29	–6.5	4.55×10^{-2}
	11.30	–6.7	1.84×10^{-2}	8.43	–6.5	4.75×10^{-2}
	11.81	–6.7	1.22×10^{-2}	8.61	–6.5	5.50×10^{-2}
	12.08	–7.4	1.20×10^{-1}	9.40	–6.7	1.75×10^{-2}
				9.61	–6.9	1.08×10^{-1}
				9.87	–6.5	1.65×10^{-2}
				9.92	–7.0	1.19×10^{-1}
				10.02	–6.6	1.87×10^{-2}
				10.13	–6.9	3.04×10^{-2}
				10.32	–7.1	1.25×10^{-1}
				11.32	–7.1	1.40×10^{-1}
				11.38	–6.9	2.53×10^{-2}
				12.17	–7.0	1.39×10^{-1}
				12.26	–7.1	1.48×10^{-1}
				12.50	–7.1	1.55×10^{-1}
				13.03	–6.9	6.93×10^{-2}

Table 3-2 Conditional equilibrium constants, log K_1 and log K_2, of reactions (3-10) and (3-11)

Ionic strength (mol dm^{-3})	Equilibrium constant	
	$\log K_1$	$\log K_2$
0.1	−6.53±0.09	−16.24±0.09
1.0	−6.23±0.12	−15.79±0.12
2.0	−6.38±0.10	−15.68±0.10

Table 3-3 Equilibrium constants and standard molar free energies of formation of amorphous selenium, hydrogen selenide and polyselenide species

Species	Reaction	$\log K^0$	Reference	$\Delta_f G_m^0$ (kJ mol^{-1})	Previously reported [1)]
Se(am)	$Se(am) + H^+ + 2e^- = HSe^-$	−6.57±0.15	This work	6.0±2.2	—
$H_2Se(aq)$	$H_2Se(g) = H_2Se(aq)$	−1.10±0.01	[3]	same as on the right	21.495±2.003
HSe^-	$H_2Se(aq) = HSe^- + H^+$	−3.85±0.05	[3]	same as on the right	43.471±2.024
Se^{2-}	$HSe^- = Se^{2-} + H^+$	−14.91±0.20	[3]	same as on the right	128.600±3.000
Se_2^{2-}	$Se_3^{2-} + Se^{2-} = 2Se_2^{2-}$	0.7±0.1	[4]	111.64±1.61	112.670±6.294
Se_3^{2-}	$2Se_4^{2-} + Se^{2-} = 3Se_3^{2-}$	4.0±0.1	[4]	98.68±1.02	100.590±9.198
Se_4^{2-}	$4Se(cr) + 2e^- = Se_4^{2-}$	−16.67±0.03	This work	95.14±0.17	97.580±12.149

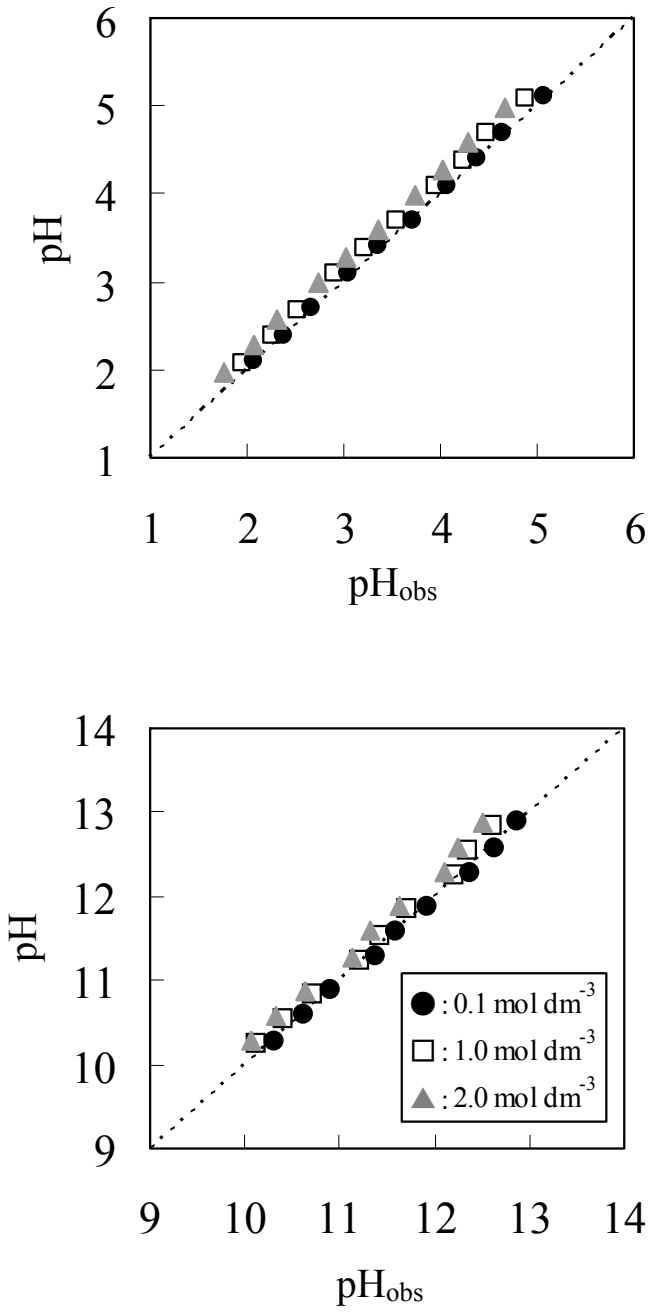

Fig. 3-1 Plot of pH (= −log a_{H+}) versus observed pH (pH_{obs}) obtained by measuring NaCl/HCl and NaCl/NaOH solutions of known H^+ and OH^- concentration

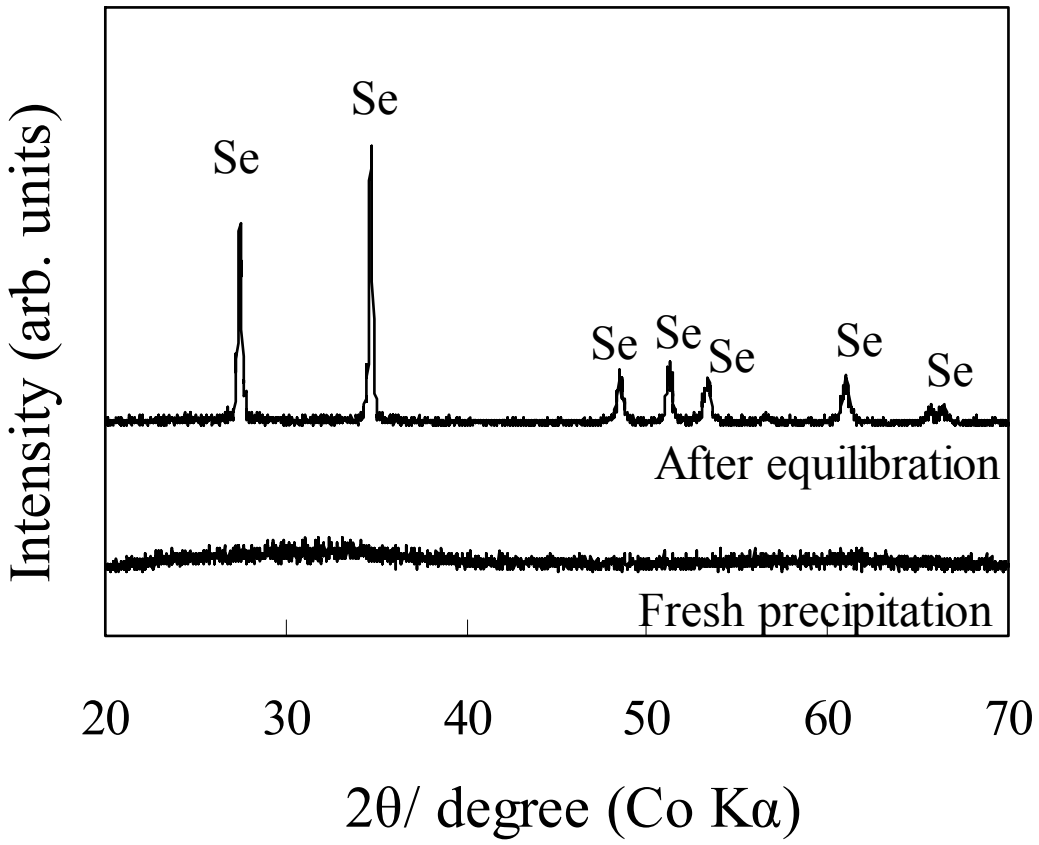

Fig. 3-2 XRD pattern of the fresh precipitation from aqueous solutions (lower) and the solid obtained after equilibration (upper) in the oversaturation experiment. The broad pattern (lower) indicates amorphous phase. Only solid elemental selenium (trigonal) was identified after equilibration, and the same patterns were observed in undersaturation experiments for the solid phase before and after equilibration.

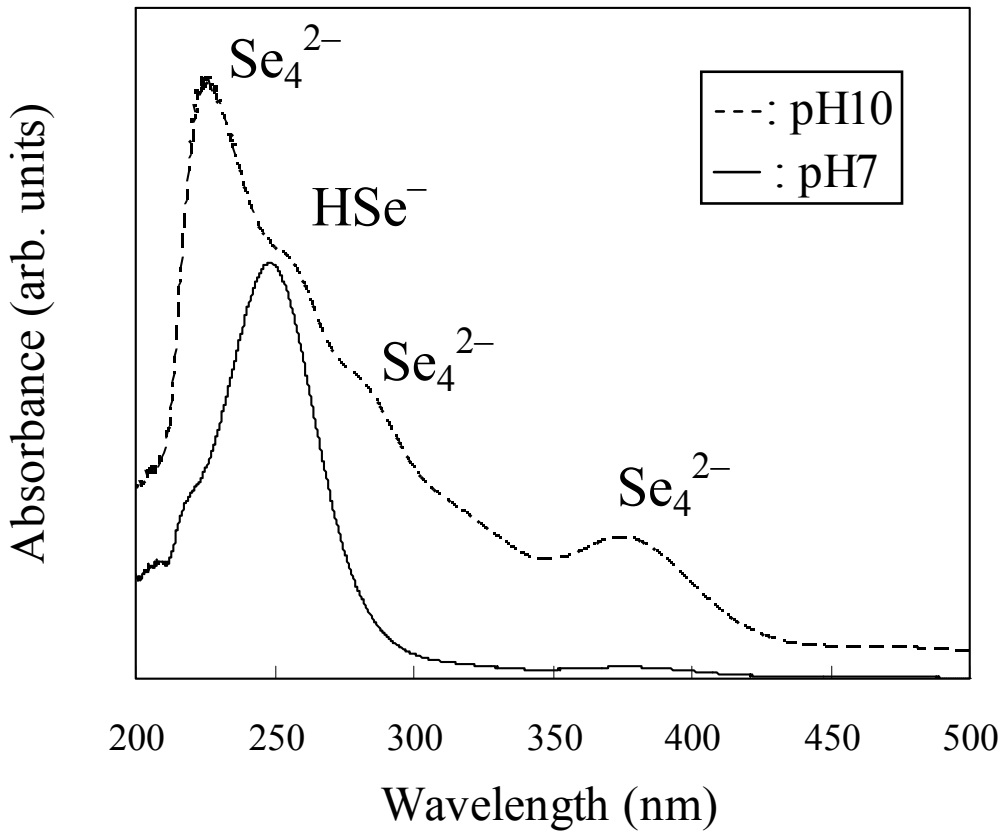

Fig. 3-3 UV-Vis spectra of the sample solutions. The absorption band at 245 nm was assigned to HSe^- anion, and the absorption bands at 220, 282, and 377 nm were assigned to Se_4^{2-} anion.

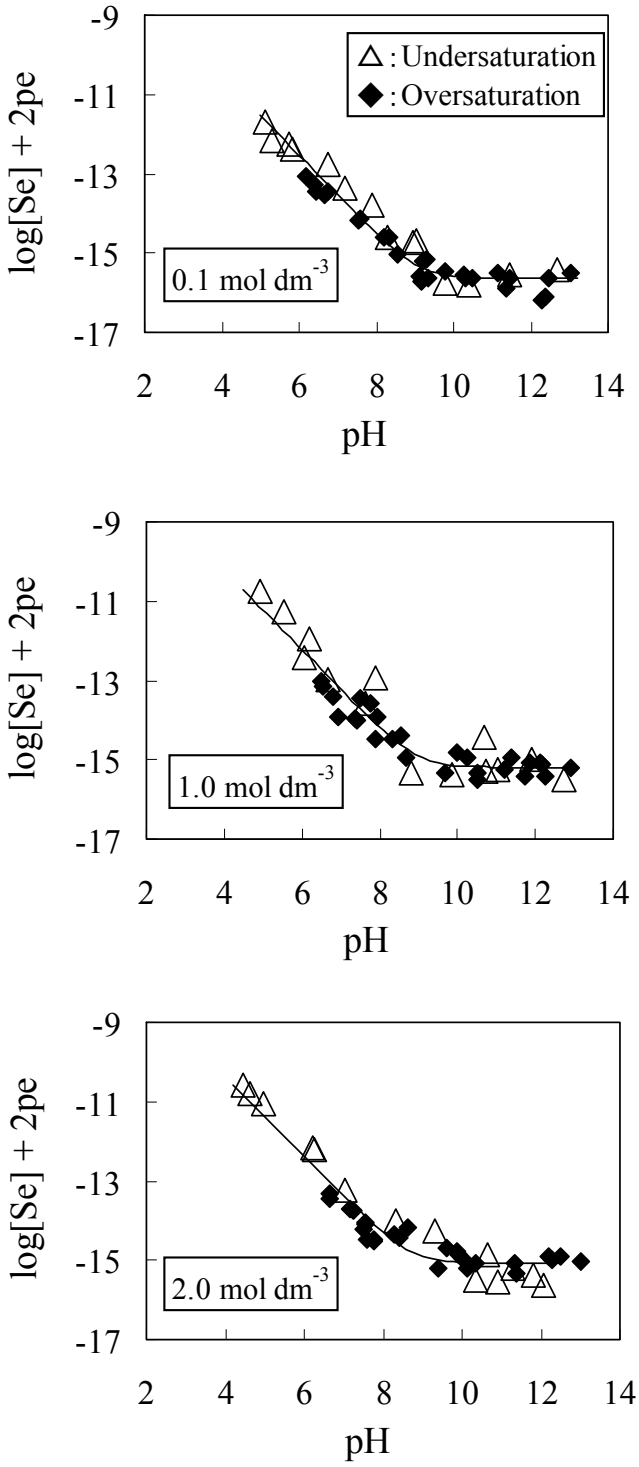

Fig. 3-4 Plot of (log [total selenium concentration] + 2pe) *vs*. pH. The open triangles represent the data obtained from the undersaturation experiments; the closed diamonds represent the data obtained from the oversaturation experiments. The curve represents the least-squares fit of the data to Eq. (3-14).

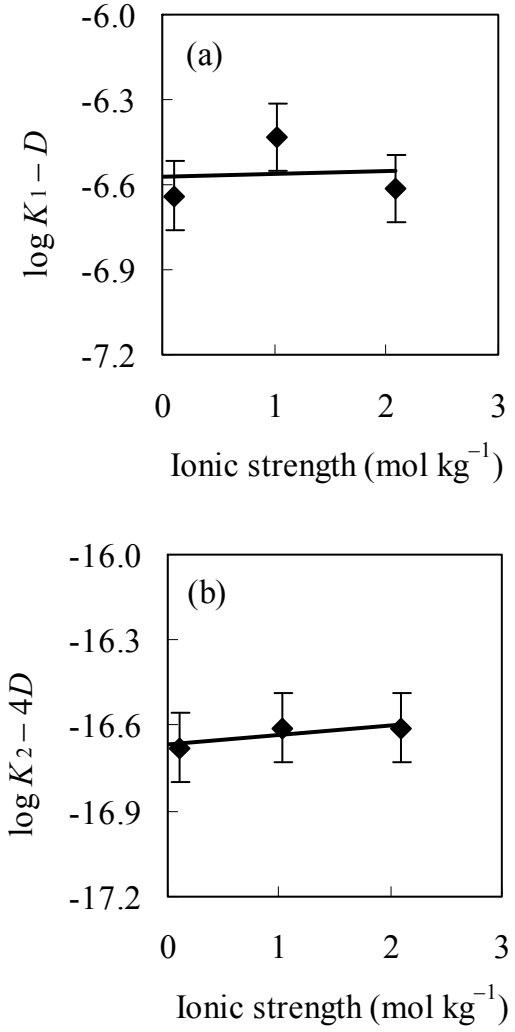

Fig. 3-5 Extrapolation of the equilibrium constant of the dissolution reaction of $Se(s) + H^+ + 2e^- = HSe^-$ (a) and $4Se(s) + 2e^- = Se_4^{2-}$ (b) to infinite dilution using SIT

4. Diffusion of Selenium in the Bentonite Buffer Material

4.1. Introduction

The bentonite buffer material is designed to consist of 70 wt% bentonite and 30 wt% sand, and its dry density is 1600 kg m^{-3}.[1)] Compacted bentonite/sand mixture shows low hydraulic conductivity because of swelling of montmorillonite which is the main component of bentonite.[1,2)] Migration of radionuclides in the buffer material can be assessed with effective diffusion coefficients (D_e) and distribution coefficients (K_d) when advection is negligible.[1,2)] In the long term, the diffusion behavior of radionuclides would change because the swelling characteristic of bentonite is likely to be deteriorated by contact with saline groundwater or alteration of montmorillonite by alkaline groundwater originating from cementitious materials.[2)] For a long-term safety assessment of geological disposal of HLW, it is necessary to evaluate the variation in diffusion coefficient of radionuclides under geological disposal conditions and understand the diffusion behavior based on diffusion mechanisms.

In this chapter, systematic D_e data of Se(−II) species through compacted bentonite/sand mixture were obtained under reducing conditions by the through-diffusion method. Effective diffusion coefficients of Se(IV) species were also obtained under anaerobic conditions for the comparison. Experiments were carried out under variable bentonite content and porewater salinity. Diffusion behaviors of anionic Se species were modeled based on the electric double layer theory and the pore diffusion model to quantitatively explain the variations in diffusivity of Se species.

4.2. Experimental

4.2.1. Selenium Stock Solutions

Selenium(−II) stock solution was prepared in a controlled atmosphere glove box under Ar by the following procedure. An appropriate amount of powdered Se was washed by soaking in a 0.01 mol dm^{-3} NaOH solution for 7 days in a polypropylene test tube to remove soluble impurities. About 0.1 g of washed powdered Se was dissolved in a 0.5 cm^3 volume of 98% $N_2H_4 \cdot H_2O$ solution to be diluted with 100 cm^3 volume of 0.1 mol dm^{-3} NaOH solution.[3)] The concentration of Se was approximately 0.01 mol dm^{-3}. The solution was stored for 3 days to reduce the Se and filtered through 10,000 NMWL ultrafilter to remove precipitated Se.

Selenium(IV) stock solution was prepared by dissolving 0.87 g of sodium selenite (Na_2SeO_3, Wako Pure Chemical Ind. Ltd.) in 100 cm^3 of 0.01 mol dm^{-3} NaOH solution under Ar. The concentration of Se was 0.05 mol dm^{-3}.

4.2.2. Through-Diffusion Experiments

Through-diffusion experiments were carried out under variable bentonite content and porewater salinity. Experimental conditions are summarized in **Table 4-1**. The employed bentonite material was Kunigel V1 (Kunimine Industries Co. Ltd.), which contained 46 - 49 wt% Na-montmorillonite.[4] Mixtures of Kunigel V1 and silica sand were compacted to an acrylic diffusion column of 20 mm diameter and 10 mm thickness. The dry density of the mixture specimen was 1600 kg m^{-3}. Sodium chloride solutions with three types of salinities, 0.05, 0.1, and 0.5 mol dm^{-3}, were employed, simulating brackish groundwater and sea water. The pH of the solution was adjusted to around 12 by adding 1 mol dm^{-3} NaOH solution, simulating alkaline groundwater originating from cementitious materials.[2] Kubo *et al*. reported that montmorillonite was scarcely altered at pH 11.5 and 50°C for 360 days.[5] In addition, the amount of montmorillonite in compacted bentonite/sand mixtures did not decrease in a few months at pH 13 and 130°C in a previous study;[6] bentonite is not likely to be altered at pH 12 and room temperature during the experimental period.

Acrylic diffusion cells[7] were used in this study. Each side of the bentonite/sand mixture was covered with sintered stainless steel filters with a porosity of 40% and 1 mm thickness, to avoid expansion of the bentonite into the reservoirs. The assembled diffusion cell was soaked in the NaCl/NaOH mixed solution of the same composition as used in the subsequent diffusion experiment under vacuum to evacuate all air from the pores in the specimens.

Through-diffusion experiments for Se(−II) were performed in the controlled atmosphere glove box under Ar at 25 ± 3°C. The mixture ratio of Kunigel V1 and silica sand was varied as 7:3, 6:4, 5:5, 4:6, 3:7, and 2:8 in dry weight. The reservoirs were filled with 110 cm^3 volume of NaCl/NaOH mixed solutions. The bentonite/sand mixtures were preconditioned prior to diffusion runs to avoid precipitation of Se in the porewater. A 0.5 cm^3 volume of 98% $N_2H_4 \cdot H_2O$ solution was added to one side of the reservoirs; the concentration of $N_2H_4 \cdot H_2O$ was 0.1 mol dm^{-3}. After 3 months, the *E*h of the solution on the other side of the reservoirs was confirmed to be sufficiently low by using a platinum electrode combined with a Ag/AgCl reference electrode after checking its accuracy with saturated quinhydrone solutions.

The blank solution was prepared by adding a 2.5 cm^3 volume of 98 % $N_2H_4 \cdot H_2O$ solution to a 1000 cm^3 volume of the NaCl/NaOH mixed solution, so the concentration of N_2H_4 was 0.05 mol dm^{-3}. The starting solution was prepared by adding a 4 cm^3 volume of the Se(−II) stock solution to a 1000 cm^3 volume of the blank solution. The concentration of Se was 5×10^{-5} mol dm^{-3}. A 1 cm^3 aliquot of the solution was sampled to determine the aqueous Se species by UV-Vis spectrometry. The pH was measured with a combination glass electrode (ROSS 8172BNWP, Thermo Fisher Scientific Inc.) which is suitable for the measurement of

high-ionic-strength samples, calibrated with standard pH buffer solutions of 7.00, 10.01, and 12.46. The *E*h was determined in relation to NHE.

Through-diffusion runs were started by placing the starting solution in the "high-concentration reservoir" and the blank solution in the "low-concentration reservoir". At 3- to 7-day intervals, 0.02 and 0.2 cm^3 aliquots were taken from the high-concentration and the low-concentration reservoirs, respectively, to determine the concentration of Se. The 0.2 cm^3 aliquot removed from the low-concentration reservoir was replaced by an equal volume of the blank solution to maintain the water levels in the two reservoirs. This balancing avoids the occurrence of a pressure difference that leads to advective transport from the high-concentration to the low-concentration reservoir. The concentration of Se in the low-concentration reservoir (c_2) was corrected as[8)]

$$c_{2,n} = c'_{2,n} + \sum_{i=1}^{n-1}\left(\frac{V_i}{V}c'_{2,i}\right) \quad (n = 2, 3, 4\cdots) \tag{4-1}$$

$$c_{2,1} = c'_{2,1} \quad (n = 1),$$

where $c_{2,n}$ is the corrected concentration of Se in the n-th sampling solution (mol dm^{-3}), $c'_{2,n}$ the measured concentration in the n-th sampling solution (mol dm^{-3}), V the volume of the solution in the low-concentration reservoir (110 cm^3), and V_i the volume of i-th sampling solution (0.2 cm^3). The sample solutions were removed from the glove box and oxidized by adding a 0.1 cm^3 volume of 30% hydrogen peroxide (H_2O_2) to prevent the precipitation and volatilization of Se. After diluting the solution with 3% nitric acid, the concentration of Se was determined by ICP-MS. After diffusion experiments, the pH and *E*h of the solutions were measured. The remaining solution was used to determine the aqueous selenium species by UV-Vis spectrometry.

Through-diffusion experiments for Se(IV) were also performed in the controlled atmosphere glove box under Ar at 25 ± 3°C. The mixture ratio of Kunigel V1 and silica sand was varied as 7:3, 5:5, and 2:8 in dry weight. The NaCl/NaOH mixed solutions with the desired concentration were used as blank solutions. The starting solution was prepared by adding a 1 cm^3 volume of the Se(IV) stock solution to a 1000 cm^3 volume of the blank solution, so the concentration of Se(IV) was 5×10^{-5} mol dm^{-3}. Through-diffusion runs for Se(IV) were performed in the same manner as mentioned above.

4.3. Experimental Results

The experimental conditions are plotted on pH-pe diagrams for the system Se-O-H[9] shown in **Fig. 4-1**. Based on the pH and pe conditions, the dominant Se species in the experimental solution was estimated to be HSe^- and SeO_3^{2-} for Se(−II) and Se(IV), respectively.

Figure 4-2 shows the UV-Vis spectra of the Se(−II) starting solution of 0.1 mol dm^{-3} NaCl and the experimental solution in the high-concentration reservoir of 2-9 cells (0.1 mol dm^{-3} NaCl, bentonite/sand = 5/5) after diffusion experiment as representative examples. The UV-Vis spectra show an absorption band at 245 nm, which was assigned to HSe^-,[10,11] and the ones assigned to Se_4^{2-} at 282 and 377 nm.[10,11] The same patterns were observed in samples under other conditions. The concentration of Se, C_{Se}, present as HSe^- in the starting solution was determined to be 1.9×10^{-5} mol dm^{-3} from the absorbance (a = 0.142 at 245 nm), molar extinction coefficient, (ε = 7500 cm^{-1} mol^{-1} dm^3 at 245 nm for HSe^-),[10] and path length, l (1 cm) according to the Beer-Lambert law[11]

$$C_{Se} = \frac{a}{\varepsilon l} \quad , \tag{4-2}$$

and that present as Se_4^{2-} was 2.3×10^{-5} mol dm^{-3} from a (= 0.041 at 377 nm) and ε (= 1804 cm^{-1} mol^{-1} dm^3 at 377 nm for Se_4^{2-}).[10] The total concentration of Se in the starting solution determined by UV-Vis spectrometry (4.2×10^{-5} mol dm^{-3}) roughly agreed with that determined by ICP-MS (4.5×10^{-5} mol dm^{-3}). After diffusion experiments, the concentration of Se present as HSe^- in the high-concentration reservoir of 2-9 cells was determined to be 1.5×10^{-5} mol dm^{-3} from a (= 0.114 at 245 nm), and that present as Se_4^{2-} was 1.8×10^{-5} mol dm^{-3} from a (= 0.032 at 377 nm). The total concentration of Se determined by UV-Vis spectrometry (3.3×10^{-5} mol dm^{-3}) also roughly agreed with that determined by ICP-MS (3.5×10^{-5} mol dm^{-3}). The concentration of HSe^- in the experimental solution was 45% of the total Se concentration through the experimental periods. Peaks assigned to any Se species were not detected in spectra of the sample solutions in the low-concentration reservoir because of the lower Se concentration than the detection limit (1×10^{-5} mol dm^{-3}).

Figures 4-3(a) and **4-3(b)** show the time dependence of the concentrations of Se(-II) in the high-concentration reservoir and in the low-concentration reservoir of 2-9 cells (0.1 mol dm^{-3} NaCl, bentonite/sand = 5/5) as representative examples. The concentration of Se(−II) in the low-concentration reservoir was compensated for the decrease caused by the sampling of the 0.2 cm^3 aliquots for analysis. Changes in the concentration of Se(−II) in both of the reservoirs are

nonlinear for 80 days after the start of the diffusion. A diffusion coefficient of Se(−II) was determined from the linear portion of the curve starting after 80 days. The Fick's 1st law of diffusion was applied to the determination of effective diffusivity,[7] D_e (m^2 s^{-1}), for Se(−II) as

$$J = -D_e \frac{\partial c}{\partial x} \quad , \tag{4-3}$$

where J is the diffusive flux (mol m^{-2} s^{-1}). Diffusive flux at the surface of the bentonite/sand mixture facing the high-concentration reservoir, J_1, and that facing the low-concentration reservoir, J_2, were determined from the rate of change in the concentration of Se in each reservoir as,

$$J_1 = -\frac{V}{S} \cdot \frac{dc_1}{dt} \quad , \quad J_2 = \frac{V}{S} \cdot \frac{dc_2}{dt} \quad , \tag{4-4}$$

where V is the volume of the solution reservoirs (1.1×10^{-4} m^3), S the cross section of the bentonite/sand mixture (3.14×10^{-4} m^2), and c_1 and c_2 the concentrations of diffusing species in the high-concentration reservoir and the low-concentration reservoir (mol m^{-3}), respectively. When J_1 was equal to J_2, diffusive mass transfer through the specimen was in steady state, and D_e was calculated. The linear concentration change of Se(−II) was fitted to a linear regression line to determine value for J_1 and J_2 tabulated in **Table 4-2**. The diffusive fluxes, J_1 and J_2, were identical, which ensured a steady state of the diffusion and allowed the calculation of D_e.

Effective diffusion coefficients of Se(−II) in the bentonite/sand mixtures, D_{eb}, were determined by correcting a loss of concentration gradient in filter by using the following equation[12]

$$D_{eb} = \frac{L_b}{\frac{L}{D_e} - 2\frac{L_f}{D_{ef}}} \quad , \tag{4-5}$$

where L is the total column length including thickness of filters (1.2×10^{-2} m), L_b the column length of the bentonite/sand mixture (1.0×10^{-2} m), L_f the thickness of the filter (1.0×10^{-3} m), and D_{ef} the effective diffusion coefficient in the filter (m^2 s^{-1}). The D_{ef} was determined from the through-diffusion experiments for the filter. **Figure 4-3(c)** shows the time dependence of the concentrations of Se(−II) in the high-concentration reservoirs and low-concentration reservoirs. The concentration changes were independent of the salinity of the experimental solution and were

analyzed by using the exact solution for the decreasing inlet concentration–increasing outlet concentration diffusion equation proposed by Zhang *et al.*[13] The concentration of diffusing species at position x and time t is described as

$$c(x,t) = \frac{c_1(0)}{\delta+\gamma+1} - 2c_1(0)\sum_{m=0}^{\infty} \frac{\exp\left(-\frac{D_{ef}\,\phi_m^2}{\alpha\,L_f^{\,2}}t\right)\left[\delta\cos\left(\phi_m^2\,\frac{L_f-x}{L_f}\right)-\gamma\,\phi_m\sin\left(\phi_m\,\frac{L_f-x}{L_f}\right)\right]}{[\gamma\phi_m^2-\delta(\delta+\gamma+1)]\cos(\phi_m)+(\delta\gamma+\delta+2\gamma)\sin(\phi_m)} \tag{4-6}$$

where $\gamma = V_2 / V_1$, $\delta = (\alpha\, S\, L_f) / V_1$, ϕ_m is the root of the following equation:

$$\tan(\phi_m) = \frac{\delta(\gamma+1)\phi_m}{\gamma\phi_m^2-\delta^2} \quad , \tag{4-7}$$

$c_1(0)$ is the initial concentration of Se in the starting solution in the high-concentration reservoir (mol m^{-3}), and V_1 and V_2 the volumes of the high-concentration reservoir and the low-concentration reservoir (1.1×10^{-4} m^3), respectively. The D_{ef} of Se(−II) was determined to be 1.2×10^{-10} m^2 s^{-1} from Eq. (4-6). The D_{eb} values of Se(−II) were determined to be within a range from 10^{-12} to 10^{-11} (m^2 s^{-1}) using Eq. (4-5) (**Table 4-2**).

Figures 4-4(a) and **4-4(b)** show the time dependence of the concentrations of Se(IV) in the high-concentration reservoir and in the low concentration reservoir of 4-5 cells (0.1 mol dm^{-3} NaCl, bentonite/sand = 5/5) as representative examples. The concentration of Se(IV) in the low-concentration reservoir was compensated for the decrease caused by the sampling of the 0.2 cm^3 aliquots for analysis. Because the Se concentration in the high-concentration reservoir was almost constant through out the experimental period, and the concentration changed linearly with time for the low-concentration reservoir in the period of 0-84th day; the D_e for Se(IV) was determined using following equation,[12,14]

$$\frac{Q(t)}{S\,L\,c_1(0)} = \frac{D_e}{L^2}t - \frac{\alpha}{6} - \frac{2\alpha}{\pi^2}\times\sum_{n=1}^{\infty}\left[\frac{(-1)^n}{n^2}\exp\left(-\frac{D_e\,n^2\,\pi^2\,t}{L^2\,\alpha}\right)\right], \tag{4-8}$$

Initial condition: $c(t, x) = 0$, $t = 0$, $0 < x < L$,

Boundary conditon: $c(t, 0) = c_1$, $t > 0$, $x = 0$,

$c(t, L) = 0$, $t > 0$, $x = L$,

where $Q(t)$ (= $c'_2(t) \times V$) is the total amount of the tracer permeated through bentonite (mol), S the surface of the column (3.14×10^{-4} m^2), t the time (s), x the distance from the interface between the high-concentration reservoir and the filter (m), and α the rock capacity factor (= $\phi + \rho_{mix} K_d$), ϕ the porosity, ρ_{mix} the dry density of the bentonite/sand mixture (kg m^{-3}), and K_d the distribution coefficient (m^3 kg^{-1}). After a long time when the mass transfer through the bentonite/sand mixture is in the steady state, Eq. (4-8) is simplified to

$$\frac{c'_2(t)V}{S L c_1(0)} = \frac{D_e}{L^2} t - \frac{\alpha}{6} \quad , \tag{4-9}$$

D_e and α can be obtained from $c'_2(t)/c_1(0)$ in the steady state phase of the diffusion by a linear regression analysis of the data. Effective diffusion coefficients of Se(IV) in the bentonite/sand mixtures, D_{eb}, were determined by correcting a loss of concentration gradient in the filter by using Eq. (4-5). **Figure 4-4(c)** shows the time dependence of the concentrations of Se(IV) in the high-concentration reservoirs and in the low-concentration reservoirs from the through-diffusion experiments for the filter. The concentration changes were independent of the salinity of the experimental solution. The D_{ef} of Se(IV) was determined to be 1.3×10^{-10} m^2 s^{-1} from Eq. (4-6). The D_{eb} values of Se(IV) were determined to be within a rage from 10^{-12} to 10^{-11} (m^2 s^{-1}) using Eq. (4-5) (**Table 4-2**).

The D_{eb} values of Se(−II) are plotted versus bentonite content in **Fig. 4-5(a)** with previously reported ones of monovalent anionic species, [15,16] Cl^- (Diffusion coefficient in free water: D_v = 2.032×10^{-9} m^2 s^{-1} [17]) and I^- ($D_v = 2.045 \times 10^{-9}$ m^2 s^{-1} [17]). **Figure 4-5(b)** shows the D_{eb} values of Se(IV) compared with the previously reported ones of SeO_3^{2-} [18] and divalent oxyanionic species, CO_3^{2-} [15,16] ($D_v = 9.23 \times 10^{-10}$ m^2 s^{-1} [17]). The D_{eb} values of Se(−II) are about a half-order of magnitude lower than the previously reported ones of Cl^- and I^-, and those of Se(IV) are in the same range as the previously reported ones of SeO_3^{2-} and CO_3^{2-}.

The D_{eb} values of Se(−II) and Se(IV) decreased with increasing bentonite content and with decreasing salinity. Similar tendencies have been reported for anionic species in bentonite by many researchers and considered to be due to anion exclusion.[19,20] The anion exclusion is primarily due to the difference in the concentration of ions between in external bulk solutions and in porewater of bentonite.[21] To quantitatively explain the diffusion behavior of anionic Se species, the concentration and diffusivity of Se in the bentonite porewater were modeled based on the electric double layer theory[22-24] and the pore diffusion model.[25,26]

4.4. Modeling

The schematic drawing of the conceptual diffusion model is depicted in **Fig. 4-6** and all the parameters required for this model are listed in **Table 4-3**. In this model, it is assumed that

- bentonite/sand mixture is homogeneous and the pores are saturated with water;
- pores in bentonite/sand mixtures consist of two types of space; one is the space between mineral particles (macro pore) and the other is the space between montmorillonite layers (interlayer pore);
- pores are treated as equidistant parallel sheets;
- the diffusion and distribution of ions are affected by the negative surface charge of montmorillonite;
- an ion is treated as a point charge;
- the basal surface of montmorillonite forms an electric double layer[27] and the surface potential was approximated using ζ potential[21,23]
- tracer anionic species diffuse through only the macro pore, because the interlayer pore is very narrow; thus, the double layers in the interlayers overlap and the electric potential in the truncated layer becomes large leading to a complete exclusion of anions from the interlayer;[28,29]
- the number of layers in montmorillonite stacks changes depending on the bentonite content and porewater salinity.[29]

The diffusive flux of anionic species, J (mol m^{-2} s^{-1}), was expressed using the effective diffusion coefficient, D_{mp} (m^2 s^{-1}), and concentration gradient in macro pore as

$$J = -D_e \frac{\Delta C_b}{\Delta x} = -D_{mp} \frac{\Delta C_{mp}}{\Delta x} \tag{4-10}$$

where C_b is the concentration of diffusing species in external bulk solution (mol m^{-3}), C_{mp} the concentration of diffusing species in macro pore (mol m^{-3}), and x the position parallel to montmorillonite layers (m).

4.4.1. Concentration of Diffusing Species in the Macro pore

The C_{mp} can be estimated by considering the ion distribution as[23]

$$C_{mp} = \frac{1}{d_{mp}} \int_0^{d_{mp}} C(X) dX \quad , \tag{4-11}$$

where d_{mp} is the macro pore width (m), and $C(X)$ the concentration of diffusing species at position X normal to montmorillonite layers (mol m^{-3}). According to the Boltzmann distribution, the ion distribution in the diffuse layer is written as[30)]

$$C(X) = C_b \exp\left(-\frac{Z_d\, e\psi_{(X)}}{k\,T} \right) \quad , \tag{4-12}$$

where Z_d is valence of diffusing species, e is elementary electric charge (1.602×10^{-19} C), $\psi_{(X)}$ is electric potential (V), k is Boltzmann constant (1.381×10^{-23} J K^{-1}), and T is temperature (K). The electric potential distribution in the diffuse layer is given by the Poisson-Boltzmann equation: [30)]

$$\frac{\partial^2\psi_{(X)}}{\partial X^2} = -\frac{4\pi}{\varepsilon}\sum_i Zi\; e\; n_{bi} \exp\left(-\frac{Zi\; e\; \psi_{(X)}}{kT} \right) \quad , \tag{4-13}$$

where ε is the permittivity (6.954×10^{-10} F m^{-1} for water), Zi the valence of electrolyte ion i (-), and n_{bi} the concentration of electrolyte ion i in the external bulk solution (m^{-3}). An analytical function of the $\psi_{(X)}$ derived by considering the overlap of electric potential distributions from pair of planes[21)] was used for an electrolyte of z^+–z^-. The surface potential, ψ_0, was determined from ζ potential measurement. Shibutani *et al.*[31)] reported that the ζ potential of montmorillonite was independent of pH but dependent on salinity. The values under 0.01 mol dm^{-3} NaCl conditions were similar to those under 0.1 mol dm^{-3} NaCl conditions, but obviously higher than those under 0.5 mol dm^{-3} NaCl conditions. The ψ_0 was assumed to be −56.5 mV for 0.05 and 0.1 mol dm^{-3} NaCl, and −30mV for 0.5 mol dm^{-3} NaCl.[23,31)]

4.4.2. Diffusivity in the Macro pore

The D_{mp} was estimated based on the pore diffusion model[25,26)] considering the viscosity of the porewater influenced by the surface negative charge of montmorillonite[23)]

$$D_{mp} = G_{mp}\frac{\eta_0}{\eta_{mp}}\phi_{mp}\,D_v \tag{4-14}$$

where G_{mp} is the geometry factor of the macro pore, η_0 the viscosity of free water (1.00×10^{-3} Pa s), η_{mp} the viscosity of porewater in the macro pore (Pa s), ϕ_{mp} the porosity of the macro pore, and

D_v the diffusion coefficient of diffusing species in free water ($m^2\ s^{-1}$). The term of $G_{mp}\frac{\eta_0}{\eta_{mp}}$ was approximated using the values in the whole pore,[32-34] $G_p\frac{\eta_0}{\eta_p}$, determined from diffusion data of HTO, $D_{e(HTO)}$, which did not interact with the surface of montmorillonite (**Fig. 4-7**).

$$G_{mp}\frac{\eta_0}{\eta_{mp}} \approx G_p\frac{\eta_0}{\eta_p} = \frac{D_{e(HTO)}}{D_{v(HTO)}\,\phi_{tot}} \quad , \tag{4-15}$$

where $D_{v(HTO)}$ is diffusivity of HTO in free water ($2.275\times10^{-9}\ m^2\ s^{-1}$),[35] and ϕ_{tot} the total porosity of bentonite/sand mixture (0.4). Applying the least-square fitting on the D_e data of HTO obtained under the various bentonite (Kunigel V1) contents at 1600 kg m^{-3} by Kato *et al.*[36] yields the term of $G_{mp}\frac{\eta_0}{\eta_{mp}}$ as a function of bentonite content in the bentonite/sand mixture, R_b (%),

$$G_{mp}\frac{\eta_0}{\eta_{mp}} = 0.7379R_b{}^{-0.3792}. \tag{4-16}$$

The porosity of the macro pore, ϕ_{mp}, can be obtained for the product of half of the surface-to-volume ratio (m^{-1}) and d_{mp} (m) as

$$\phi_{mp} = \frac{S_{mp}\,C_{mont}\,\rho_{mix}}{2}d_{mp} \quad , \tag{4-17}$$

where S_{mp} is the external surface area of montmorillonite stacks per unit weight ($m^2\ kg^{-1}$; those of accessory minerals are negligible), C_{mont} the montmorillonite content in the bentonite/sand mixture (-), and ρ_{mix} the dry density of the bentonite/sand mixture (1600 kg m^{-3}).

The d_{mp} was estimated from the cubic law of hydraulic conductivity.[7] The cubic law is based on the theory of hydrodynamics for the laminar flow between flat plates and usually used to estimate the fracture permeability.[37] Water flow between fine particles like clay is generally laminar,[37,38] the cubic law was applied to the estimation of the d_{mp} in this model. The hydraulic conductivity, K ($m\ s^{-1}$), can be described as[7]

$$K = \frac{\rho_f\,g\,\phi\,b^2}{18\eta} \quad , \tag{4-18}$$

where ρ_f is the density of fluid (kg m^{-3}), g the gravitational acceleration (9.806 m s^{-2}), ϕ the porosity, b the aperture of the parallel planar space (m), and η the viscosity of fluid (Pa s). The interlayer pores are somewhat permeable but their contribution to the overall hydraulic conductivity is probably negligible;[29] the hydraulic conductivity thorough the bentonite/sand mixture is dominated by the permeability of macro pore. Then, Eq. (4-18) can be written considering the geometry factor[39] and viscosity in the macro pore in

$$K = \frac{\rho_f \, g \, \phi_{mp} \, d_{mp}^{\,2}}{18 \eta_0} G_{mp} \frac{\eta_0}{\eta_{mp}} \quad , \tag{4-19}$$

Hydraulic conductivities for bentonite/sand mixtures have been formulated as a function of effective bentonite dry density, ρ_e (kg m^{-3}), from the previously measured values in Ref. 2). The equation for fresh water is

$$K = \exp\left(-26.535 + 2.5197 \times 10^{-3} \cdot \rho_e - 2.7755 \times 10^{-3} \cdot \rho_e^{\,2}\right) \tag{4-20}$$

and that for seawater,

$$K = \exp\left(-25.64 + 8.29 \times 10^{-3} \cdot \rho_e - 5.689 \times 10^{-3} \cdot \rho_e^{\,2}\right). \tag{4-21}$$

The ρ_e is defined as[2]

$$\rho_e = \frac{\rho_{mix}\left(100 - R_s\right)}{\left(100 - \dfrac{\rho_{mix} \, R_s}{\rho_s}\right)} , \tag{4-22}$$

where R_s is the sand content (%) and ρ_s the grain density of sand (2640 kg m^{-3}).[2] The K values for 0.05 and 0.1 mol dm^{-3} NaCl solutions were estimated from Eq. (4-20), and that for the 0.5 mol dm^{-3} NaCl solution was from Eq. (4-21).

The ϕ_{mp} can be calculated from the difference between total porosity, ϕ_{tot}, and interlayer porosity, ϕ_{ll}. The ϕ_{tot} is calculated using the ratio of ρ_{mix} (1600 kg m^{-3}) to the grain density of bentonite/sand mixture, ρ_g, (2680 kg m^{-3}),[2]

$$\phi_{mp} = \phi_{tot} - \phi_{il} = 1 - \frac{\rho_{mix}}{\rho_g} - \phi_{il} . \quad (4\text{-}23)$$

The ϕ_{il} is equal to the product of half of surface-to-volume ratio (m^{-1}) and d_{il} (m) as

$$\phi_{il} = \frac{S_{il}\, C_{mont}\, \rho_{mix}}{2} d_{il} \quad , \quad (4\text{-}24)$$

where d_{il} is the interlayer pore width (0.9 nm for 0.05 and 0.1 mol dm^{-3} NaCl, and 0.6 nm for 0.5 mol dm^{-3} NaCl)[32] and S_{il} ($m^2\ kg^{-1}$) the specific surface area of the interlayer of montmorillonite stacks per unit weight. The S_{il} is calculated from the total specific surface area of montmorillonite, S_{tot} ($8\times10^5\ m^2\ kg^{-1}$) [21,24,40]

$$S_{il} = S_{tot} - S_{mp}. \quad (4\text{-}25)$$

The d_{mp}, S_{mp}, ϕ_{mp} and ϕ_{il} were calculated by solving Eqs. (4-17) and (4-19) - (4-25) iteratively. The averaged number of layers in montmorillonite stacks, N_l , was calculated as

$$N_l = \frac{S_{tot}}{S_{mp}} . \quad (4\text{-}26)$$

4.4.3. Diffusion Model

The ion concentration in the macro porewater is proportional to that in the bulk solution (see Eqs. (4-11) and (4-12)), the ratio of the concentration difference in the macro porewater to that in external bulk water can be expressed as

$$\frac{\Delta C_{mp}}{\Delta C_b} = \frac{C_{mp}}{C_b} . \quad (4\text{-}27)$$

The D_e can be described by substituting Eqs. (4-11), (4-14), and (4-27) into Eq. (4-10) as

$$D_e = G_{mp} \frac{\eta_0}{\eta_{mp}} \phi_{mp} D_v \frac{1}{C_b\ d_{mp}} \int_0^{d_{mp}} C(X) dX \quad , \quad (4\text{-}28)$$

4.5. Model Calculation

The results of model calculations for HSe^-, Se_4^{2-}, and SeO_3^{2-} are partly summarized in **Table 4-4**. The D_v values of HSe^- (1.87×10^{-9} m^2 s^{-1}) and SeO_3^{2-} (8.87×10^{-10} m^2 s^{-1}) were calculated from the Nernst-Einstein equation[17)]

$$D_v = \frac{\lambda R T}{z^2 F^2} \quad , \tag{4-29}$$

where λ is the ionic infinite dilution molar conductivity (70.4 cm^2 Ω^{-1} mol^{-1} for HSe^- and 133.4 cm^2 Ω^{-1} mol^{-1} for SeO_3^{2-}),[17)] R the gas constant (8.3145 J K^{-1} mol^{-1}), T the temperature (298.15 K), z the electric charge, and F the Faraday constant (96485 C mol^{-1}). Since D_v data for Se_4^{2-} was not available, it was estimated to be 1.8×10^{-10} m^2 s^{-1} by chemical analogy to polysulfide.[17)]

The numbers of layers in montmorillonite stacks, N_l, were calculated to be 2 to 4 under 0.05 and 0.1 mol dm^{-3} NaCl condition, and 9 to 21 under 0.5 mol dm^{-3} NaCl conditions. Tessier *et al.*[41)] investigated the effects of salt concentration on the swelling properties of Na-smectite by transmission electron microscopy observations, and reported that Na-smectite was formed by the stacking of a few layers under 10^{-3} mol dm^{-3} NaCl condition and 20 or more layers under 1 mol dm^{-3} NaCl condition. Pusch and Karnland[29)] estimated the numbers of layers in stacks in MX-80 bentonite (dry density: 900 to 1790 kg m^{-3}) to be 3 in distilled water, 7 in 2 % NaCl solution (0.3 mol dm^{-3}) and 10 in 10% NaCl solution (1.7 mol dm^{-3}) based on microscopy observations[42)]. The N_l values calculated by using this model are consistent with these literature values.

The calculated porosities, ϕ_{mp} and ϕ_{ll}, show that the macro pore is dominant in the total pore in bentonite/sand mixtures, supporting Eq. (4-15). The ϕ_{mp} and D_{mp} values increase with decreasing bentonite content, and the values under 0.05 mol dm^{-3} NaCl conditions are similar to those under 0.5 mol dm^{-3} NaCl conditions, suggesting the independence of salinity. The d_{mp} values increase with decreasing bentonite content and with increasing salinity. The narrower d_{mp} produces a larger anion exclusion effect. The C_{mp}/C_b values of Se species also increase with decreasing bentonite content and with increasing salinity, reflecting the anion exclusion. The differences in C_{mp}/C_b values between HSe^- and Se_4^{2-}/SeO_3^{2-} show that the anion exclusion effect appears more remarkable for divalent Se_4^{2-}/SeO_3^{2-} than for monovalent HSe^-. The high C_{mp}/C_b values (0.95 - 0.99) under 0.5 mol dm^{-3} NaCl condition suggest that the anion exclusion effect is not remarkable under saline water conditions.

The calculated D_e values for HSe^-, Se_4^{2-} and SeO_3^{2-} are also listed in **Table 4-4**. The experimentally measured D_e values of Se(−II) were obviously lower than the previously reported

ones of monovalent anion, even taking into account the errors (**Table 4-2** and **Fig. 4-5**). It is found that Se(−II) includes HSe^- and Se_4^{2-} species from the UV-Vis spectrometry measurements (**Fig. 4-2**); the low diffusivity of Se(−II) is likely to be due to the low diffusivity of Se_4^{2-}. The diffusive flux of Se(−II), $J_{(Se(-II))}$ (mol m^{-2} s^{-1}), is the summation of those of HSe^- and Se_4^{2-} as

$$J_{(Se(-II))} = J_{(HSe^-)} + J_{(Se_4^{2-})} \tag{4-30}$$

$$J_{(HSe^-)} = -D_{e(HSe^-)} \frac{\partial c_{(HSe^-)}}{\partial x} \quad , \quad J_{(Se_4^{2-})} = -D_{e(Se_4^{2-})} \frac{\partial c_{(Se_4^{2-})}}{\partial x} . \tag{4-31}$$

The concentration of Se present as HSe^- in the high-concentration reservoir was determined to be 45% of the total Se(−II) concentration in most samples by UV-Vis spectrometry through the experimental periods (**Fig. 4-2**), and that present as Se_4^{2-} was 55%. Based on the constant concentration ratio of HSe^- to Se_4^{2-} through the experimental period, chemical equilibrium as[9)]

$$Se_4^{2-} + 4H^+ + 6e^- = 4HSe^- \tag{4-32}$$

was assumed. Equation (4-30) can be written as

$$-D_{e(Se(-II))} \frac{\partial c_{(Se(-II))}}{\partial x} = -D_{e(HSe^-)} \frac{0.45 \cdot \partial c_{(Se(-II))}}{\partial x} - D_{e(Se_4^{2-})} \frac{0.55 \cdot \partial c_{(Se(-II))}}{\partial x} . \tag{4-33}$$

Dividing both sides by $-\frac{\partial c_{(Se(-II))}}{\partial x}$ yields the D_e values of Se(−II) as

$$D_{e(Se(-II))} = 0.45 D_{e(HSe^-)} + 0.55 D_{e(Se_4^{2-})} \quad . \tag{4-34}$$

Figure 4-8 shows the comparison of D_e values of Se(−II) (a) and SeO_3^{2-} (b) predicted using this diffusion model with experimentally measured ones. The D_e values calculated with the Tachi *et al.*'s model[43)] for Kunigel V1,

$$D_e = \phi \frac{\delta_g \delta_{el}}{\tau^2} D_v \quad (4\text{-}35)$$

where τ is the tortuosity of the diffusive pore, δ_g is the geometric constrictivity, and δ_{el} counts electrostatic effects, with Eq. (4-34) is also shown in **Fig. 4-8**. Tachi *et al*.'s model predicted the D_e of Se(−II) and SeO_3^{2-} at low bentonite content reasonably well, but a relatively large discrepancy was observed at high bentonite content. In particular, the discrepancy was remarkable at low salinity. This discrepancy is due to the overestimation of anion exclusions caused by the underestimation of the pore width, because the model is based on the homogeneous pore structure ($N_l = 1$). On the other hand, the D_e values predicted using the model considering the two types of pore developed in this study show good agreement with the experimentally measured ones. Although the diffusivities of HSe^- and Se_4^{2-} could not be determined individually from the experiments, the model calculations assuming the constant concentration ratio of HSe^- to Se_4^{2-} and the much lower diffusivity of Se_4^{2-} than HSe^- successfully reproduced the results of the experiments.

4.6. Conclusion

Effective diffusion coefficients of Se(−II) and Se(IV) species through compacted bentonite/sand mixture were systematically obtained under reducing and anaerobic conditions, respectively, by the through-diffusion method. Experiments were carried out under variable bentonite content and porewater salinity. The D_e values of Se(−II) species were within a range of 9.7×10^{-12} - 5.9×10^{-11} $m^2\ s^{-1}$, and those of Se(IV) species were within a range of 4.6×10^{-12} - 6.7×10^{-11} $m^2\ s^{-1}$. The D_e values of Se species decreased with increasing bentonite content and decreasing salinity.

A diffusion model for anionic species was developed based on the electric double layer theory and the pore diffusion model. The calculated D_e values of Se species and the experimentally measured ones showed good agreement, which help in the understanding of the diffusion of anionic Se species in the bentonite porewater.

References

1) Japan Nuclear Cycle Development Institute (JNC), *H12: Project to Establish the Scientific and Technical Basis for HLW Disposal in Japan - Second Progress Report on Research and Development for the Geological Disposal of HLW in Japan*, JNC TN 1410 2000–001, JNC (2000).

2) Japan Atomic Energy Agency (JAEA) and Federation of Electric Power Companies of Japan (FEPC), *Second Progress Report on Research and Development for TRU Waste Disposal in Japan –Repository Design, Safety Assessment and Means of Implementation in the Generic Phase*-, JAEA-Review 2007–010, FEPC TRU–TR2–2007–01, JAEA and FEPC (2007).

3) L. Syper, J. Mlochowski, "The convenient syntheses of organoselenium reagents," *Synthesis*, 439–442 (1984).

4) M. Ito, M. Okamoto, M. Shibata, Y. Sasaki, T. Danhara, K. Suzuki, T. Watanabe, "*Mineral Composition Analysis of Bentonite*," PNC TN 8430 93–003, Power Reactor and Nuclear Fuel Development Corporation (1993), [in Japanese].

5) H. Kubo, Y. Kuroki, M. Mihara, "Experimental investigation on alteration of bentonite by concrete pore fluids," *Soils Found.*, 46 (10), 31–34 (1998), [in Japanese].

6) S. Nakayama, Y. Sakamoto, T. Yamaguchi, M. Akai, T. Tanaka, T. Sato, Y. Iida, "Dissolution of montmorillonite in compacted bentonite by highly-alkaline aqueous solutions and diffusivity of hydroxide ions," *Appl. Clay Sci*. **27**, 53–65 (2004).

7) T. Yamaguchi, S. Nakayama, S. Nagao, M. Kizaki, "Diffusive transport of neptunium and plutonium through compacted sand–bentonite mixtures under anaerobic conditions," *Radiochim. Acta*, **95**, 115–125 (2007).

8) Atomic Energy Society of Japan (AESJ), *Measurement Method of the Distribution Coefficient on the Sorption Process*, Standard AESJ–SC–TR001 (2006), [in Japanese].

9) A. Olin, B. Nolang, E. G. Osadchii, L.- O. Ohman, E. Rosen, *Chemical Thermodynamics of Selenium*, Elsevier, Amsterdam (2005).

10) S. Licht, F. Forouzan, "Speciation analysis of aqueous polyselenide solutions," *J. Electrochem. Soc*., **142**[5], 1546–1551 (1995).

11) L. Lyons, T. Young, "Alkaline selenide, polyselenide electrolytes: concentrations, absorption-spectra and formal potentials," *Aust. J. Chem*., **39**[3], 511–527 (1986).

12) H. Sato, S. Suzuki, "Fundamental study on the effect of an orientation of clay particles on diffusion pathway in compacted bentonite," *Appl. Clay Sci*., **23**, 51–60 (2003).

13) M. Zhang, M. Takeda, H. Nakajima, "Determining the transport properties of rock specimens using an improved laboratory through diffusion technique," *Mater. Res. Soc. Symp. Proc*., **932**, 135–142 (2006).
14) J. Crank, *The Mathematics of Diffusion*, 2nd edition, Oxford University Press, Oxford (1975).
15) H. Kato, T. Nakazawa, S. Ueta, M. Muroi, I. Yasutomi, H. Fujihara, "Effective diffusivities of iodine, chlorine and carbon in bentonite buffer material," *Mater. Res. Soc. Symp. Proc.*, **556**, 687–694 (1999).
16) T. Ishidera, S. Miyamoto, H. Sato, *The Effect of Silica Sand Content and $NaNO_3$ Concentration Diffusions of C, Cl and I in Compacted Bentonite*, JNC TN8400 2004–001, JNC (2004), [in Japanese].
17) Y. Marcus, *Ion Properties*, Marcus Dekker, Inc., New York (1997).
18) H. Sato, *Acquisitions of Effective Diffusion Coefficients (De) for Ni(II), Am(III), Sm(III) and Se(IV) in Bentonite by Through-Diffusion Method*, JNC TN8400 99–062, JNC (1999).
19) T. E. Eriksen, M. Jansson, *Diffusion of I^-, Cs^+ and Sr^{2+} in Compacted Bentonite –Anion Exclusion and Surface Diffusion*, SKB Technical Report 96-16, SKB (1996).
20) P. Wersin, L. R. Van Loon, J. M. Soler, A. Yllera, J. Eikenberg, T. Gimmi, P. Hernan, J. Y. Boisson, "Long–term diffusion experiment at Mont Terri: first results from field and laboratory data," *Appl. Clay Sci.*, **26**[1–4], 123–135 (2004).
21) A. Muurinen, O. Karnland, J. Lehikoinen, "Ion concentration caused by an external solution into the porewater of compacted bentonite," *Phys. Chem. Earth*, 29, 119–127 (2004).
22) H. Sato, M. Yui, H. Yoshikawa, "Diffusion behavior for Se and Zr in sodium bentonite," *Mater. Res. Soc. Symp. Proc.,* **353**, 269–276 (1995).
23) H. Kato, M. Muroi, N. Yamada, H. Ishida, H. Sato, "Estimation of effective diffusivity in compacted bentonite," *Mater. Res. Soc. Symp. Proc.*, **353**, 277–284 (1995).
24) M. Ochs, B. Lothenbach, H. Wanner, H. Sato, M. Yui, "An integrated sorption-diffusion model for the calculation of consistent distribution and diffusion coefficients in compacted bentonite," *J. Contam. Hydrol*., **47**, 283–296 (2001).
25) J. V. Brakel, P. M. Heertjes, "Analysis of diffusion in macroporous media in terms of a porosity, a tortuosity and a constrictivity factor," *Int. J. Heat Mass Transfer*, **17**, 1093–1103 (1974).
26) I. Neretnieks, "Diffusivities of some constituents in compacted wet bentonite clay and the impact on radionuclide migration in the buffer", *Nucl. Technol*., **71**, 458–470 (1985).
27) W. Stumm, J. J. Morgan, *Aquatic Chemistry*, 3rd edition, John Wiley & Sons, Inc., New York (1996).
28) L. R. Van Loon, M. A. Glaus, W. Müller, "Anion exclusion effects in compacted bentonites:

towards a better understanding of anion diffusion," *Appl. Geochem.* 2536–2552 (2007).

29) R. Pusch, O. Karnland, *GMM – A General Microstructural Model for Qualitative and Quantitative Studies of Smectite Clays*, SKB Technical Report 90–43, SKB (1990).

30) F. Kitahara, A. Watanabe, *Kaimen Denki Gensho*, Kyoritsu Shuppan, Tokyo (1972), [in Japanese].

31) T. Shibutani, Y. Kohara, C. Oda, M. Kubota, Y. Kuno, M. Shibata, *Physico-Chemical Characteristics of Purified Na-smectite and Protonation/Deprotonation Behavior of Smectite Surface in NaCl Media*, JNC TN8400 99–066, JNC (1999), [in Japanese].

32) T. Kozaki, J. Liu, S. Sato, "Diffusion mechanism of sodium ions in compacted montmorillonite under different NaCl concentration," *Phys. Chem. Earth.*, **33**, 957–961 (2008).

33) I. C. Bourg, G. Sposito, A. C. M. Bourg, "Tracer diffusion in compacted, water–saturated bentonite," *Clays Clay Miner*., **54**, 363–374 (2006).

34) J. Lyklema, S. Rovillard, J. De Coninck, "Electrokinetics: The properties of the stagnant layer unraveled," *Langmuir* **14**, 5659–5663 (1998).

35) A. J. Easteal, A. V. Edge, L. A. Woolf, "Isotope effects in water: tracer diffusion coefficients for $H_2{}^{18}O$ in ordinary water," *J. Phys. Chem*., **88**, 6060–6063 (1984).

36) H. Kato, T. Nakazawa, S. Ueta, T. Yato, "Measurements of effective diffusivities of tritiated water in sand-mixed bentonite," *Proc. Radioactive Waste Management and Environmental Remediation-ASME 1999*, Nagoya, Japan, Sep. 26-30, 1999 (1999).

37) The Japanese Geotechnical Society, *Handbook on Geotechnical Engineering*, Maruzen, Tokyo (1999), [in Japanese].

38) The Japanese Geotechnical Society, *Doshitsu Shiken no Houhou to Kaisetsu,* 1st revised edition, The Japanese Geotechnical Society, Tokyo, Japan (2002), [in Japanese].

39) H. S. Wong, N. R. Buenfeld, M. K. Head, "Estimating transport properties of mortars using image analysis on backscattered electron images," *Cem. Concr. Res*., **36**[8] 1556–1566 (2006).

40) T. Kozaki, H. Sato, A. Fujishima, N. Saito, S. Sato, H. Ohashi, "Effect of dry density on activation energy for diffusion of strontium in compacted sodium montmorillonite," *Mater. Res. Soc. Symp. Proc*., **465**, 893–900 (1997).

41) D. Tessier, G. Pedro, "Electron microscopy study of Na smectite fabric –Role of layer charge, salt concentration and suction parameters," *Proc. Int. Clay Conf. 1981*, 165–176 (1982).

42) R. Pusch, "Identification of Na-smectite hydration by use of "humid cell" high voltage microscopy," *Appl. Clay Sci.*, **2**, 343–352 (1987).

43) Y. Tachi, K. Yotsuji, Y. Seida, M. Yui, " Diffusion of cesium and iodine in compacted

montmorillonite under different saline conditions" *Mater. Res. Soc. Symp. Proc.*, **1193**, 545–552 (2009).

Table 4-1 Experimental conditions for through-diffusion experiments

Oxidation state	Dry density of specimen	Salinity of solution	Bentonite/sand ratio	Cell number
Se(–II)	1600 kg m^{-3}	0.05 mol dm^{-3} NaCl	7/ 3	2-1
			6/ 4	2-2
			5/ 5	2-3
			4/ 6	2-4
			3/ 7	2-5
			2/ 8	2-6
		0.1 mol dm^{-3} NaCl	7/ 3	2-7
			6/ 4	2-8
			5/ 5	2-9
			4/ 6	2-10
			3/ 7	2-11
			2/ 8	2-12
		0.5 mol dm^{-3} NaCl	7/ 3	2-13
			6/ 4	2-14
			5/ 5	2-15
			4/ 6	2-16
			3/ 7	2-17
			2/ 8	2-18
Se(IV)	1600 kg m^{-3}	0.05 mol dm^{-3} NaCl	7/ 3	4-1
			5/ 5	4-2
			2/ 8	4-3
		0.1 mol dm^{-3} NaCl	7/ 3	4-4
			5/ 5	4-5
			2/ 8	4-6
		0.5 mol dm^{-3} NaCl	7/ 3	4-7
			5/ 5	4-8
			2/ 8	4-9

Table 4-2 Analysis of diffusion of Se(−II) and Se(IV) in the bentonite/sand mixture

Diffusing species	Cell number	J_1 (mol m^{-2} s^{-1})	J_2 (mol m^{-2} s^{-1})	c_1 (mol m^{-3})	c_2 (mol m^{-3})	D_{eb} (m^2 s^{-1})
Se(–II)	2-1	$(3.3 \pm 1.4)\times10^{-11}$	$(3.4 \pm 0.1)\times10^{-11}$	$(3.9 \pm 0.2)\times10^{-2}$	$(2.0 \pm 0.1)\times10^{-3}$	$(9.7 \pm 0.6)\times10^{-12}$
	2-2	$(5.4 \pm 2.3)\times10^{-11}$	$(5.2 \pm 0.2)\times10^{-11}$	$(4.0 \pm 0.2)\times10^{-2}$	$(2.6 \pm 0.1)\times10^{-3}$	$(1.4 \pm 0.1)\times10^{-11}$
	2-3	$(7.0 \pm 2.1)\times10^{-11}$	$(5.5 \pm 0.2)\times10^{-11}$	$(3.8 \pm 0.2)\times10^{-2}$	$(2.8 \pm 0.2)\times10^{-3}$	$(1.6 \pm 0.1)\times10^{-11}$
	2-4	$(1.0 \pm 0.3)\times10^{-10}$	$(7.7 \pm 0.2)\times10^{-11}$	$(3.9 \pm 0.2)\times10^{-2}$	$(3.3 \pm 0.2)\times10^{-3}$	$(2.3 \pm 0.1)\times10^{-11}$
	2-5	$(1.2 \pm 0.3)\times10^{-10}$	$(1.2 \pm 0.1)\times10^{-10}$	$(3.8 \pm 0.2)\times10^{-2}$	$(3.7 \pm 0.2)\times10^{-3}$	$(3.6 \pm 0.3)\times10^{-11}$
	2-6	$(1.0 \pm 0.4)\times10^{-10}$	$(1.2 \pm 0.1)\times10^{-10}$	$(3.8 \pm 0.2)\times10^{-2}$	$(4.0 \pm 0.2)\times10^{-3}$	$(3.7 \pm 0.3)\times10^{-11}$
	2-7	$(5.8 \pm 2.3)\times10^{-11}$	$(6.6 \pm 0.2)\times10^{-11}$	$(3.7 \pm 0.2)\times10^{-2}$	$(3.1 \pm 0.2)\times10^{-3}$	$(2.0 \pm 0.2)\times10^{-11}$
	2-8	$(6.5 \pm 2.6)\times10^{-11}$	$(7.3 \pm 0.2)\times10^{-11}$	$(3.7 \pm 0.2)\times10^{-2}$	$(3.6 \pm 0.2)\times10^{-3}$	$(2.2 \pm 0.2)\times10^{-11}$
	2-9	$(7.8 \pm 4.2)\times10^{-11}$	$(9.6 \pm 0.2)\times10^{-11}$	$(3.8 \pm 0.3)\times10^{-2}$	$(3.3 \pm 0.2)\times10^{-3}$	$(2.9 \pm 0.3)\times10^{-11}$
	2-10	$(9.4 \pm 4.4)\times10^{-11}$	$(1.2 \pm 0.1)\times10^{-10}$	$(3.8 \pm 0.3)\times10^{-2}$	$(4.0 \pm 0.2)\times10^{-3}$	$(3.7 \pm 0.3)\times10^{-11}$
	2-11	$(1.0 \pm 0.4)\times10^{-10}$	$(1.3 \pm 0.1)\times10^{-10}$	$(3.8 \pm 0.2)\times10^{-2}$	$(3.9 \pm 0.2)\times10^{-3}$	$(4.1 \pm 0.3)\times10^{-11}$
	2-12	$(1.4 \pm 0.5)\times10^{-10}$	$(1.5 \pm 0.1)\times10^{-10}$	$(3.6 \pm 0.2)\times10^{-2}$	$(4.5 \pm 0.2)\times10^{-3}$	$(5.3 \pm 0.5)\times10^{-11}$
	2-13	$(1.3 \pm 0.5)\times10^{-10}$	$(1.4 \pm 0.1)\times10^{-10}$	$(3.9 \pm 0.2)\times10^{-2}$	$(3.4 \pm 0.2)\times10^{-3}$	$(4.0 \pm 0.3)\times10^{-11}$
	2-14	$(1.6 \pm 0.5)\times10^{-10}$	$(1.5 \pm 0.1)\times10^{-10}$	$(3.9 \pm 0.2)\times10^{-2}$	$(3.7 \pm 0.2)\times10^{-3}$	$(4.5 \pm 0.3)\times10^{-11}$
	2-15	$(1.7 \pm 0.8)\times10^{-10}$	$(1.4 \pm 0.1)\times10^{-10}$	$(3.8 \pm 0.3)\times10^{-2}$	$(3.6 \pm 0.2)\times10^{-3}$	$(4.5 \pm 0.4)\times10^{-11}$
	2-16	$(1.5 \pm 1.2)\times10^{-10}$	$(1.4 \pm 0.1)\times10^{-10}$	$(3.8 \pm 0.5)\times10^{-2}$	$(4.3 \pm 0.3)\times10^{-3}$	$(4.6 \pm 0.8)\times10^{-11}$
	2-17	$(1.9 \pm 1.0)\times10^{-10}$	$(1.6 \pm 0.1)\times10^{-10}$	$(3.6 \pm 0.4)\times10^{-2}$	$(4.2 \pm 0.3)\times10^{-3}$	$(5.4 \pm 0.8)\times10^{-11}$
	2-18	$(2.0 \pm 0.8)\times10^{-10}$	$(1.7 \pm 0.1)\times10^{-10}$	$(3.7 \pm 0.3)\times10^{-2}$	$(4.8 \pm 0.2)\times10^{-3}$	$(5.9 \pm 0.6)\times10^{-11}$
Se(IV)	4-1	-	-	-	-	$(4.6 \pm 0.1)\times10^{-12}$
	4-2	-	-	-	-	$(6.9 \pm 0.1)\times10^{-12}$
	4-3	-	-	-	-	$(3.1 \pm 0.1)\times10^{-11}$
	4-4	-	-	-	-	$(7.7 \pm 0.1)\times10^{-12}$
	4-5	-	-	-	-	$(1.4 \pm 0.1)\times10^{-11}$
	4-6	-	-	-	-	$(5.4 \pm 0.1)\times10^{-11}$
	4-7	-	-	-	-	$(3.7 \pm 0.1)\times10^{-11}$
	4-8	-	-	-	-	$(4.1 \pm 0.1)\times10^{-11}$
	4-9	-	-	-	-	$(6.7 \pm 0.1)\times10^{-11}$

Table 4-3 Notations used for the model calculation

Symbol	Description	Unit
J	diffusive flux	mol m^{-2} s^{-1}
D_e	effective diffusion coefficient	m^2 s^{-1}
D_{mp}	diffusion coefficient in macro pore	m^2 s^{-1}
D_v	diffusion coefficient in free water	m^2 s^{-1}
C_b	concentration of diffusing species in external bulk solution	mol m^{-3}
C_{mp}	concentration of diffusing species in macro pore	mol m^{-3}
$C(X)$	concentration of diffusing species at position X	mol m^{-3}
d_{mp}	macro pore width	m
d_{il}	interlayer pore width	m
x	position parallel to montmorillonite layers	m
X	position normal to montmorillonite layers	m
n_{bi}	concentration of electrolyte ion i in external bulk solution	m^{-3}
Z_d	valence of diffusing species	-
Zi	valence of electrolyte ion i	-
ψ_0	surface potential	V
$\psi_{(X)}$	electric potential at position X	V
G_{mp}	geometry factor of macro pore	-
G_p	geometry factor of whole pore	-
ρ_{mix}	dry density of bentonite/sand mixture	kg m^{-3}
ρ_g	grain density of bentonite	kg m^{-3}
ρ_s	grain density of sand	kg m^{-3}
ρ_e	effective bentonite dry density	kg m^{-3}
ρ_f	density of fluid	kg m^{-3}
S_{tot}	total surface area of montmorillonite stacks	m^2 kg^{-1}
S_{mp}	external surface area of montmorillonite stacks	m^2 kg^{-1}
S_{il}	specific surface area of interlayer of montmorillonite	m^2 kg^{-1}
C_{mont}	montmorillonite content in bentonite/sand mixture	-
R_b	bentonite content in bentonite/sand mixture	%
R_s	sand content in bentonite/sand mixture	%
η_{mp}	viscosity of macro porewater	Pa s
η_0	viscosity of water	Pa s
ϕ_{tot}	porosity of diffusion medium	-
ϕ_{mp}	porosity of macro pore	-
ϕ_{il}	porosity of interlayer pore	-
K	hydraulic conductivity	m s^{-1}
N_l	the number of layers in montmorillonite stack	-

Table 4-4 Results of model calculations for Se species

Salinity (mol dm^{-3})	Bentonite/sand ratio	N_1 (-)	ϕ_{mp} (-)	ϕ_{il} (-)	d_{mp} (nm)	C_{mp}/C_b			D_{mp} (m^2 s^{-1})			D_e (m^2 s^{-1})		
						HSe^-	Se_4^{2-}	SeO_3^{2-}	HSe^-	Se_4^{2-}	SeO_3^{2-}	HSe^-	Se_4^{2-}	SeO_3^{2-}
0.05	7/ 3	4	0.26	0.15	5.1	0.37	0.16	0.16	7.1×10^{-11}	6.8×10^{-12}	3.4×10^{-11}	2.6×10^{-11}	1.1×10^{-12}	5.3×10^{-12}
	6/ 4	4	0.28	0.12	6.0	0.44	0.23	0.23	8.2×10^{-11}	7.9×10^{-12}	3.9×10^{-11}	3.6×10^{-11}	1.8×10^{-12}	8.8×10^{-12}
	5/ 5	4	0.30	0.10	7.2	0.52	0.31	0.31	9.5×10^{-11}	9.1×10^{-12}	4.5×10^{-11}	4.9×10^{-11}	2.8×10^{-12}	1.4×10^{-11}
	4/ 6	3	0.33	0.07	8.5	0.58	0.39	0.39	1.1×10^{-10}	1.1×10^{-11}	5.3×10^{-11}	6.5×10^{-11}	4.2×10^{-12}	2.1×10^{-11}
	3/ 7	2	0.35	0.05	9.6	0.63	0.45	0.45	1.3×10^{-10}	1.3×10^{-11}	6.4×10^{-11}	8.4×10^{-11}	5.8×10^{-12}	2.9×10^{-11}
	2/ 8	2	0.38	0.02	10.0	0.64	0.47	0.47	1.7×10^{-10}	1.6×10^{-11}	8.0×10^{-11}	1.1×10^{-10}	7.7×10^{-12}	3.8×10^{-11}
0.1	7/ 3	4	0.26	0.15	5.1	0.51	0.31	0.31	7.1×10^{-11}	6.8×10^{-12}	3.4×10^{-11}	3.6×10^{-11}	2.1×10^{-12}	1.0×10^{-11}
	6/ 4	4	0.28	0.12	6.0	0.58	0.39	0.39	8.2×10^{-11}	7.9×10^{-12}	3.9×10^{-11}	4.8×10^{-11}	3.1×10^{-12}	1.5×10^{-11}
	5/ 5	4	0.30	0.10	7.2	0.65	0.48	0.48	9.5×10^{-11}	9.1×10^{-12}	4.5×10^{-11}	6.1×10^{-11}	4.4×10^{-12}	2.2×10^{-11}
	4/ 6	3	0.33	0.07	8.5	0.70	0.55	0.55	1.1×10^{-10}	1.1×10^{-11}	5.3×10^{-11}	7.8×10^{-11}	6.0×10^{-12}	2.9×10^{-11}
	3/ 7	2	0.35	0.05	9.6	0.73	0.61	0.61	1.3×10^{-10}	1.3×10^{-11}	6.4×10^{-11}	9.9×10^{-11}	7.8×10^{-12}	3.9×10^{-11}
	2/ 8	2	0.38	0.02	10.0	0.75	0.62	0.62	1.7×10^{-10}	1.6×10^{-11}	8.0×10^{-11}	1.3×10^{-10}	1.0×10^{-11}	5.0×10^{-11}
0.5	7/ 3	20	0.28	0.12	25.9	0.97	0.95	0.95	7.7×10^{-11}	7.5×10^{-12}	3.7×10^{-11}	7.5×10^{-11}	7.1×10^{-12}	3.5×10^{-11}
	6/ 4	21	0.30	0.10	34.4	0.98	0.96	0.96	8.7×10^{-11}	8.4×10^{-12}	4.1×10^{-11}	8.5×10^{-11}	8.1×10^{-12}	4.0×10^{-11}
	5/ 5	21	0.32	0.09	44.7	0.98	0.97	0.97	9.9×10^{-11}	9.5×10^{-12}	4.7×10^{-11}	9.7×10^{-11}	9.2×10^{-12}	4.6×10^{-11}
	4/ 6	20	0.33	0.07	55.0	0.99	0.98	0.98	1.1×10^{-10}	1.1×10^{-11}	5.4×10^{-11}	1.1×10^{-10}	1.1×10^{-11}	5.3×10^{-11}
	3/ 7	16	0.35	0.05	60.6	0.99	0.98	0.98	1.3×10^{-10}	1.3×10^{-11}	6.3×10^{-11}	1.3×10^{-10}	1.3×10^{-11}	6.2×10^{-11}
	2/ 8	9	0.37	0.03	54.1	0.99	0.98	0.98	1.6×10^{-10}	1.6×10^{-11}	7.8×10^{-11}	1.6×10^{-10}	1.5×10^{-11}	7.6×10^{-11}

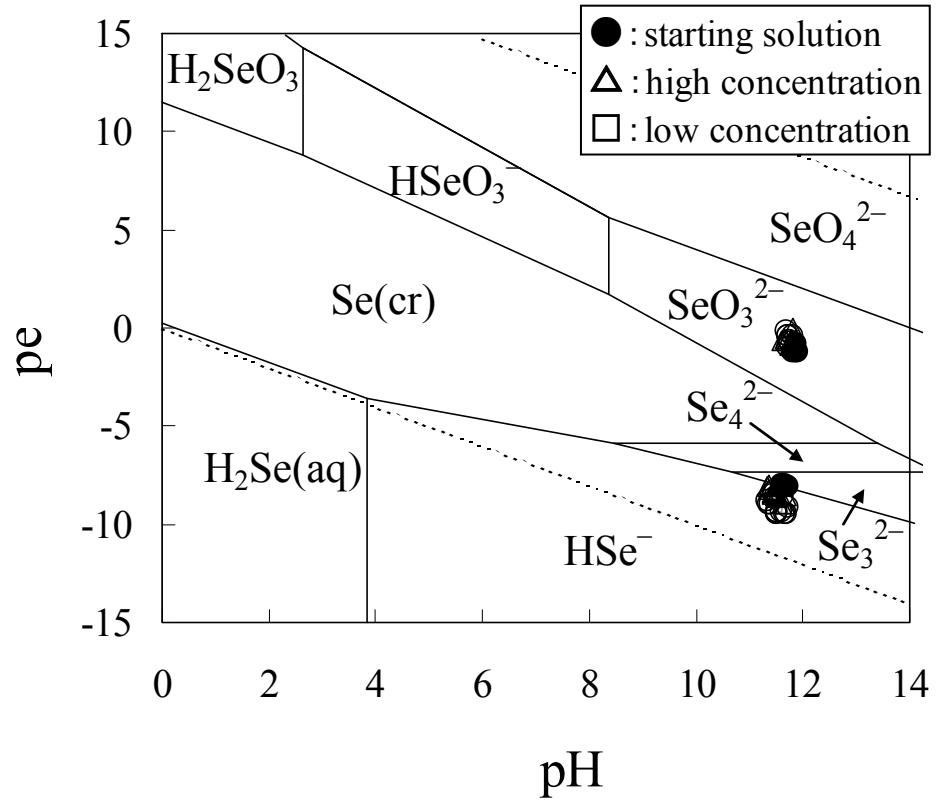

Fig. 4-1 Experimental conditions of starting solutions (filled symbols) and solutions after experiments (open symbols) in a pH-pe diagram for the H-O-Se system under standard conditions. The total concentration of Se is 5×10^{-5} mol dm^{-3}. The triangles and squares represent the conditions for the experimental solutions in the high-concentration reservoirs and the low-concentration reservoirs, respectively.

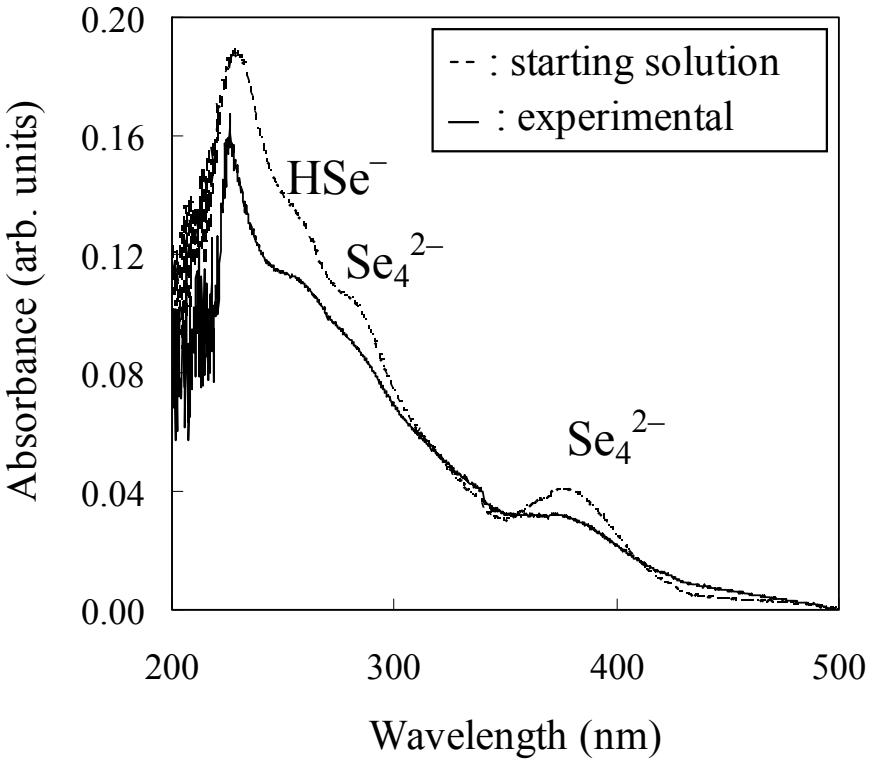

Fig. 4-2 UV-Vis spectra of the Se(−II) starting solution of 0.1 mol dm^{-3} NaCl and the experimental solution in the high-concentration reservoir of 2-9 cells after the through-diffusion experiment. The absorption band at 245 nm was assigned to HSe^- and those at 282 and 377 nm were assigned to Se_4^{2-}.

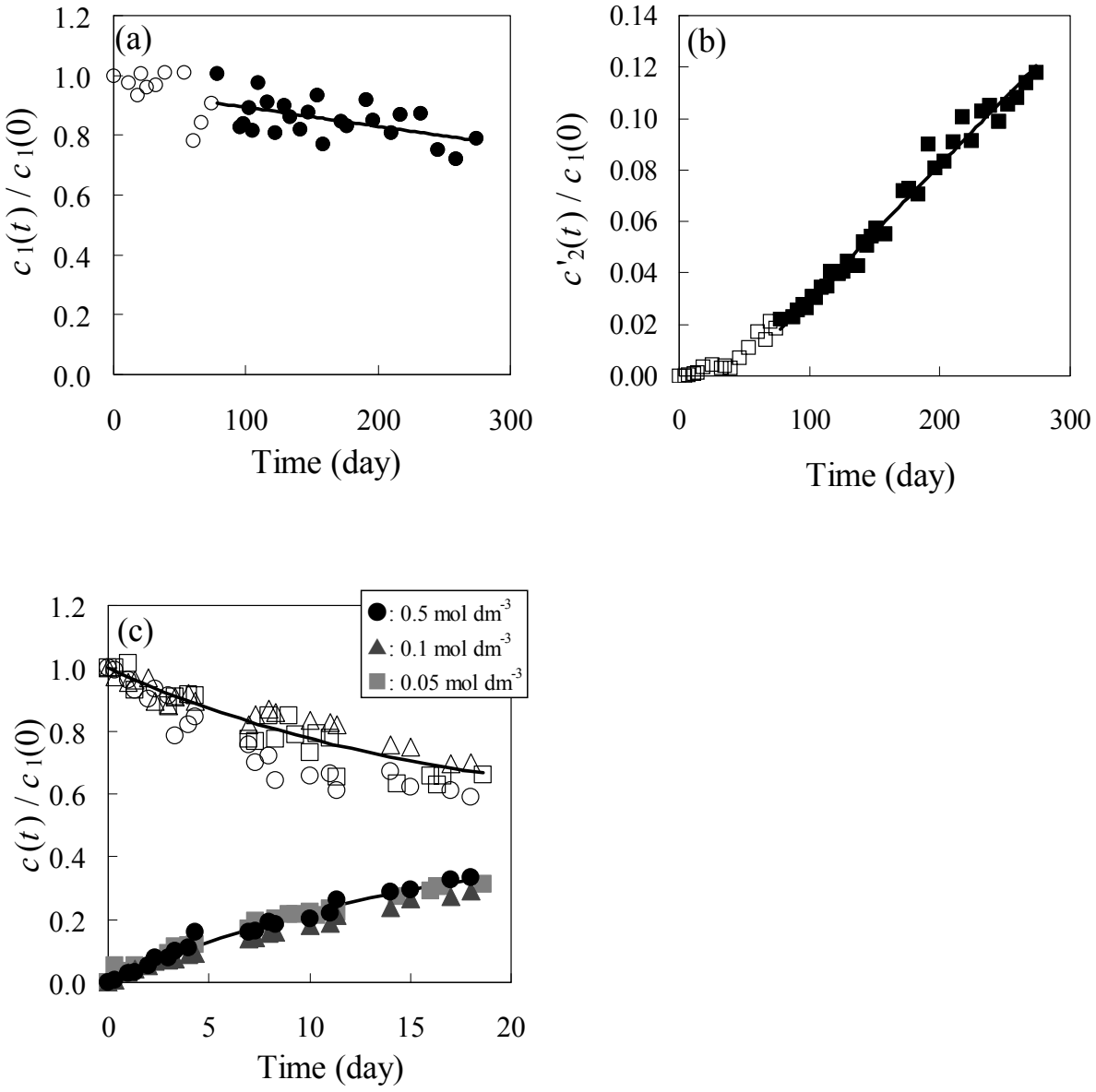

Fig. 4-3 Changes in concentrations of Se(−II) in the high-concentration reservoir (a) and those in the low-concentration reservoir (b) of 2-9 cells. The D_e was determined by using data after the 80th day (filled symbols). Changes in concentrations of Se(−II) in the high-concentration reservoirs (open symbols) and low-concentration reservoirs (filled symbols) from the through-diffusion experiments for the filter (c).

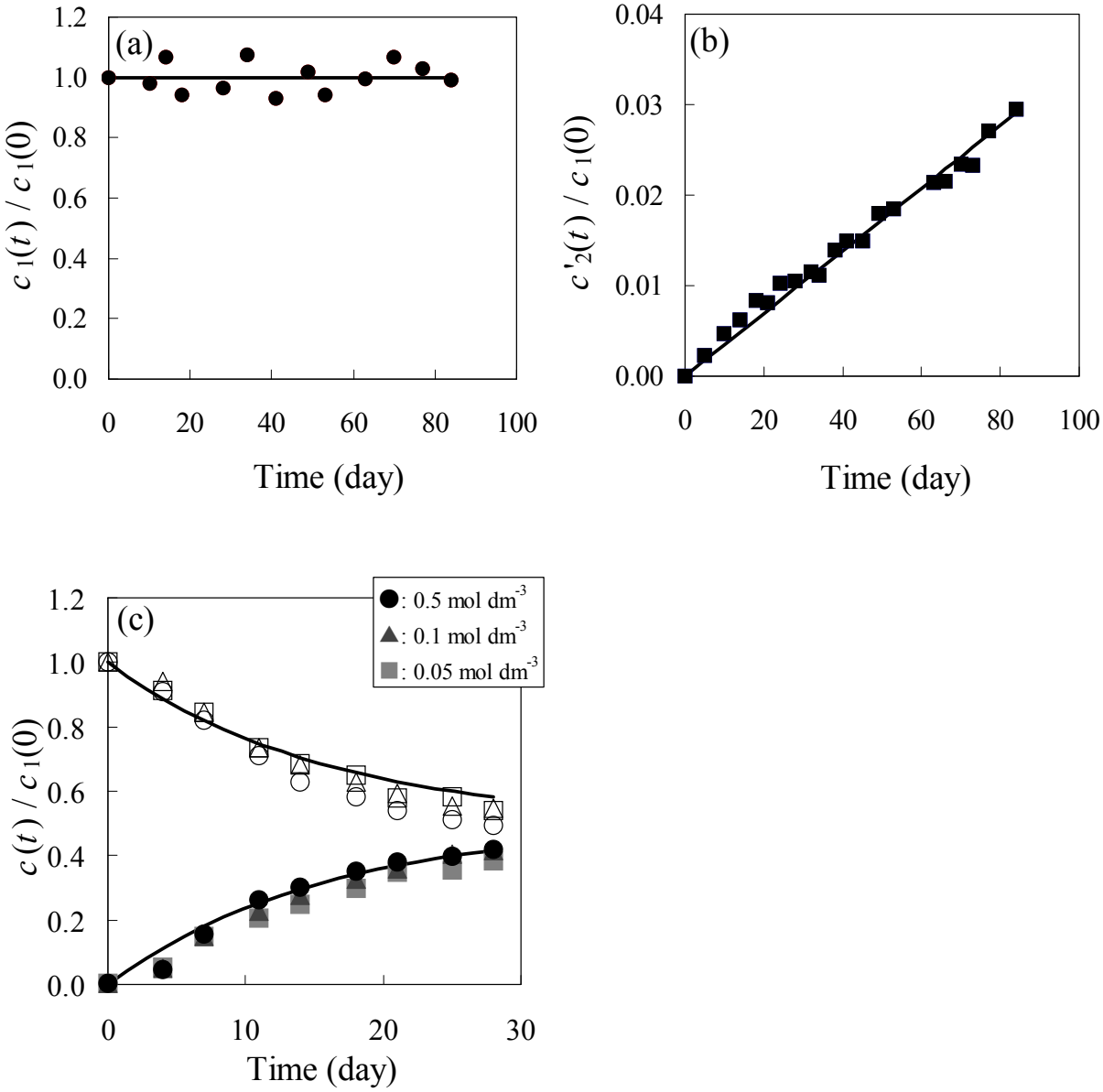

Fig. 4-4 Changes in concentrations of Se(IV) in the high-concentration reservoir (a) and low-concentration reservoir (b) of 4-5 cells. The D_e was determined by using data of 0-84th day. Changes in concentrations of Se(IV) in the high-concentration reservoirs (open symbols) and low-concentration reservoirs (filled symbols) from the through-diffusion experiments for the filter (c).

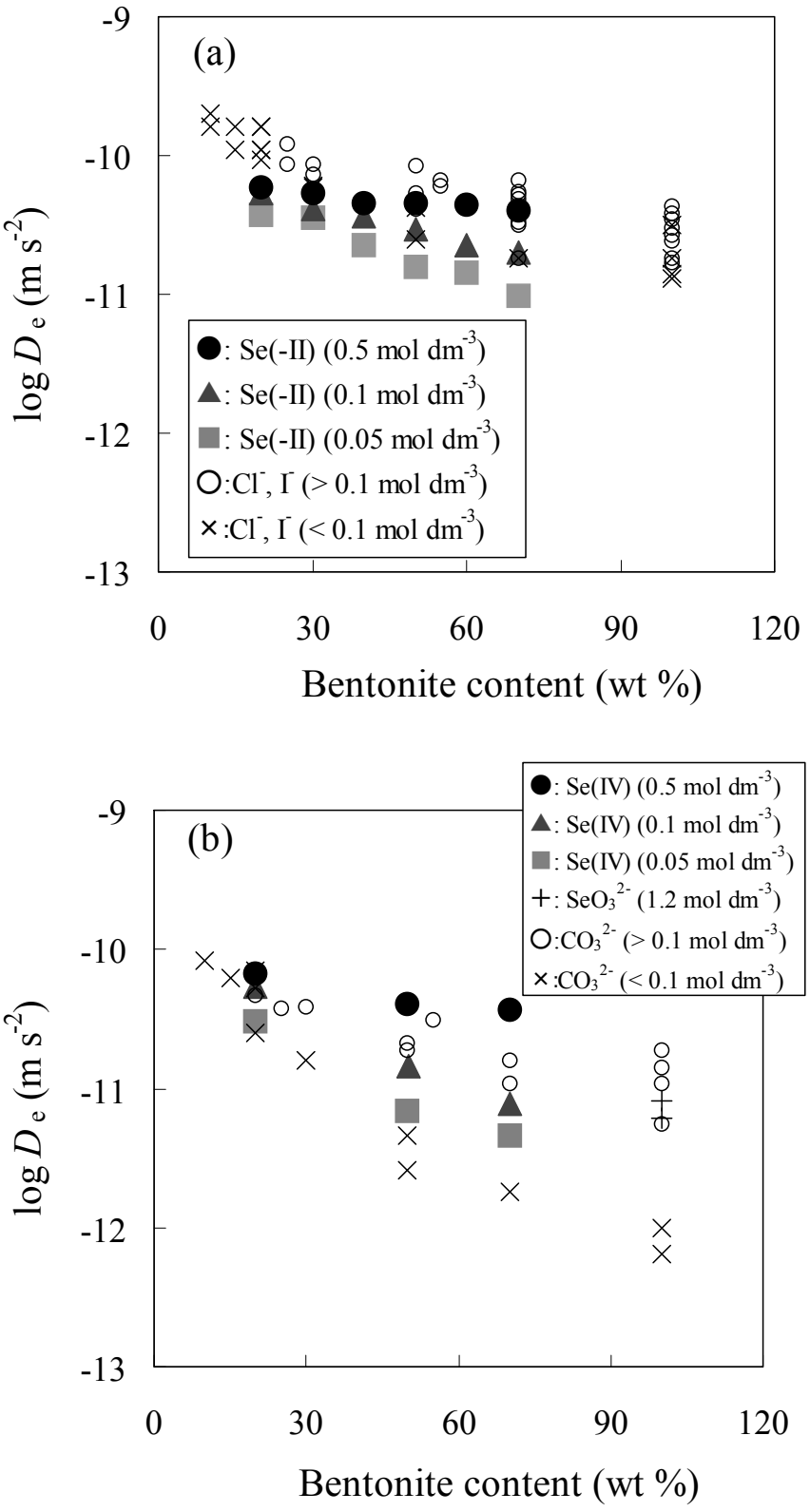

Fig. 4-5 Comparison of measured diffusion coefficients (filled symbols) of Se(−II) with previously reported ones (open symbols) of Cl^- and I^- (a),[15,16] and those of Se(IV) with previously reported ones of SeO_3^{2-} [18] and CO_3^{2-} [15,16] (b)

(a)

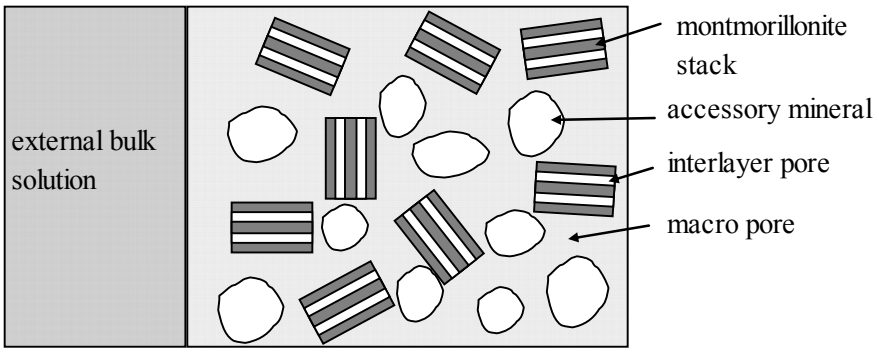

(b)

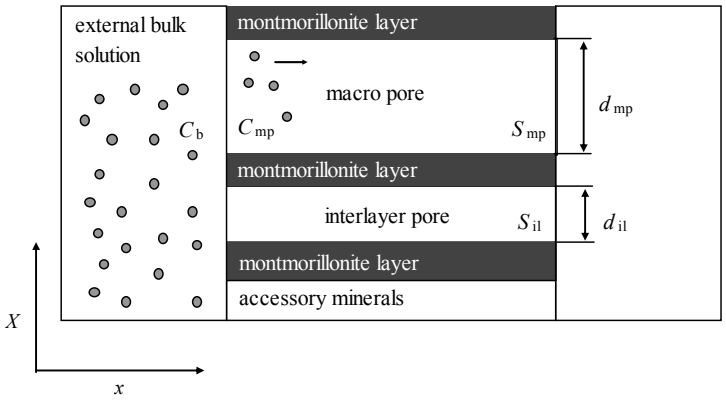

(c)

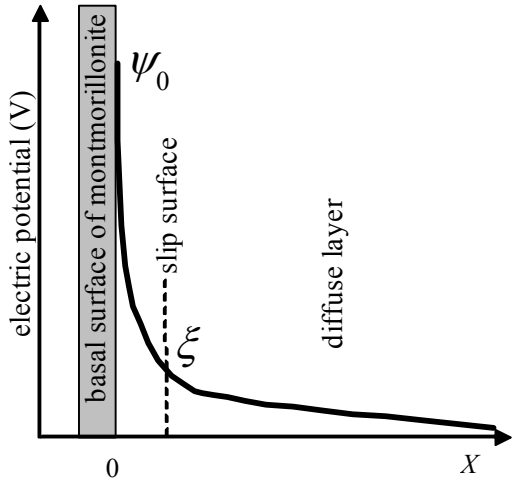

Fig. 4-6 Schematic drawing of the bentonite/sand mixture (a) and the diffusion pathways through the macro pore (b), and sketch of the electric double layer (c).

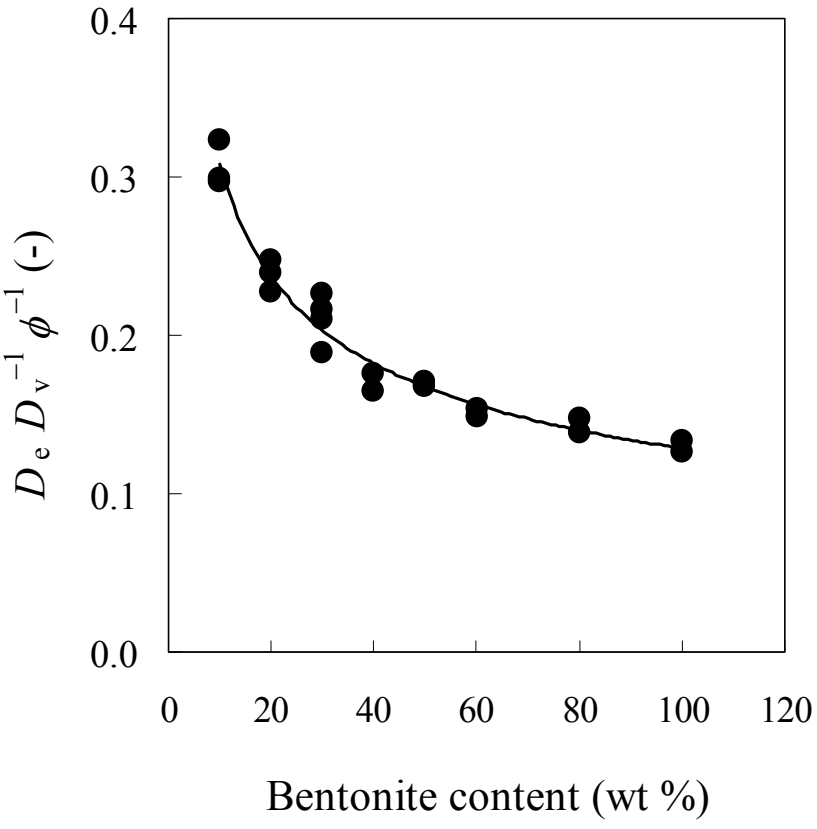

Fig. 4-7 Estimation of geometry factor for various bentonite contents [36)]

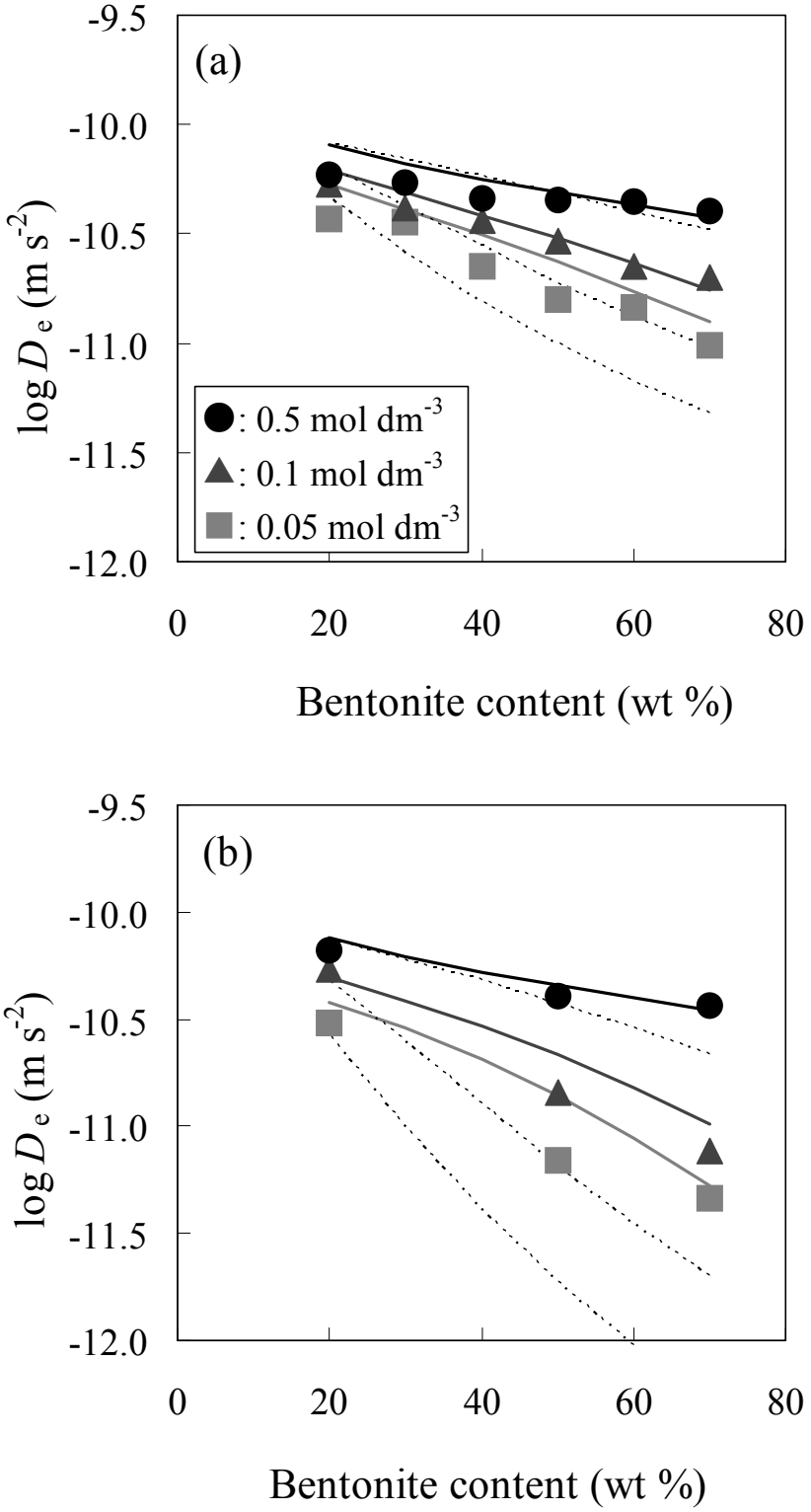

Fig. 4-8 Comparison of diffusion coefficients of Se(−II) (a) and SeO_3^{2-} (b) predicted using this diffusion model (solid lines) with experimentally measured ones and the prediction using Tachi *et al.*'s model[43] (dashed lines)

5. Sorption of Selenium onto Rocks

5.1. Introduction

The retardation of radionuclide migration by sorption onto a host rock is one of the main geologic factors that influence the performance of HLW disposal system. For a long-term safety assessment of geological disposal of HLW, it is necessary to evaluate the variation in sorption distribution coefficients (K_d) of Se(−II) species under the disposal conditions, and understand the sorption behavior based on sorption mechanisms. Although a considerable amount of Se sorption data has been obtained under aerobic conditions,[e.g. 1-8] where Se(IV) and Se(VI) species are dominant, data obtained under reducing conditions are limited[6-10] and the sorption behavior of Se(−II) species has not been clarified.

Batch sorption experiments were carried out to study the sorption behavior of Se(−II) onto rocks under reducing conditions. Granodiorite was used to represent crystalline rocks, and sandy mudstone and tuffaceous sandstone were used to represent sedimentary rocks. The major constituent minerals and accessory minerals of these rocks were also employed to identify which minerals were the most sorbent for Se(−II) and to discuss the sorption mechanisms.

5.2. Materials

5.2.1. Groundwater Samples

To minimize oxidation, groundwater samples were collected with a special care to avoid exposure to air. The procedure is described in detail in Ref. 11), and summarized as follows. Groundwater from the granodiorite, sandy mudstone, and tuffaceous sandstone aquifer was obtained from three separate boreholes, each of which was drilled with degassed water obtained by bubbling Ar gas into the local surface water as part of the drilling procedure. Groundwater was sampled from the granodiorite aquifer at a depth interval of GL −328 m to −352 m (GL: ground level), from the sandy mudstone aquifer at a depth interval of GL −129 m to −130 m, and from the tuffaceous sandstone aquifer at a depth interval of GL −330 m to −340 m. The upper surface of the borehole water also was covered with Ar gas to prevent exposing the water to oxygen in the air. The pH, oxidation-reduction potential (ORP) and dissolved oxygen concentration of the borehole water were measured by using an *in situ* groundwater monitor. The ORP measured by a platinum electrode against a Ag/AgCl reference electrode was converted to electric potential against the normal hydrogen electrode (*E*h *vs*. NHE). The pumped-out groundwater was immediately frozen with dry ice and stored at −20°C in a freezer. The groundwater samples were

analyzed according to Japanese Industrial Standards to determine dissolved cations, anions, and organic compounds.[10,11] Chemical compositions of the groundwater samples are summarized in **Table 5-1**.

5.2.2. Rock Samples

Rock cores were sampled from a depth of GL −310 m to −320 m in the granodiorite, from a depth of GL −150 m to −155 m in the sandy mudstone, and from a depth of GL −330 m to −340 m in the tuffaceous sandstone. The cores received a special treatment to minimize their exposure to air.[11] The rock cores were cut into cylindrical pieces with diameters of 50 mm and lengths of 200 mm in the degassed water, and were temporarily stored in three-dimensional pressurizing vessels. The cylindrical rock pieces were further cut into disks 5 mm thick by using an automatic horizontal cutting machine in a controlled atmosphere glove box under Ar gas. The disk specimens were also stored in three dimensional pressurizing vessels filled with pressurized degassed water.

The rock samples were analyzed to determine their specific gravity, water content, and porosity (**Table 5-2**).[10,11] The rock samples were crushed and passed through a 63 μm sieve, then analyzed to determine their cation and anion exchange capacities by the semi-micro Schollenberger[12] and $BaCl_2$-$MgSO_4$ methods[13], respectively (**Table 5-2**). Rock-forming and clay minerals were identified by XRD analysis, and chemical compositions of the rock samples were determined by X-ray fluorescence spectrometry (XRF) (**Table 5-3**). In addition, the mineral content of the granodiorite was determined by petrographic analysis of thin sections using polarization microscopy (**Table 5-4**).

5.2.3. Minerals

The main constituent minerals of the rock samples, as identified by XRD analysis (**Table 5-3**), were selected for sorption experiments. Quartz and feldspar were represented by commercially available samples of silica (SiO_2; Aerosil Corp.) and albite ($NaAlSi_3O_8$, Nichika Inc.), respectively. Calcite ($CaCO_3$) and chlorite ($(Mg, Fe(II), Al)_6(Al, Si)_4O_{10}(OH)_8$) samples were purchased from Nichika Inc., and pyrite (FeS_2) was purchased from Rare Metallic Co., Ltd. The mica group minerals were represented by biotite ($K(Mg, Fe(II))_3(Al, Fe(III)Si_3O_{10})(OH, F)_2$, Nichika Inc.) and the smectite group minerals by montmorillonite ($(Ca_{0.5},Na)_{0.33}(Al,Mg)_2Si_4O_{10}(OH)_2 \cdot nH_2O$, Kunipia F, Kunimine Industries Co. Ltd.). Iron oxide minerals were represented in the sorption experiments by samples of goethite (α-FeOOH), which can be formed by alteration of Fe-bearing minerals,[14] such as pyrite, biotite and chlorite, all of which were detected in the rock samples by XRD or petrographic analysis and are known as

sorbent minerals for Se.[1,2,9,15] All of the purchased mineral samples were in granulated form and used without pretreatment. Their specific surface areas, as measured by the BET method, were 309.4 $m^2\ g^{-1}$ (silica), 1.1 $m^2\ g^{-1}$ (albite), 0.4 $m^2\ g^{-1}$ (calcite), 0.9 $m^2\ g^{-1}$ (pyrite), 4.6 $m^2\ g^{-1}$ (biotite), 1.7 $m^2\ g^{-1}$ (chlorite), 15.5 $m^2\ g^{-1}$ (montmorillonite), and 17.6 $m^2\ g^{-1}$ (goethite).

5.2.4. Selenium Stock Solution

Selenium(−II) stock solution was prepared in a controlled atmosphere glove box under Ar by the following procedure. A solution of ^{75}Se (4 MBq cm^{-3}, carrier: 50μg cm^{-3} Na_2SeO_3) was purchased from GE Healthcare Limited. A 0.5cm^3 volume of 98% aqueous solution of $N_2H_4 \cdot H_2O$ was mixed with a 0.5 cm^3 volume of the ^{75}Se solution in a polypropylene test tube and the mixture was stored for 3 days to reduce Se.[16] The mixture was diluted with distilled deionized water to 10 cm^3. The solution was filtered through a 10,000 NMWL ultrafilter to remove a precipitated fraction of Se. A 3 cm^3 volume of the filtrate was sampled to analyze aqueous Se species by UV-Vis spectrometry.

5.3. Sorption Experiments

The experimental runs were made following the procedure of the "Measurement Method of the Distribution Coefficient on the Sorption Process" compiled by the Atomic Energy Society of Japan.[17] The experimental procedures departed from Ref. 17) insofar as the rock disks used as samples in this study were unprocessed to maintain the sampled condition of the underground environments. All the experiments, except for analytical procedures, were performed in a controlled atmosphere glove box under Ar at 25 ± 3°C. The frozen groundwater was thawed in the controlled atmosphere glove box for a day, after which it was filtered through a 0.45 μm filter to remove suspended solids. A 5 cm^3 volume of 98 % $N_2H_4 \cdot H_2O$ solution was added to a 1,000 cm^3 volume of the filtered groundwater to prepare reduced groundwater. The concentration of $N_2H_4 \cdot H_2O$ in the reduced groundwater was 0.1 mol dm^{-3}.

Batch sorption experiments were carried out using two different Se concentrations to confirm that the obtained distribution coefficients were independent of Se concentration. First, a 0.2 cm^3 volume of the Se(−II) stock solution was spiked into a 600 cm^3 volume of the reduced groundwater. This Se solution was filtered through a 0.45μm filter to produce experimental solutions of higher Se concentration (Se solution "H", Se: 1×10^{-8} mol dm^{-3}). Then, this Se solution (H) was diluted with the reduced groundwater and passed through a 0.45μm filter to prepare the lower Se concentration experimental solutions (Se solution "L", Se: 2×10^{-9} mol dm^{-3}). The pH of the solutions was adjusted to 8.5, 9.5, 10.5 and 11.5 with NaOH solution or HCl. The

pH was measured with a combination glass electrode (ROSS 8172BNWP, Thermo Fisher Scientific Inc.) which is suitable for the measurement of high-ionic-strength samples. The electrode was calibrated with standard pH buffer solutions of 7.00, 10.01, and 12.46. The *E*h was determined against NHE using a platinum electrode combined with a Ag/AgCl reference electrode after checking its accuracy with saturated quinhydrone solutions. A 1 cm^3 aliquot was sampled and the radioactivity of the solution was measured by γ- spectrometry (LOAX-51370/20-P, SEIKO EG&G) with a peak at 0.136 MeV to determine the initial concentration of Se.

Blank tests were carried out to check for precipitation and/or adsorption of Se onto vessel walls. A 60 cm^3 volume of Se solution (H) or (L) was poured into a screw-capped Teflon PFA vessel and stored for 2 weeks. A 2 cm^3 aliquot was sampled and filtered through a 10,000 NMWL ultrafilter preconditioned with a small amount of the sample solution. One cm^3 of the filtrate was sampled and its radioactivity was measured by γ- spectrometry. It was confirmed that the Se concentration did not decrease from the initial concentration, indicating that precipitation and/or adsorption of Se onto vessel walls was negligible.

The rock samples were preconditioned prior to sorption runs by immersion in the reduced groundwater for 3 months to avoid precipitation of Se from original porewater leaching out of the pores of rock samples. The sorption runs were initiated by contacting the disk rock samples with Se solution (H) or Se solution (L). The samples were agitated once a day. The sorption period for sandy mudstone was set at 2 weeks after it was confirmed in a previous work[10] that the sorption process reached equilibrium within 2 weeks in batch sorption experiments for the same type of rock sample. The sorption period for tuffaceous sandstone was also set at 2 weeks, because its porosity (26.3%) is as high as that of sandy mudstone (29.0%). The sorption period for granodiorite, which has a low porosity (1.17%), was extended until a decrease in Se concentration in solution was no longer observed. The pH and *E*h of the sample solutions were measured at the end of the sorption period. A 2 cm^3 aliquot was sampled and filtered through a 10,000 NMWL ultrafilter preconditioned with a small amount of the sample solution. One cm^3 of the filtrate was sampled, and the radioactivity of the solution was measured by γ- spectrometry to determine the equilibrated concentration of Se.

Sorption experiments using sterilized groundwater and rock samples were also carried out to investigate the possibility that microorganisms might be affecting the sorption process. Experimental runs were made at pH 10.5. The disk rock sample was soaked in the groundwater in a Teflon PTFE container. The container was enclosed in a stainless steel jacket and stored at 130°C for half an hour.[18] After this sterilization, the container was carried out in the controlled atmosphere glove box under Ar. A 0.5 cm^3 volume of 98% $N_2H_4 \cdot H_2O$ solution was added to a

100 cm^3 volume of the sterilized groundwater to prepare reduced sterilized groundwater. The sterilized rock samples were preconditioned by immersion in the reduced sterilized groundwater for a month. A 0.03 cm^3 volume of the Se(−II) stock solution was spiked into a 100 cm^3 volume of the reduced sterilized groundwater. By filtering this solution through a 0.45μm filter, an experimental solution for sterilized samples (Se solution "S", Se: 1×10^{-8} mol dm^{-3}) was prepared. The pH, *E*h, and radioactivity of the solution were measured. A 58 cm^3 volume of the Se solution (S) was poured in a screw-capped Teflon PFA vessel and the preconditioned sterilized disk rock sample was put into the solution. The sorption period for sandy mudstone and tuffaceous sandstone was set at 2 weeks, and that for granodiorite at 4 months. The pH, *E*h, and radioactivity of the solutions were measured after the sorption periods in the same manner as mentioned above.

Sorption experiments for constituent and accessory minerals were carried out by the following procedure. A 1.5 cm^3 volume of 98% $N_2H_4{\cdot}H_2O$ solution was added to a 300 cm^3 volume of 0.05 or 0.5 mol dm^{-3} NaCl solution. A 0.1 cm^3 volume of Se(−II) stock solution was spiked into a 300 cm^3 volume of the NaCl solution. By filtering this solution through a 0.45 μm filter, experimental solutions for minerals (Se solution "M", Se: 1×10^{-8} mol dm^{-3}) were prepared. The pH of the solution was adjusted to 8.5, 10.5, and 12 with NaOH solution or HCl. The pH and *E*h of the solutions were measured. A 1 cm^3 aliquot was sampled, and the radioactivity of the solution was measured by γ- spectrometry to determine the initial concentration of Se. A 0.1 g of granulated mineral sample was immersed in a 10 cm^3 volume of the Se solution (M) in a polypropylene test tube. Blank tests were carried out in parallel with the sorption runs to confirm that precipitation and/or adsorption of Se onto vessel walls was negligible. After 2 weeks, the pH, *E*h, and radioactivity of the solutions were measured in the same manner as mentioned above.

5.4. Results and Discussion

5.4.1. Selenium Species

The UV-Vis spectrum of the Se(−II) stock solution shows absorption bands at 247 and 377 nm, as shown in **Fig. 5-1**. These peaks were assigned to HSe^- and Se_4^{2-}, respectively,[19,20] showing that Se was dissolved as stable species under the reducing condition.[21] Experimental data from the sorption experiments using rocks and minerals are summarized in **Tables 5-5** and **5-6**, respectively. Based on the pH and reducing conditions of the initial and equilibrated experimental solutions in all of the experimental runs, the dominant Se species in solution was estimated to be HSe^- (**Fig. 5-2**).

5.4.2. Sorption Behavior onto Mineral Samples

The sorption ratio, R_s (%), and the distribution coefficient, K_d (m^3 kg^{-1}), for mineral samples were calculated using

$$R_s = \frac{C_{ini} - C_{eq}}{C_{ini}} \times 100 \quad (5\text{-}1)$$

$$K_d = \frac{\left(C_{ini} - C_{eq}\right)}{C_{eq}} \frac{V_{ini}}{M} \quad (5\text{-}2)$$

where C_{ini} is the initial concentration of Se (mol dm^{-3}), C_{eq} the equilibrated concentration of Se (mol dm^{-3}), V_{ini} the initial volume of solution (m^3), and M the weight of the solid phase (kg). The R_s and K_d values determined for the mineral samples are listed in **Table 5-6**.

Sorption phenomena comprise a variety of possible mechanisms, such as ion exchange, surface complexation, and precipitation/mineralization.[22,23] Generally, ion exchange is influenced by ionic strength, and surface complexation is affected by pH.[24] Redox sensitive elements, such as Se, are also subject to precipitation/mineralization processes due to changes in redox conditions, in addition to effects from the concentration of other ions and changes in pH. The K_d values obtained from the mineral samples are plotted versus pH in **Fig. 5-3** to summarize their effects on the sorption mechanism of Se(−II) on minerals.

The R_s and K_d values for tectosilicates (quartz and albite) were less than 10% and 1×10^{-2} m^3 kg^{-1}, respectively, at any pH. Sorption experiments under various redox conditions include the measurement of K_ds for Se(IV) on these tectosilicates, and the K_ds were also very low (K_d < 1×10^{-2} m^3 kg^{-1}) at pHs 2 - 12.[1,6] Such a low sorption for Se(−II) as well as Se(IV) is due to the low point of zero charge (pzc) of quartz (< 2.2) and albite (3.0).[6] Surface sites of these minerals are negatively charged at neutral-alkaline pH, so that neither the Se(−II) nor Se(IV) anion can be easily sorbed onto these minerals.

The pH dependences of K_ds for phyllosilicates (biotite, chlorite, and montmorillonite) show the same tendency (**Fig. 5-3**). The R_s values for Se(−II) on phyllosilicates decreased with increasing pH from 34 to 76% at pH 8.5 to about 6 to 20% at pH 12. The K_d values show a negative dependence on pH and are independent of NaCl concentration, indicating that the dominant sorption mechanism of Se(−II) onto phyllosilicates is surface complexation. **Figure 5-4** compares the K_ds obtained in this study and previously reported values for Se under various redox conditions. The pH dependences of K_ds for Se(−II) on biotite and chlorite are similar to those obtained for Se(IV) by Shibutani *et al.*[1] and Ticknor *et al.*[6] (**Figs. 5-4(a)** and **5-4(b)**). On the

other hand, the K_ds on montmorillonite obtained for Se(IV) by Shibutani *et al.*[1] are much lower than those for Se(−II) obtained in this study (**Fig. 5-4(c)**), suggesting a difference in sorption mechanism between Se(−II) and Se(IV). Phyllosilicate minerals consist of an alumina octahedral sheet sandwiched between two silica tetrahedral sheets,[25] and they include aluminol sites (≡AlOH) and silanol sites (≡SiOH) on the edge surfaces. Biotite and chlorite with Fe in their mineral structures possibly include ferrol sites (≡FeOH).[1] The ≡SiOH sites (pzc < 2.2) are negatively charged at neutral-alkaline pH; thus, anionic Se species cannot be sorbed electrostatically. The ≡AlOH sites (pzc = 9.5 [26]) and the ≡FeOH sites (pzc = 7.2 [26]) are partially positively charged at alkaline pH, and they are expected to contribute to the surface complexation of anionic Se species. Shibutani *et al.*[1] modeled the sorption of Se(IV) on biotite and chlorite as surface complexation with ≡FeOH sites but not with ≡AlOH sites, because the sorption of Se(IV) onto montmorillonite was not observed. However, ≡AlOH sites are expected to have contributed to the sorption of Se(−II) onto phyllosilicates in addition to ≡FeOH sites, given that the sorption of Se(−II) onto montmorillonite was observed in this study, and the pH dependence of K_d for Se(−II) onto montmorillonite was similar to that onto biotite and chlorite. This result suggests that the surface complexation constant for Se(−II) with ≡AlOH sites is higher than that for Se(IV).

The K_d values for Se(−II) on goethite were as high as those on phyllosilicates at pH 12, but are about 2 orders of magnitude higher at pH 8.5 (**Fig. 5-3**). Hayes *et al.*[3] investigated the sorption behavior of Se(IV) onto goethite in 0.005, 0.1, and 1.0 mol dm^{-3} sodium nitrate ($NaNO_3$) solution, and that of Se(VI) in 0.001, 0.01, 0.1, and 1.0 mol dm^{-3} $NaNO_3$ solutions (**Fig. 5-4(d)**). The sorption behavior of Se(IV) was independent of the ionic strength and explained by inner-sphere complexation with ≡FeOH sites using a triple layer model. Hayes *et al.*[3] explained the sorption dependence of Se(VI) on ionic strength as being due to outer-sphere complexation. Shibutani *et al.*[1] also modeled the sorption behavior of Se(IV) onto goethite as surface complexation with ≡FeOH sites. The pH dependence of K_d for Se(−II) is similar to that for Se(IV), but it clearly differs from that for Se(VI) (**Fig. 5-4(d)**). The sorption mechanism of Se(−II), as well as Se(IV), onto goethite is likely to be surface complexation with ≡FeOH sites.

The R_s values for Se(−II) on calcite were 19 to 48% (**Table 5-6**). The obtained K_ds were 0.02 to 0.08 m^3 kg^{-1}, independent of pH. The K_ds for Se(−II) were nearly identical to those for Se(IV) reported by Fujikawa and Fukui,[4] and Ticknor *et al.*[6] (**Fig. 5-4(e)**). The sorption behavior of Se(−II) is likely to be similar to that of Se(IV), though the sorption mechanism onto calcite is not clarified at present.

The R_s values for Se(−II) on pyrite were more than 90% at any pH (**Table 5-6**). The obtained

K_ds, 1.3 to 9.9 m^3 kg^{-1}, show a slightly negative dependence on pH and are independent of NaCl concentration. Shibutani *et al*.[1] and Tachi *et al*.[2] reported that the sorbed amount of Se(IV) on pyrite was large at pH < 9 but sharply decreased at pH > 10 (**Fig. 5-4(f)**). The sorption behavior of Se(IV) onto pyrite was explained by surface complexation with an ≡FeOH site, which was generated by weathering of pyrite.[1] On the other hand, the strong sorption of Se(−II) was observed even at pH 12 in this study, suggesting that the sorption mechanism of Se(−II) onto pyrite is different from surface complexation.

The sorption mechanisms of Se(−II)[9,27] and Se(IV)[28,29] onto pyrite have been studied by spectroscopy. Xia *et al*.[9] carried out sorption experiments of Se(−II)/Se(0) on sedimentary rock samples containing pyrite under reducing conditions. Selenium(IV) in a test solution was reduced to Se(−II)/Se(0) by a mixed gas (H_2 (4.9%) + N_2) in the presence of a platinum (Pt) catalyst. Most of the Se sorbed onto the sedimentary rock was determined to be Se(0) by X-ray absorption near-edge structure (XANES) analysis, and the sorption mechanism was explained as incorporation into pyrite as

$$FeS_2 + Se(0)_{aq} = FeSe(0)S(-II) + S(0)_{aq}. \quad (5\text{-}3)$$

Liu *et al*.[27] carried out the sorption experiments of Se(−II) on synthesized pyrite under reducing conditions. The results of XRD and *in situ* XANES analyses indicated the presence of Se(0) on the pyrite surface ($Se(0)_s$), and the results of X-ray photoelectron spectroscopy (XPS) analysis indicated the formation of S(−II) on the pyrite surface. The sorption mechanism of Se(−II) was explained as the surface redox reaction as

$$FeS_2 + HSe^- = FeS + Se(0)_s + HS^-. \quad (5\text{-}4)$$

In both studies, the oxidation state of sorbed Se was identified as Se(0), and the sorption mechanism was interpreted as interactions with sulfur. Naveau *et al*.[28] and Breynaert *et al*.[29] reported that the sorption mechanism of Se(IV) onto pyrite was a redox reaction with sulfur but not iron, supporting the interpretation by Xia *et al*.[9] and Liu *et al*.[27] Although it is not clarified whether Se can be incorporated into pyrite, it seems not to occur easily because the crystalline system of ferroselite ($FeSe_2$; orthorhombic) is different from that of pyrite (FeS_2; cubic).[14] Thus, the sorption mechanism of Se(−II) onto pyrite is probably a local redox reaction with sulfur at the surface, as shown in Eq. (5-4).

5.4.3. Sorption Behavior onto Rock Samples

(1) Granodiorite

Changes over time in Se concentration due to sorption onto granodiorite are shown in **Fig. 5-5**. Decreases in Se concentration in the pH 10.5 and 11.5 solutions were not observed from the 100th day through the conclusion of the experiment on the 230th day, indicating that the solution attained a steady state by the 100th day. The pH 8.5 and 9.5 solutions attained a steady state a bit later, by the 170th day.

The R_s and K_d values for granodiorite, except for the sterilized sample, were calculated using

$$R_s = \frac{C_{ini} V_{ini} - C_{eq} V_{eq} - \sum_{i=1}^{n-1} C_i V_i}{C_{ini} V_{ini}} \times 100 \quad (5\text{-}5)$$

$$K_d = \frac{C_{ini} V_{ini} - C_{eq} V_{eq} - \sum_{i=1}^{n-1} C_i V_i}{M C_{eq}} \quad (5\text{-}6)$$

where C_{ini} is the initial concentration of Se (mol dm^{-3}), V_{ini} the initial volume of solution (m^3), C_{eq} the equilibrated concentration of Se (mol dm^{-3}), V_{eq} the volume of sample solution after equilibrium (m^3), C_i the concentration of Se in the sampling solution (mol dm^{-3}), V_i the volume of sampling solution (m^3), and M the weight of the solid phase (kg). The R_s and K_d for the sterilized sample were determined according to Eqs. (5-1) and (5-2), respectively.

R_s and K_d values determined for granodiorite are listed in **Table 5-5**, and the pH dependences of K_ds are shown in **Fig. 5-6(a)**. The K_ds obtained from the lower Se concentration experimental runs agree with those obtained from the higher Se concentration experimental runs, suggesting the linear sorption of Se(−II) onto granodiorite under the experimental conditions. The K_d for the sterilized sample shows an agreement with those for the nonsterilized samples, indicating a negligible effect of microorganisms on sorption in the nonsterilized samples. The R_s values for Se(−II) on granodiorite decreased from about 60% at pH 8.5 to about 10% at pH 11.5. The obtained K_ds, 2.2×10^{-4} to 4.0×10^{-3} m^3 kg^{-1}, showed a negative pH dependence.

The K_ds obtained for granodiorite were compared to previously reported ones for granite or granodiorite[4-6,30] (**Fig. 5-7**). The K_d profile for Se(−II) obtained in this study is similar to that previously reported for Se(IV) but is about 1 order of magnitude lower than that obtained for Se(−II) under the reducing condition (0.08 mol dm^{-3} N_2H_4) by Ticknor *et al.*[6] The K_ds

obtained under reducing conditions by Ticknor *et al*. are higher than those obtained under aerobic conditions, even though they were obtained in a higher pH region (**Fig. 5-7**), where anionic Se species do not readily form surface complexes. The higher K_ds obtained by Ticknor *et al*. might be caused by precipitation of Se, because the solubility of Se is low under the reducing conditions.[21)]

The pH dependence of Se(−II) sorption on granodiorite is similar to the sorption of Se(−II) onto phyllosilicate minerals (**Figs. 5-3** and **5-7**). Biotite is the only phyllosilicate mineral detected by XRD analysis in the sampled granodiorite (**Table 5-3**), and is likely to be a dominant sorbent mineral for Se(−II) in granodiorite at neutral-alkaline pH. The K_d values obtained for granodiorite (2.2×10^{-4} to 4.0×10^{-3} m^3 kg^{-1}) are about 5% of those for biotite by itself (6.1×10^{-3} to 7.9×10^{-2} m^3 kg^{-1}). The differences are roughly proportional to the mass fraction of biotite in the granodiorite, which was determined to be 5 to 20% by polarization microscopy (**Table 5-4**) and is about 5% in general.[1,6,31)]

In addition, Jan *et al*.[15)] reported that crystalline iron oxides dominate the sorption of Se(IV) on granite. Iron oxides were not identified by XRD analysis in the sampled granodiorite, but they can be formed by weathering of biotite.[32)] The K_ds for Se(−II) on goethite (1.5×10^{-2} to 7.9×10^{0} m^3 kg^{-1}) are about 2 to 3 orders of magnitude higher than those on granodiorite (2.2×10^{-4} to 4.0×10^{-3} m^3 kg^{-1}); thus, there is a possibility that a small amount of iron oxides, such as goethite, can dominate the sorption of Se(−II) on granodiorite especially at or below neutral pH.

(2) Sandy Mudstone

The R_s and K_d values for sandy mudstone were determined according to Eqs. (5-1) and (5-2), respectively (**Table 5-5**). The pH dependences of K_ds are shown in **Fig. 5-6(b)**. The K_ds obtained from the lower Se concentration experimental runs agree with those from the higher Se concentration experimental runs, suggesting the linear sorption of Se(−II) onto sandy mudstone under the experimental conditions. The K_d for the sterilized sample is in agreement with those for the nonsterilized samples, suggesting that the effect of microorganisms on sorption in the nonsterilized sample was negligible. The R_s values for Se(−II) on sandy mudstone were more than 90% at any pH. The obtained K_d values, 3.3×10^{-2} to 5.6×10^{-2} m^3 kg^{-1}, were independent of pH.

The K_ds obtained for sandy mudstone were compared to previously reported ones for mudstone and shale[4,8,9)] (**Fig. 5-8)**. The K_ds for Se(−II) obtained in this study were about 1 order of magnitude higher than those for Se(IV) obtained by Fujikawa and Fukui[4)] and Igarashi *et al*.[8)] In addition, the pH dependence of K_d for Se(−II) is less pronounced than that for Se(IV); thus, the sorption mechanism of Se(−II) onto sandy mudstone is likely to be different from that of Se(IV).

The K_ds for Se under reducing conditions were reported by Igarashi *et al*. (0.08 mol dm^{-3} N_2H_4 condition),[8] Xia *et al*. (H_2 (4.9 %) + N_2 condition),[9] and the authors (0.2 mol dm^{-3} N_2H_4 condition)[10]. The values obtained by Igarashi *et al*.[8] cannot be compared easily with the values obtained in this study, because they vary over a wide range and were obtained at lower pH regions. The K_d values obtained in the previous study by the author[10] using the same types of groundwater and rock samples under higher ionic strengths (0.1 to 1 mol dm^{-3}) and higher Se(−II) concentrations (1.2×10^{-5} to 3.4×10^{-5} mol dm^{-3}) agree with the results in this study. Xia *et al*.[9] carried out the sorption experiments for Se using 4 types of mudstone/shale. The K_d values varied according to the rock type ((A) – (D) in **Fig. 5-8**), but the pH dependences of K_ds were similar. Xia *et al*.[9] reported that the differences in the K_d values between the rocks were related to their differences in pyrite content, thus pyrite was a major contributor to the sorption of Se. The K_ds obtained in this study agree with those for the rock sample (A) employed by Xia *et al*., which contains the largest amount of pyrite (0.192%). Pyrite is the only mineral that shows high adsorbability at alkaline pH, and the pH dependence of the K_d values for sandy mudstone is similar to that for pyrite. Therefore, pyrite is likely to be a dominant sorbent mineral for Se(−II) in sandy mudstone at neutral-alkaline pH. The very weak peak for pyrite in the XRD analysis (detection limit of about 1%[33]) and the presence of reduced iron (FeO) and S (2.3% as SO_3) in the XRF analysis, indicate the presence of about 1 to 2% pyrite in the sandy mudstone samples. The K_ds obtained for sandy mudstone (3.3×10^{-2} to 5.6×10^{-2} m^3 kg^{-1}) range from 0.5 to 3% of those for pyrite (1.3 to 9.9 m^3 kg^{-1}), a value that is comparable to the estimated mass fraction of pyrite (1 to 2%) in the rock. The difference in K_d between Se(−II) and Se(IV) on sandy mudstone is likely to be caused by the difference in sorption behavior onto pyrite for these two species.

(3) Tuffaceous Sandstone

The R_s and K_d values for tuffaceous sandstone were determined according to Eqs. (5-1) and (5-2), respectively (**Table 5-5**). The pH dependences of K_ds are shown in **Fig. 5-6(c)**. The K_d values obtained from the lower Se concentration experimental runs agree with those from the higher Se concentration experimental runs, suggesting the linear sorption of Se(−II) onto tuffaceous sandstone under the experimental conditions. The K_d value for the sterilized sample shows an agreement with those for nonsterilized samples, suggesting that the effect of microorganisms on sorption in the nonsterilized sample was negligible. The R_s values for Se(−II) on tuffaceous sandstone were more than 90% at any pH. The obtained K_ds, 2.9×10^{-2} to 8.2×10^{-2} m^3 kg^{-1}, decreased slightly with increasing pH.

The obtained K_ds for tuffaceous sandstone were compared to previously reported ones for tuff

and sandstone[1,7] (**Fig. 5-9**). The values obtained using 0.05 mol dm^{-3} N_2H_4 by Barney[7] are the only data obtained under reducing conditions and are similar to those for Se(IV) under aerobic conditions (**Fig. 5-9**). The K_ds for Se(−II) obtained in this study were about 1 order of magnitude higher than those for Se(IV) obtained by Shibutani *et al.*[1] and Barney[7]. In addition, the pH dependence of K_d for Se(−II) is less pronounced than that for Se(IV), suggesting that the sorption mechanism of Se(−II) onto tuffaceous sandstone is likely to be different from that of Se(IV).

The very weak peak for pyrite in the XRD analysis (detection limit of about 1%[33]) and the presence of Fe and S (0.5% as SO_3) in the XRF analysis (**Table 5-3**) indicate the presence of about 0.5 to 1% pyrite in the tuffaceous sandstone samples. The obtained K_ds for tuffaceous sandstone (2.9×10^{-2} to 8.2×10^{-2} m^3 kg^{-1}) are about 0.8 to 2 % of those for pyrite (1.3 to 9.9 m^3 kg^{-1}), and these values are comparable to the mass fraction of pyrite (0.5 to 1%).

Moreover, the values and pH dependences of K_d for Se(−II) on tuffaceous sandstone were similar to those on sandy mudstone. It is likely, therefore, that pyrite also acts as the dominant sorbent mineral for Se(−II) in the tuffaceous sandstone at neutral-alkaline pH. The difference in K_d between Se(−II) and Se(IV) on tuffaceous sandstone is likely to be caused by the difference in sorption behavior onto pyrite. A lower pyrite content in the samples used by Barney[13] may have led to lower K_d values under reducing conditions than those in this study.

5.5. Conclusion

The obtained K_d values of Se(−II) species were in the ranges of 2.2×10^{-4} to 4.0×10^{-3} m^3 kg^{-1} for granodiorite, 3.3×10^{-2} to 5.6×10^{-2} m^3 kg^{-1} for sandy mudstone and 2.9×10^{-2} to 8.2×10^{-2} m^3 kg^{-1} for tuffaceous sandstone at pHs 8.5 to 11.5. The values and pH dependence of K_d for Se(−II) species on granodiorite obtained in this study agree with previously reported ones for Se(IV) species obtained under other redox conditions. Experimental results suggest that biotite dominates the sorption of Se(−II) species onto granodiorite at neutral-alkaline pH, and the sorption mechanism is surface complexation with ≡AlOH sites and ≡FeOH sites. The K_d values for Se(−II) on sandy mudstone and tuffaceous sandstone obtained in this study were about 1 order of magnitude higher than previously reported ones for Se(IV) species. Experimental results suggest that pyrite is the dominant sorbent mineral for Se(−II) species in sandy mudstone and tuffaceous sandstone at neutral-alkaline pH. The higher K_d values for Se(−II) species are likely to be due to the strong sorption of Se(−II) species onto pyrite in sandy mudstone and tuffaceous sandstone. The sorption mechanism of Se(−II) species onto pyrite is estimated to be a local redox reaction with sulfur at the surface.

References

1) T. Shibutani, Y. Nishikawa, S. Inui, N. Uchidate, M. Yui, *Study on Sorption Behavior of Se on Rocks and Minerals*, PNC TN8410 94-395, Power Reactor and Nuclear Fuel Development Corporation (1994), [in Japanese].
2) Y. Tachi, T. Shibutani, H. Sato, M. Yui, "Sorption and diffusion behavior of selenium in tuff," *J. Contam. Hydrol*., **35**, 77– 89 (1998).
3) K. F. Hayes, C. Papelis, J. O. Leckie, "Modeling ionic strength effects on anion adsorption at hydrous oxide/solution interfaces," *J. Colloid Interface Sci.*, **125**[2], 717–726 (1988).
4) Y. Fujikawa, M. Fukui, "Radionuclide sorption to rocks and minerals: Effect of pH and inorganic anion. Part. 2. Sorption and speciation of selenium," *Radiochim. Acta*, **76**, 163–172 (1997).
5) K. V. Ticknor, J. McMurry, "A study of selenium and tin sorption on granite and goethite," *Radiochim. Acta*, **73**, 149–156 (1996).
6) K. V. Ticknor, D. R. Harris, T. T. Vandergraaf, *Sorption/Desorption Studies of Selenium on Fracture-Filling Minerals under Aerobic and Anaerobic Conditions*, AECL TR-453, Atomic Energy of Canada Limited (1988).
7) G. S. Barney, *Radionuclide Sorption on Basalt-Interbed Materials*, FY 1981 Annual Report, RHO-BW-ST-35P (1982)
8) T. Igarashi, T. Nakazawa, S. Ueda, *Redox Potential and its Effects to Distribution Coefficients*, KURRI KR-44, 177–182 (2000), [in Japanese].
9) X. Xia, G. Kamei, K. Iijima, M. Shibata, T. Ohnuki, N. Kozai, "Selenium sorption in a sedimentary rock/saline groundwater system and spectroscopic evidence," *Mater. Res. Soc. Symp. Proc*., **932,** 933–942 (2006).
10) Y. Iida, Y. Kimura, T. Yamaguchi, M. Ueda, T. Tanaka, S. Nakayama, "Sorption distribution coefficients of selenium on a sandy mudstone under reducing conditions of underground," *J. Nucl. Fuel Cycle Environ.*, **15** [2], 57–67 (2009), [in Japanese].
11) K. Ebashi, T. Yamaguchi, T. Tanaka, K. Araki, M. Saitou, *Sampling and Treatment of Rock Cores and Groundwater under Reducing Environments of Deep Underground*. JAERI-Conf 2005-007, 242–247 (2005).
12) C. J. Schollenberger, R. H. Simon, "Determination of exchange capacity and exchangeable bases in soil-ammonium acetate method," *Soil Sci.,* **59**, 13–24 (1945).
13) G. P. Gillman, "A proposed method for the measurement of exchange properties of highly weathered soils," *Aust. J. Soil Res*. **17**, 129–139 (1979).
14) K. Makino, *Encyclopedia of Minerals*, Nikkan Kogyo Shinbunsha, Tokyo (1999), [in

Japanese].

15) Y. L. Jan, T. H. Wang, M. H. Li, S. C. Tsai, Y. Y. Wei, C. N. Hsu, S. P. Teng, "Evaluating adsorption ability of granite to radioselenium by chemical sequential extraction." *J. Radioanal. Nucl. Chem.*, **273**, 299–306 (2007).

16) L. Syper, J. Mlochowski, "The convenient syntheses of organoselenium reagents," *Synthesis*, **5**, 439–442 (1984).

17) Atomic Energy Society of Japan (AESJ), *Measurement Method of the Distribution Coefficient on the Sorption Process*, Standard AESJ-SC-TR001 (2006), [in Japanese].

18) G. E. Jenneman, M. J. McInerney, M. E. Crocker, R. M. Knapp, "Effect of sterilization by dry heat or autoclaving on bacterial penetration through Berea sandstone," *Appl. Environ. Microbiol.*, **51**, 39–43 (1986).

19) S. Licht, F. Forouzan, "Speciation analysis of aqueous polyselenide solutions," *J. Electrochem. Soc*., **142**[5], 1546–1551 (1995).

20) L. Lyons, T. Young, "Alkaline selenide, polyselenide electrolytes: concentrations, absorption-spectra and formal potentials," *Aust. J. Chem*., **39**[3], 511–527 (1986).

21) A. Olin, B. Nolang, E. G. Osadchii, L.-O. Ohman, E. Rosen, *Chemical Thermodynamics of Selenium*, Elsevier, Amsterdam (2005).

22) O. Tochiyama, A. Takasu, T. Ikeda, H. Kimura, S. Sato, S. Nagasaki, S. Nakayama, Y. Niibori, H. Furuya, T. Mitsugashira, T. Yamaguchi, "Concept and applicability of sorption distribution coefficient in the radionuclide transport model," *J. Nucl. Fuel Cycle Environ.*, **5**[3], 3–19 (1998), [in Japanese].

23) J. A. Davis, M. Ochs, M. Olin, T. E. Payne, C. J. Tweed, *NEA Sorption Project Phase II: Interpretation and Prediction of Radionuclide Sorption onto Substrates Relevant for Radioactive Waste Disposal Using Thermodynamic Sorption Models*, Nuclear Energy Agency Report No 5992, OECD (2005).

24) D. L. Zhao, S. J. Feng, C. L. Chen, S. H. Chen, D. Xu, X. K. Wang, "Adsorption of Thorium(IV) on MX-80 bentonite: Effect of pH, ionic strength and temperature," *Appl. Clay Sci*., **41**, 17–23 (2008).

25) H. Shirozu, *Clay Mineralogy*, Asakura press, Tokyo (1988), [in Japanese].

26) W. Stumm, J. J. Morgan, *Aquatic Chemistry*, 3rd edition, John Wiley & Sons, Inc., New York (1996).

27) X. Liu, M. Fattahi, G. Montavon, B. Grambow, "Selenide retention onto pyrite under reducing conditions," *Radiochim. Acta*, **96**, 473–479 (2008).

28) A. Naveau, F. M. Rivera, E. Guillon, J. Dumonceau, "Interactions of aqueous selenium (−II)

and (IV) with metallic sulfide surfaces," *Environ. Sci. Technol*., **41**[15], 5376–5382 (2007).

29) E. Breynaert, C. Bruggeman, A. Maes, "XANES-EXAFS analysis of Se solid-phase reaction products formed upon contacting Se(IV) with FeS_2 and FeS." *Environ. Sci. Technol*., **42**[10], 3595–3601 (2008).

30) H. Sato, T. Shibutani, Y. Tachi, K. Ota, K. Amano, M. Yui, *Diffusion Behavior of Nuclides Considering Pathways in Fractured Crystalline Rocks*, PNC TN8410 97-127 (1997).

31) K. Idemitsu, H. Furuya, K. Murayama, T. Asao, Y. Inagaki, "Diffusivity of uranium(VI) in water-saturated Inada granite," *Mater. Res. Soc. Symp. Proc*., **257**, 625–632 (1992).

32) C. R. Twidale, J. A. Bourne, J. R. Vidal Romani, "Origin of miniature mogotes in granite, King Rocks, southern Yilgarn Block, Western Australia," *Cuaternario y Geomorfologia*, **13**, 33–43 (1999).

33) M. Kato, *X-ray Diffraction Analysis*, Uchida Rokakuho, Tokyo (1990), [in Japanese].

Table 5-1 Chemical compositions of groundwater

		Granodiorite	Sandy mudstone	Tuffaceous sandstone
pH		7.9	8.1	7.1
*E*h (mV)		–74 ± 27	–118 ± 20	–205 ± 4
Dissolved oxgen (ppm)		<0.17	0.2±0.1	1.1±0.1
Dissolved ion (mol dm^{-3})	Na^+	9.6×10^{-4}	7.4×10^{-2}	1.3×10^{-1}
	K^+	9.2×10^{-5}	8.0×10^{-4}	6.1×10^{-4}
	Mg^{2+}	3.5×10^{-4}	1.6×10^{-3}	3.8×10^{-3}
	Ca^{2+}	6.0×10^{-4}	5.2×10^{-3}	9.0×10^{-3}
	NH_4^+	$<5.6\times10^{-6}$	3.6×10^{-3}	2.0×10^{-4}
	Cl^-	7.3×10^{-4}	1.2×10^{-1}	1.4×10^{-1}
	HCO_3^-	1.8×10^{-3}	1.6×10^{-3}	1.0×10^{-3}
	SO_4^{2-}	8.3×10^{-5}	1.0×10^{-5}	4.5×10^{-4}
	HS^-	$<1.6\times10^{-5}$	Not determined	1.3×10^{-3}
	NO_3^-	5.6×10^{-5}	1.0×10^{-5}	$<1.6\times10^{-6}$
	NO_2^-	4.3×10^{-6}	Not determined	$<2.2\times10^{-6}$
	CH_4	1.1×10^{-8}	Not determined	4.5×10^{-4}
Organic carbon (mg dm^{-3})		0.5	1.4	<0.5
Organic nitrogen （mg dm^{-3}）		<0.1	<0.1	<0.1

Table 5-2 Properties of rock samples

	Granodiorite	Sandy mudstone	Tuffaceous sandstone
Specific gravity (kg m^{-3})	2.73×10^{3}	2.67×10^{3}	2.23×10^{3}
Water content (wt%)	0.35	15.1	13.1
Porosity (vol%)	1.17	29.0	26.3
Cation exchange capacity (eq kg^{-1})	1.2×10^{-2}	2.3×10^{-1}	7.0×10^{-3}
Anion exchange capacity (eq kg^{-1})	$<1\times10^{-3}$	1.7×10^{-2}	$<1\times10^{-3}$

Table 5-3 Mineral and chemical compositions of rock sample

			Granodiorite	Sandy mudstone	Tuffaceous sandstone
Mineral compositions*	Rock forming minerals	Quartz	+++	+++	+++
		Albite	++	+	+
		Anorthite	++	+	–
		Microcline	+	++	–
		Tremolite	+	–	–
		Calcite	–	–	+++
		Pyrite	–	(+)	(+)
	Clay minerals	Mica group	++	+	(+)
		Chlorite	–	+	(+)
		Smectite group	–	+	–
		Kaolin mineral	–	+	–
Chemical compositions (mass%)		SiO_2	63.0	52.2	57.2
		Al_2O_3	15.0	20.0	12.6
		CaO	4.4	3.3	18.8
		K_2O	3.3	7.8	1.2
		MgO	3.5	1.0	2.8
		Na_2O	3.6	1.2	3.3
		FeO	–	10.9	–
		Fe_2O_3	5.6	–	2.5
		TiO_2	0.7	1.3	0.2
		SO_3	–	2.3	0.5
		BaO	0.5	–	–
		SrO	0.1	–	–
		MnO	0.1	–	0.6
		P_2O_5	0.2	–	–

* Relative intensity; +++: strong, ++: medium, +: weak, (+): very weak, –: not detected.

Table 5-4 Mineral composition of granodiorite identified by polarization microscopy

		Quantitative ratio (%)
Main constituent minerals	Quartz	20 – 50
	Plagioclase	20 – 50
	Biotite	5 – 20
	Amphibole	5 – 20
Accessory minerals	K-feldspar	< 1
	Apatite	< 1
	Zircon	< 1
	Sphene	< 1
Altered minerals	Sericite	< 5
	Actinolite	< 1
	Chlorite	< 1
	Epidote	< 1

Table 5-5 Experimental variables and data for Se sorption on rock samples

	Experimental condition	Solution volume (cm^3)	Solid weight (g)	Initial solution			Equilibrated solution			K_d ($m^3\ kg^{-1}$)	R_s (%)
				pH	Eh (V)	Concentration of Se (mol dm^{-3})	pH	Eh (V)	Concentration of Se (mol dm^{-3})		
Granodiorite	Lower Se concentration	58	26.6 ± 0.2	8.68	-0.30	$(1.20 \pm 0.03)\times10^{-9}$	8.61	-0.29	$(4.00 \pm 0.67)\times10^{-10}$	$(4.0 \pm 0.9)\times10^{-3}$	62
				9.44	-0.30		9.35	-0.31	$(5.63 \pm 0.80)\times10^{-10}$	$(2.2 \pm 0.5)\times10^{-3}$	48
				10.40	-0.39		10.05	-0.34	$(8.05 \pm 0.84)\times10^{-10}$	$(1.0 \pm 0.3)\times10^{-3}$	31
				11.50	-0.40		10.96	-0.40	$(1.03 \pm 0.09)\times10^{-9}$	$(3.5 \pm 2.8)\times10^{-4}$	14
	Higher Se concentration	58	26.6 ± 0.2	8.64	-0.31	$(8.92 \pm 0.15)\times10^{-9}$	8.43	-0.33	$(3.40 \pm 0.16)\times10^{-9}$	$(3.3 \pm 0.2)\times10^{-3}$	58
				9.49	-0.33		9.34	-0.35	$(4.92 \pm 0.18)\times10^{-9}$	$(1.6 \pm 0.1)\times10^{-3}$	41
				10.54	-0.37		10.10	-0.37	$(6.31 \pm 0.20)\times10^{-9}$	$(8.6 \pm 1.2)\times10^{-4}$	28
				11.57	-0.39		11.06	-0.41	$(8.08 \pm 0.22)\times10^{-9}$	$(2.2 \pm 0.9)\times10^{-4}$	9
	Sterilized	58	26.6 ± 0.2	10.67	-0.40	$(8.56 \pm 0.10)\times10^{-9}$	10.45	-0.33	$(7.34 \pm 0.18)\times10^{-9}$	$(3.6 \pm 0.8)\times10^{-4}$	14
Sandy mudstone	Lower Se concentration	58	17.9 ± 0.3	8.59	-0.27	$(6.30 \pm 0.08)\times10^{-10}$	8.85	-0.37	$(3.47 \pm 2.11)\times10^{-11}$	$(5.6 \pm 3.4)\times10^{-2}$	94
				9.30	-0.31		9.25	-0.38	$(4.47 \pm 2.30)\times10^{-11}$	$(4.2 \pm 2.2)\times10^{-2}$	93
				9.95	-0.33		9.18	-0.38	$(5.49 \pm 2.12)\times10^{-11}$	$(3.4 \pm 1.3)\times10^{-2}$	91
				11.36	-0.40		9.59	-0.39	$(3.62 \pm 2.48)\times10^{-11}$	$(5.3 \pm 3.7)\times10^{-2}$	94
	Higher Se concentration	58	17.9 ± 0.3	8.77	-0.29	$(3.85 \pm 0.10)\times10^{-9}$	9.21	-0.39	$(3.14 \pm 0.34)\times10^{-10}$	$(3.7 \pm 0.4)\times10^{-2}$	92
				9.48	-0.32		9.60	-0.40	$(3.46 \pm 0.36)\times10^{-10}$	$(3.3 \pm 0.4)\times10^{-2}$	91
				10.07	-0.35		9.50	-0.41	$(3.16 \pm 0.32)\times10^{-10}$	$(3.6 \pm 0.4)\times10^{-2}$	92
				10.94	-0.39		9.97	-0.42	$(3.02 \pm 0.35)\times10^{-10}$	$(3.8 \pm 0.5)\times10^{-2}$	92
	Sterilized	58	17.9 ± 0.3	10.96	-0.43	$(4.12 \pm 0.10)\times10^{-9}$	10.42	-0.42	$(1.71 \pm 0.40)\times10^{-10}$	$(7.5 \pm 1.8)\times10^{-2}$	96
Tuffaceous sandstone	Lower Se concentration	58	19.4 ± 0.8	8.08	-0.30	$(1.79 \pm 0.03)\times10^{-9}$	9.14	-0.39	$(6.31 \pm 2.28)\times10^{-11}$	$(8.2 \pm 3.0)\times10^{-2}$	96
				9.36	-0.37		10.15	-0.42	$(8.59 \pm 2.46)\times10^{-11}$	$(5.9 \pm 1.7)\times10^{-2}$	95
				10.10	-0.39		10.35	-0.42	$(1.04 \pm 0.26)\times10^{-10}$	$(4.8 \pm 1.2)\times10^{-2}$	94
				10.98	-0.41		10.55	-0.42	$(1.02 \pm 0.24)\times10^{-10}$	$(5.0 \pm 1.2)\times10^{-2}$	94
	Higher Se concentration	58	19.4 ± 0.8	8.77	-0.33	$(8.26 \pm 0.14)\times10^{-9}$	9.66	-0.40	$(3.84 \pm 0.36)\times10^{-10}$	$(6.1 \pm 0.6)\times10^{-2}$	95
				9.50	-0.36		10.34	-0.42	$(5.23 \pm 0.58)\times10^{-10}$	$(4.4 \pm 0.5)\times10^{-2}$	94
				10.25	-0.38		10.61	-0.42	$(6.19 \pm 0.34)\times10^{-10}$	$(3.7 \pm 0.3)\times10^{-2}$	93
				11.00	-0.39		10.91	-0.43	$(7.74 \pm 0.50)\times10^{-10}$	$(2.9 \pm 0.2)\times10^{-2}$	91
	Sterilized	58	19.4 ± 0.8	10.86	-0.38	$(6.12 \pm 0.08)\times10^{-9}$	11.01	-0.45	$(2.99 \pm 0.70)\times10^{-10}$	$(5.8 \pm 1.4)\times10^{-2}$	95

Table 5-6 Experimental variables and data for Se sorption on minerals

		Concentration of NaCl (mol dm^{-3})	pH	Eh (V)	Concentration of Se (mol dm^{-3})	K_d (m^3 kg^{-1})	R_s (%)
Initial solution		0.05	8.22	-0.35	$(6.12 \pm 0.08) \times 10^{-9}$	—	—
			10.24	-0.35		—	—
			11.83	-0.49		—	—
		0.5	8.50	-0.32	$(6.21 \pm 0.08) \times 10^{-9}$	—	—
			10.43	-0.37		—	—
			11.71	-0.47		—	—
Equilibrated solution	Quartz	0.05	8.66	-0.48	$(5.98 \pm 0.15) \times 10^{-9}$	$(2.0 \pm 3.3) \times 10^{-3}$	2
			9.54	-0.50	$(5.96 \pm 0.15) \times 10^{-9}$	$(2.5 \pm 3.7) \times 10^{-3}$	3
			10.53	-0.51	$(6.58 \pm 1.55) \times 10^{-9}$	0	0
		0.5	8.50	-0.49	$(6.05 \pm 0.20) \times 10^{-9}$	$(2.4 \pm 4.4) \times 10^{-3}$	3
			9.36	-0.50	$(6.11 \pm 0.21) \times 10^{-9}$	$(1.5 \pm 4.5) \times 10^{-3}$	2
			10.25	-0.51	$(5.68 \pm 0.20) \times 10^{-9}$	$(8.5 \pm 4.8) \times 10^{-3}$	8
	Albite	0.05	8.68	-0.49	$(5.71 \pm 0.15) \times 10^{-9}$	$(6.8 \pm 3.7) \times 10^{-3}$	7
			10.21	-0.52	$(6.08 \pm 0.16) \times 10^{-9}$	$(0.5 \pm 3.4) \times 10^{-3}$	1
			12.11	-0.52	$(6.31 \pm 0.15) \times 10^{-9}$	0	0
		0.5	8.55	-0.50	$(5.73 \pm 0.20) \times 10^{-9}$	$(7.2 \pm 4.6) \times 10^{-3}$	8
			10.14	-0.51	$(5.63 \pm 0.20) \times 10^{-9}$	$(9.6 \pm 4.8) \times 10^{-3}$	9
			11.96	-0.53	$(5.63 \pm 0.19) \times 10^{-9}$	$(1.0 \pm 0.5) \times 10^{-2}$	9
	Calcite	0.05	8.70	-0.43	$(3.18 \pm 0.11) \times 10^{-9}$	$(7.9 \pm 0.6) \times 10^{-2}$	48
			10.53	-0.47	$(3.41 \pm 0.12) \times 10^{-9}$	$(7.3 \pm 0.6) \times 10^{-2}$	44
			12.18	-0.50	$(4.62 \pm 0.13) \times 10^{-9}$	$(3.1 \pm 0.4) \times 10^{-2}$	25
		0.5	8.61	-0.47	$(4.77 \pm 0.18) \times 10^{-9}$	$(2.9 \pm 0.6) \times 10^{-2}$	23
			10.54	-0.50	$(5.42 \pm 0.20) \times 10^{-9}$	$(1.3 \pm 0.5) \times 10^{-2}$	13
			12.03	-0.51	$(5.00 \pm 0.18) \times 10^{-9}$	$(2.3 \pm 0.5) \times 10^{-2}$	19
	Biotite	0.05	8.59	-0.32	$(4.07 \pm 0.07) \times 10^{-9}$	$(5.0 \pm 0.3) \times 10^{-2}$	34
			10.41	-0.37	$(5.31 \pm 0.09) \times 10^{-9}$	$(1.2 \pm 0.2) \times 10^{-2}$	13
			11.99	-0.57	$(5.75 \pm 0.09) \times 10^{-9}$	$(6.1 \pm 2.4) \times 10^{-3}$	6
		0.5	8.50	-0.40	$(3.45 \pm 0.12) \times 10^{-9}$	$(7.9 \pm 0.6) \times 10^{-2}$	44
			10.22	-0.42	$(5.45 \pm 0.15) \times 10^{-9}$	$(1.4 \pm 0.4) \times 10^{-2}$	12
			11.89	-0.57	$(5.01 \pm 0.14) \times 10^{-9}$	$(2.2 \pm 0.4) \times 10^{-2}$	19
	Chlorite	0.05	8.77	-0.49	$(2.75 \pm 0.10) \times 10^{-9}$	$(1.2 \pm 0.1) \times 10^{-1}$	55
			10.72	-0.47	$(3.94 \pm 0.12) \times 10^{-9}$	$(5.5 \pm 0.5) \times 10^{-2}$	36
			12.42	-0.60	$(5.41 \pm 0.14) \times 10^{-9}$	$(1.3 \pm 0.4) \times 10^{-2}$	12
		0.5	8.67	-0.46	$(3.79 \pm 0.12) \times 10^{-9}$	$(6.5 \pm 0.6) \times 10^{-2}$	39
			10.69	-0.52	$(5.39 \pm 0.14) \times 10^{-9}$	$(1.6 \pm 0.4) \times 10^{-2}$	13
			12.25	-0.58	$(5.40 \pm 0.14) \times 10^{-9}$	$(1.6 \pm 0.4) \times 10^{-2}$	13
	Montmorillonite	0.05	8.78	-0.34	$(1.46 \pm 0.09) \times 10^{-9}$	$(2.9 \pm 0.2) \times 10^{-1}$	76
			10.51	-0.35	$(4.99 \pm 0.14) \times 10^{-9}$	$(1.8 \pm 0.4) \times 10^{-2}$	18
			12.03	-0.53	$(5.61 \pm 0.15) \times 10^{-9}$	$(7.9 \pm 3.6) \times 10^{-3}$	8
		0.5	8.60	-0.37	$(2.84 \pm 0.11) \times 10^{-9}$	$(1.0 \pm 0.1) \times 10^{-1}$	54
			9.86	-0.38	$(3.25 \pm 0.14) \times 10^{-9}$	$(8.9 \pm 0.8) \times 10^{-2}$	48
			11.81	-0.55	$(4.99 \pm 0.14) \times 10^{-9}$	$(1.9 \pm 0.3) \times 10^{-2}$	20
	Goethite	0.05	8.65	-0.37	$(6.83 \pm 3.12) \times 10^{-11}$	$(7.9 \pm 3.6) \times 10^{0}$	99
			10.00	-0.43	$(8.32 \pm 0.62) \times 10^{-10}$	$(5.2 \pm 0.4) \times 10^{-1}$	86
			12.32	-0.56	$(5.22 \pm 0.14) \times 10^{-9}$	$(1.5 \pm 0.4) \times 10^{-2}$	15
		0.5	8.54	-0.36	$(1.31 \pm 0.36) \times 10^{-10}$	$(4.5 \pm 1.2) \times 10^{0}$	98
			10.01	-0.40	$(9.96 \pm 0.68) \times 10^{-10}$	$(4.7 \pm 0.3) \times 10^{-1}$	84
			12.35	-0.52	$(5.25 \pm 0.14) \times 10^{-9}$	$(1.7 \pm 0.4) \times 10^{-2}$	15
	Pyrite	0.05	9.86	-0.55	$(1.11 \pm 0.35) \times 10^{-10}$	$(5.9 \pm 1.8) \times 10^{0}$	98
			10.90	-0.57	$(7.20 \pm 3.22) \times 10^{-11}$	$(7.4 \pm 3.3) \times 10^{0}$	99
			12.27	-0.60	$(4.78 \pm 0.52) \times 10^{-10}$	$(1.3 \pm 0.1) \times 10^{0}$	92
		0.5	9.91	-0.51	$(6.02 \pm 3.34) \times 10^{-11}$	$(9.9 \pm 5.5) \times 10^{0}$	99
			11.04	-0.55	$(1.20 \pm 0.38) \times 10^{-10}$	$(5.7 \pm 1.8) \times 10^{0}$	98
			12.06	-0.62	$(2.93 \pm 0.42) \times 10^{-10}$	$(2.2 \pm 0.3) \times 10^{0}$	95

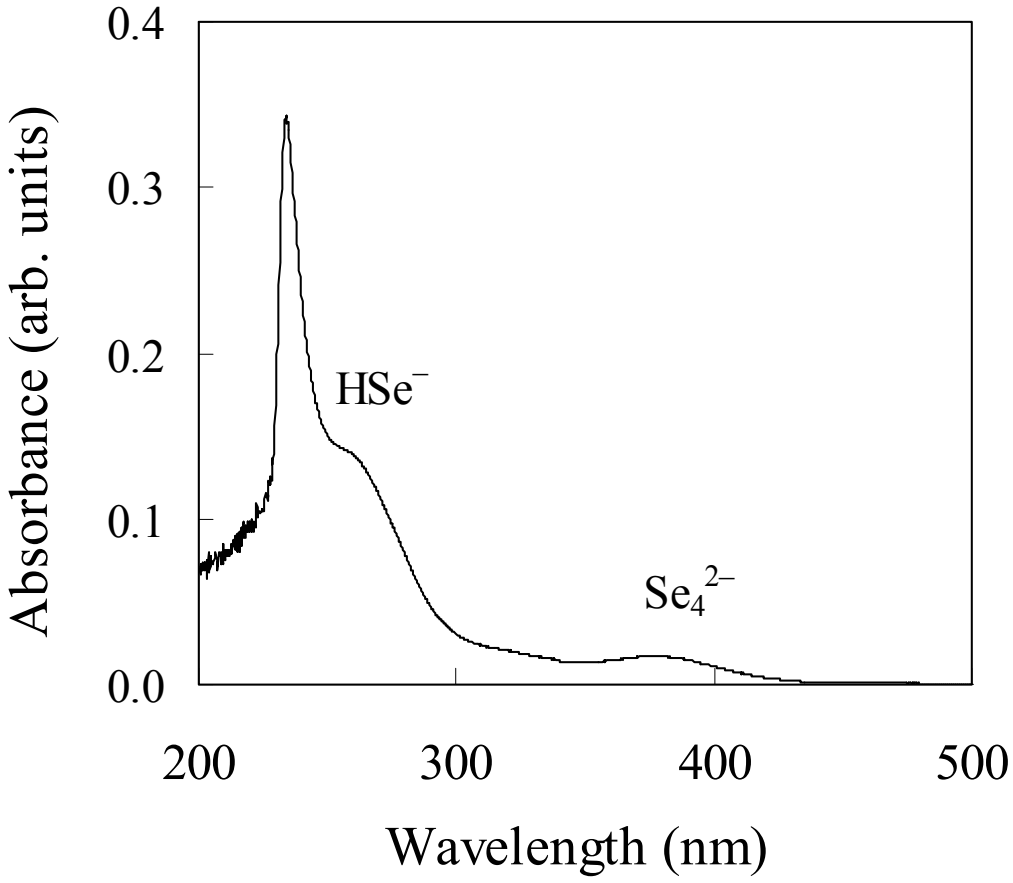

Fig. 5-1 UV-Vis spectrum of the Se(−II) stock solution (Se concentration: 3×10^{-5} mol dm^{-3}, pH: 11.05 and *E*h: −0.42 V). The absorption band at 245 nm was assigned to the HSe^- ion, and the absorption band at 377 nm was assigned to the Se_4^{2-} ion.

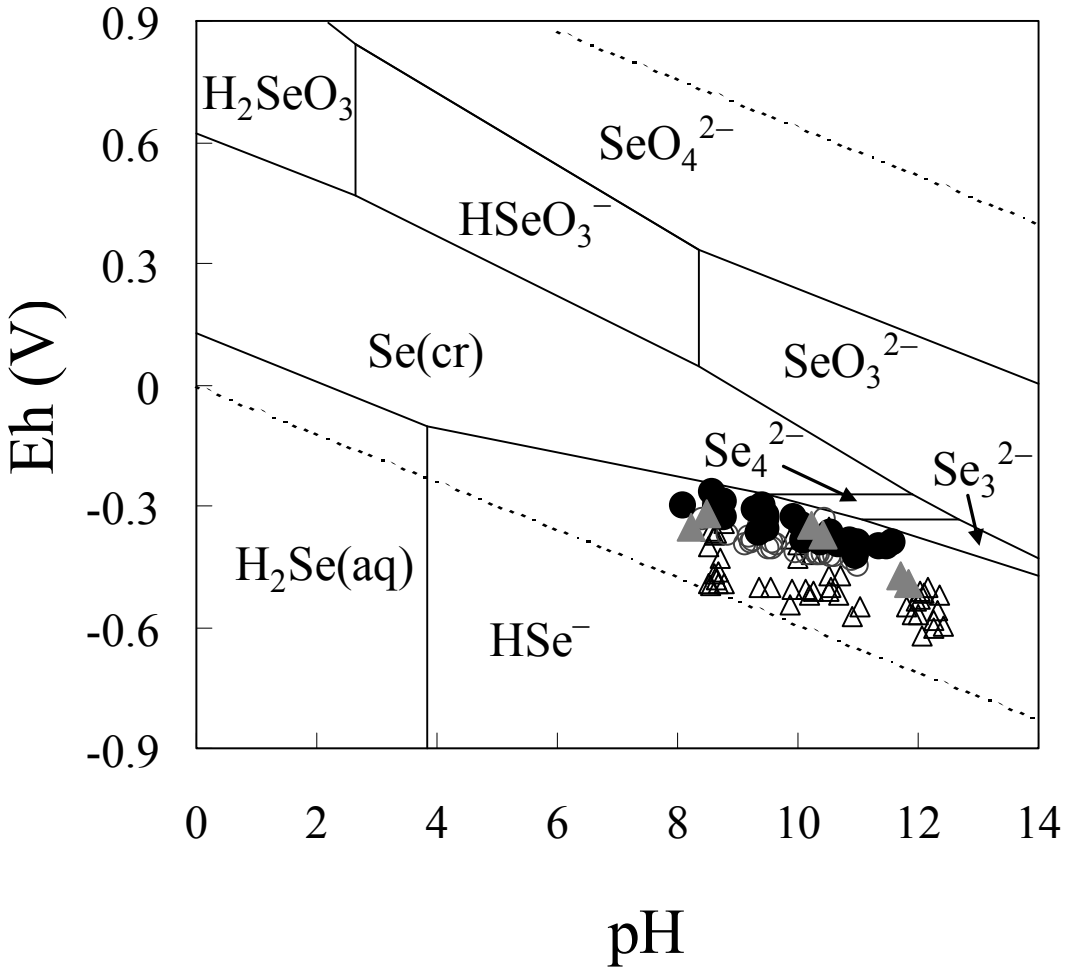

Fig. 5-2 Experimental conditions of initial (open symbols) and equilibrated (filled symbols) solutions in a pH-*E*h diagram for the H-O-Se system under standard conditions. The total concentration of Se is 10^{-8} mol dm^{-3}. The circles and triangles represent the conditions for the sorption experiments using rocks and minerals, respectively.

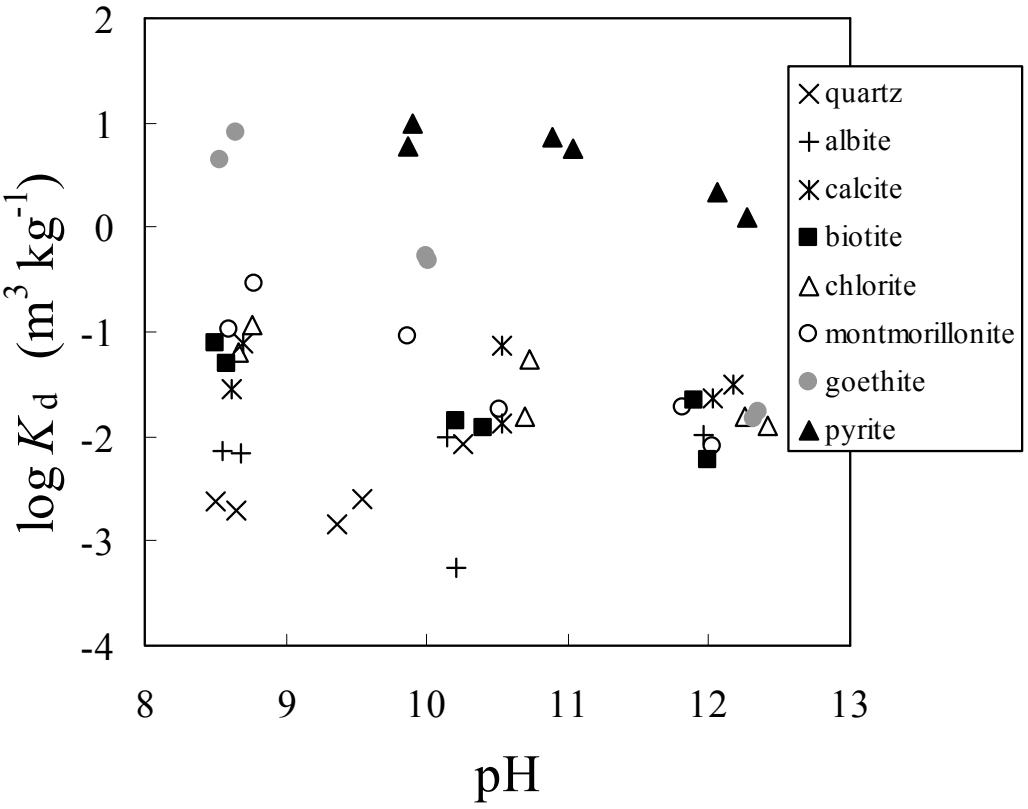

Fig. 5-3 Plots of K_d for mineral samples *vs*. pH

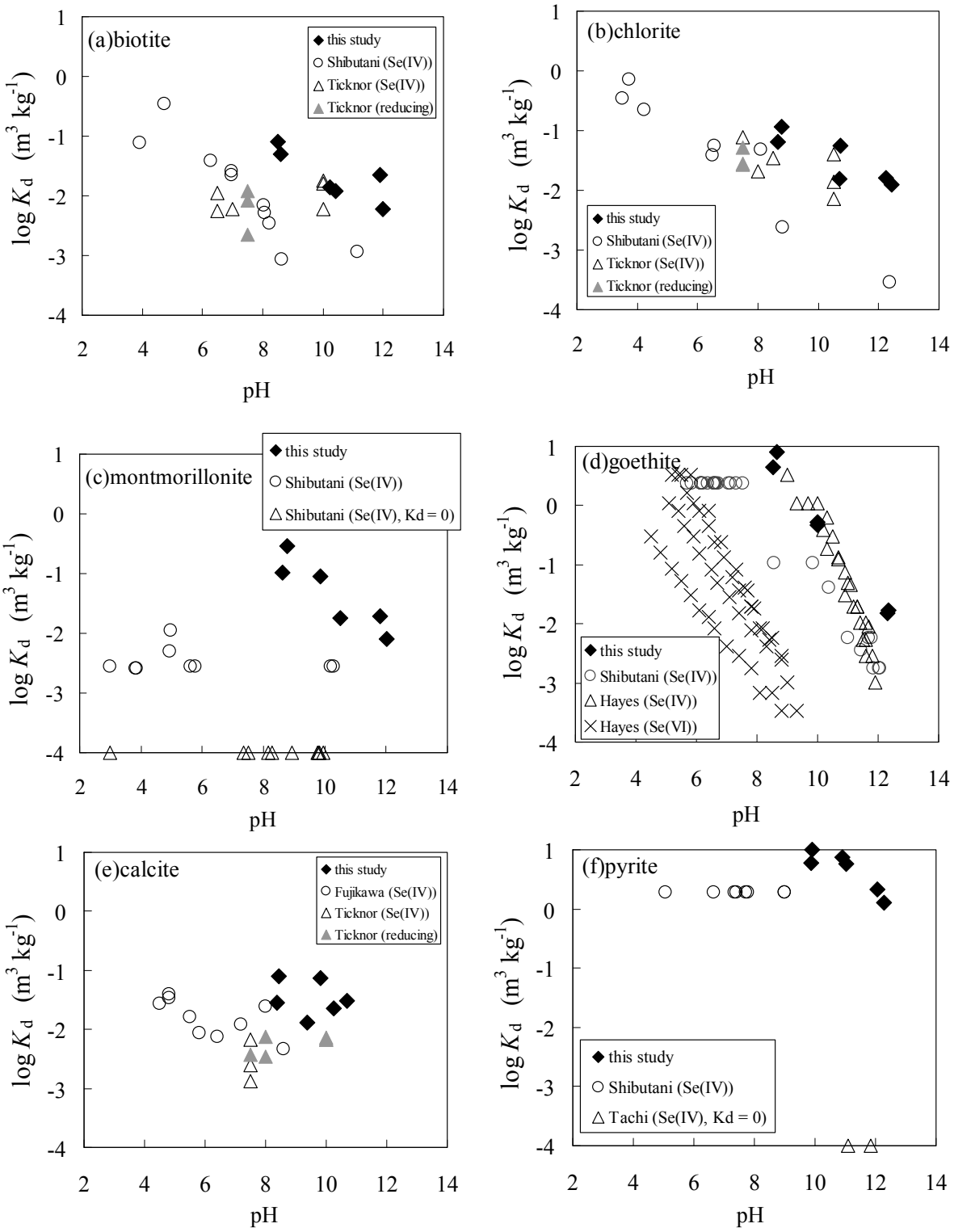

Fig.5-4 Comparison of K_d for minerals obtained in this study and previously reported ones ((a) biotite,[1,6] (b) chlorite,[1,6] (c) montmorillonite,[1] (d) goethite,[1,3] (e) calcite,[4,6] and (f) pyrite[1,2]).

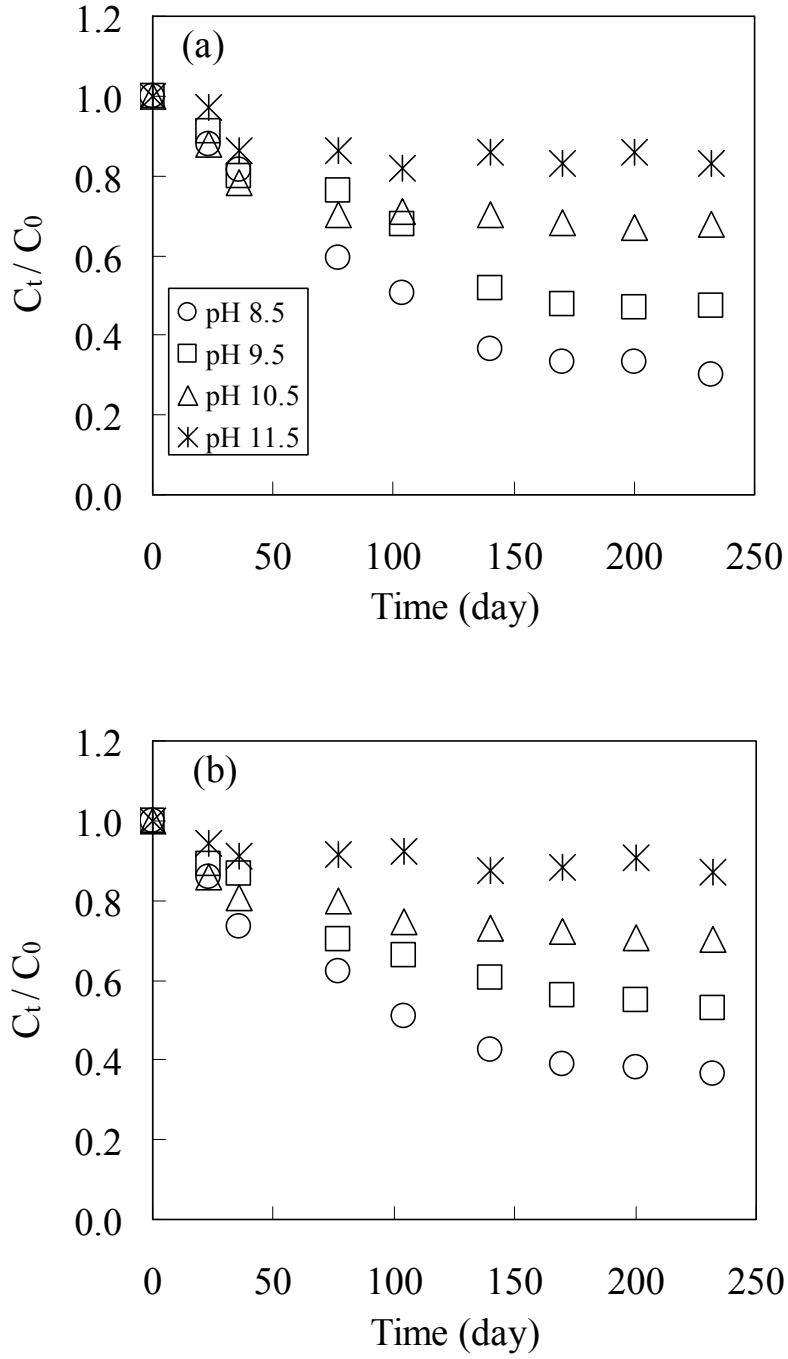

Fig. 5-5 Time dependences of Se concentrations in the sorption experimental runs using granodiorite in the lower Se concentration experimental runs (a) and the higher Se concentration experimental runs (b)

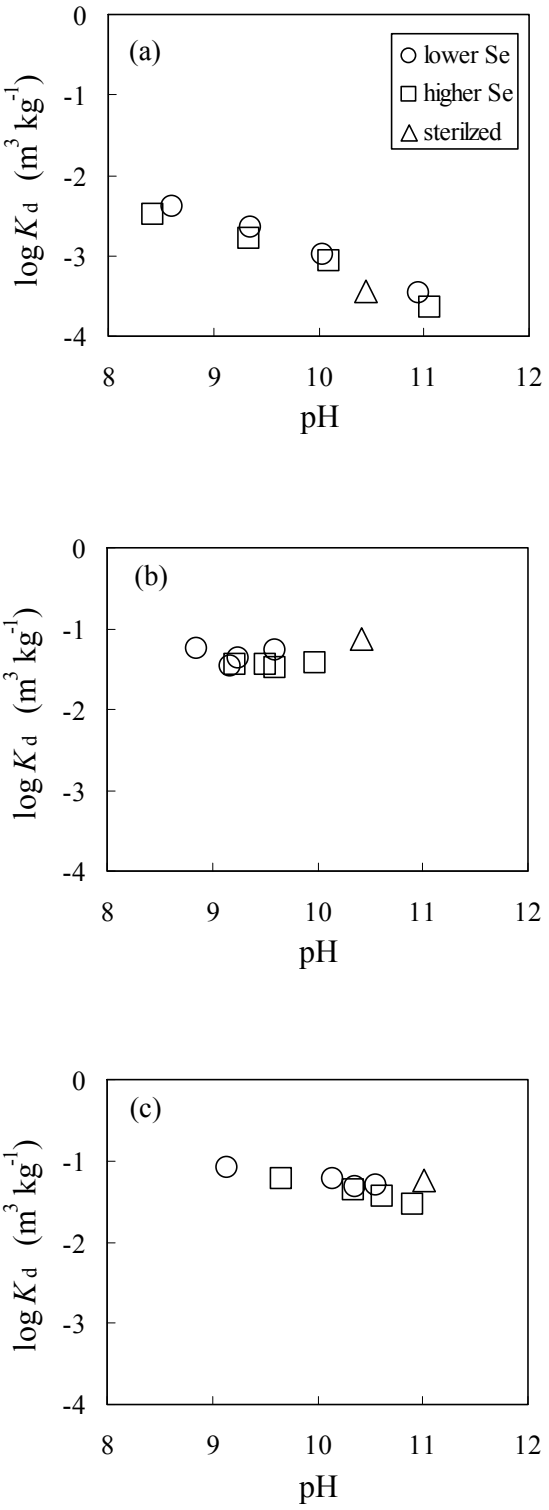

Fig. 5-6 Plots of K_d for granodiorite (a), sandy mudstone (b), and tuffaceous sandstone (c) *vs.* pH. Circles represent data from the lower Se concentration experimental runs; squares represent data from the higher Se concentration experimental runs; triangles represent data for sterilized rock samples.

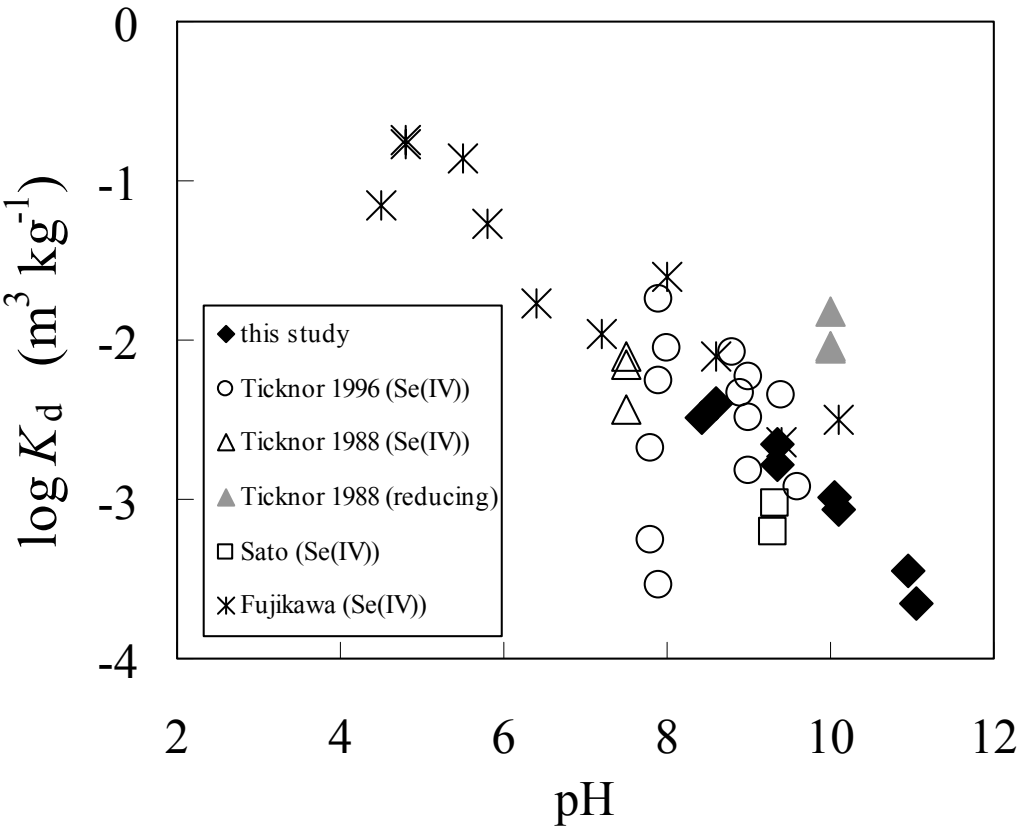

Fig. 5-7 Comparison of selenium K_d values for granodiorite obtained in this study and previously reported studies[4-6,30)]

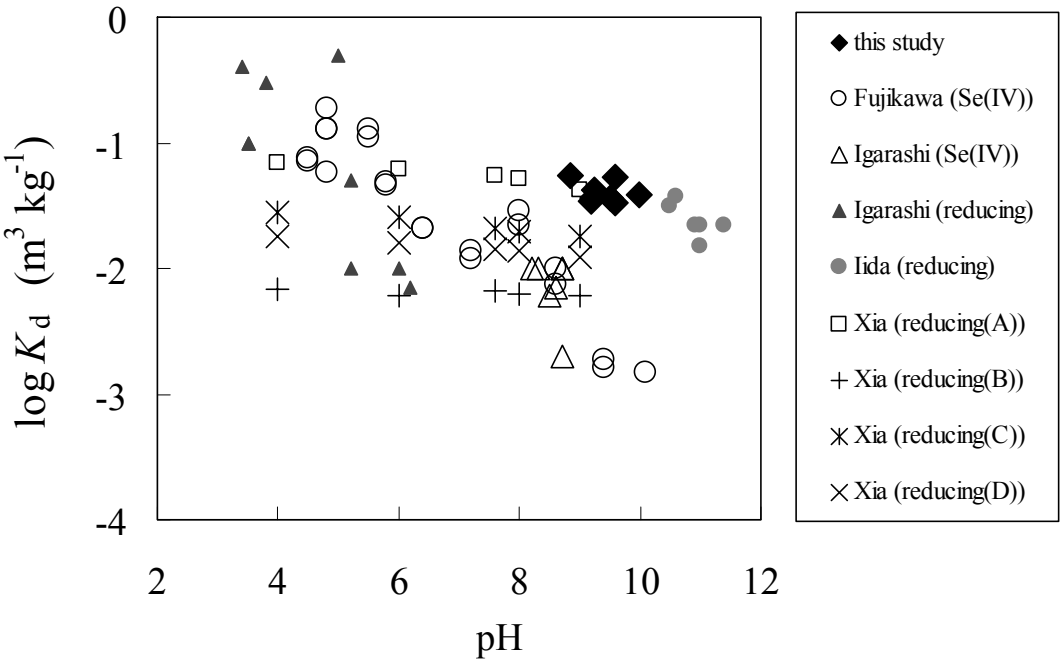

Fig. 5-8 Comparison of selenium K_d values for sandy mudstone obtained in this study and previously reported studies[4,6-8)]

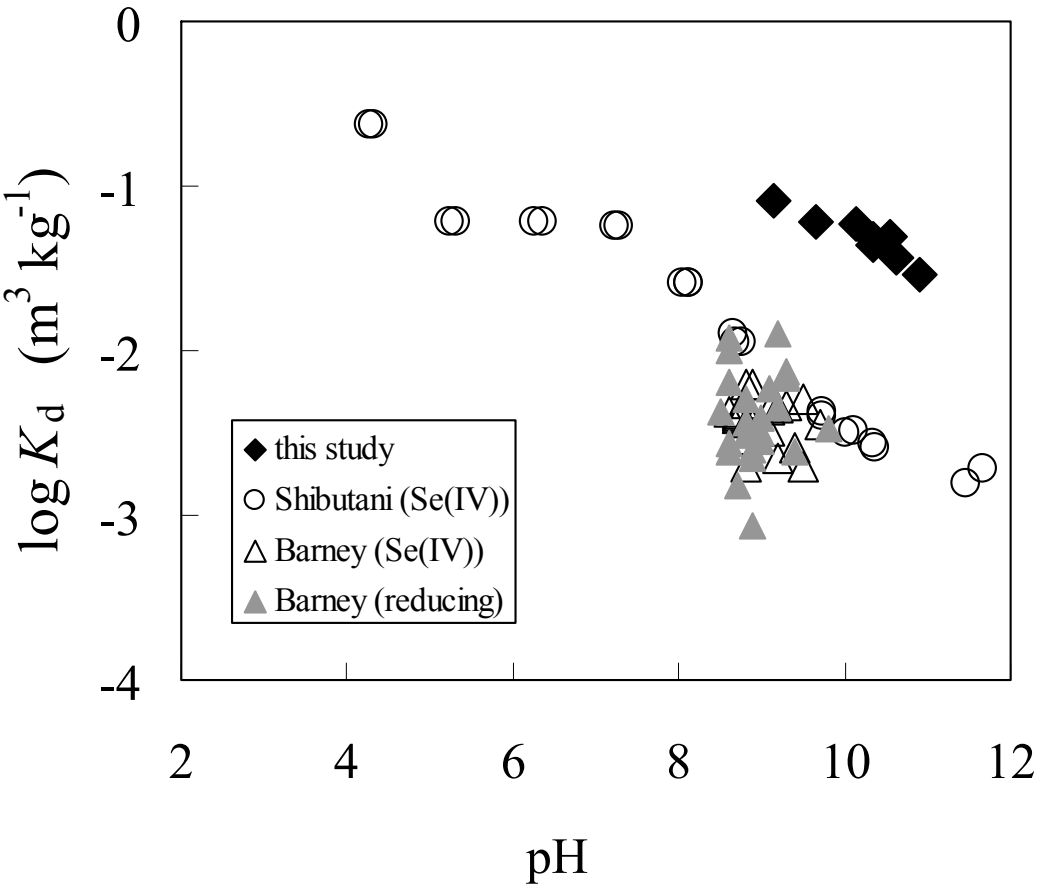

Fig. 5-9 Comparison of selenium K_d values for tuffaceous sandstone obtained in this study and previously reported studies[1,7)]

6. Concluding remarks

6.1. Summary

The geochemical information on the migration of Se in the disposal environments of HLW was obtained with laboratory experiments, to improve reliability of the safety assessment of HLW disposal system.

The solubility limiting solid of Se near the vitrified waste and overpack in the disposal environments was determined by dissolution experiments in the presence of Fe under reducing conditions in chapter 2. Ferroselite ($FeSe_2$) which was the most thermodynamically stable solid phase under the experimental conditions was employed as the starting solid in the undersaturation experiments and formed in the oversaturation experiments. However, the obtained values of ion activity product for the reaction of $0.5FeSe_2 + H^+ + e^- = 0.5Fe^{2+} + HSe^-$ were 3 to 4 orders of magnitude higher than the equilibrium constants calculated from existing thermodynamic data. The dominant dissolution reaction of Se was determined as $Se(s) + H^+ + 2e^- = HSe^-$ and its equilibrium constant was determined to be $\log K^0 = -7.46 \pm 0.11$. This value agrees with the value of $\log K^0 = -7.62 \pm 0.06$ calculated from existing thermodynamic data of Se(cr) and HSe^- within errors, which suggests that the solubility limiting solid is Se(cr) in the disposal environments even if Fe-Se compounds are formed.

The equilibrium constants of the dissolution reaction of Se were obtained by dissolution experiments in chapter 3. The solubility limiting solid and the dominant dissolved species were determined as Se(am) and HSe^- at pH between 5 and 8. The equilibrium constant of dissolution reaction was obtained as

$$Se(am) + H^+ + 2e^- = HSe^- \qquad \log {}^0K_1 = -6.57 \pm 0.15. \qquad (6\text{-}1)$$

The solubility of Se limited by Se(am) can be about 1 order of magnitude higher than that limited by Se(cr), however, the solubility of Se is likely to be limited by Se(cr) near overpacks in the disposal environments, because the concentration of HSe^- was limited by Se(cr) in the presence of Fe (chapter 2). The solubility limiting solid and the dominant dissolved species were determined as Se(cr) and Se_4^{2-} at pH between 9 and 13. The equilibrium constant of dissolution reaction was obtained as

$$4Se(cr) + 2e^- = Se_4^{2-} \qquad \log {}^0K_2 = -16.67 \pm 0.03. \qquad (6\text{-}2)$$

This value agrees with the value calculated from existing thermodynamic data. The validity of the solubility evaluations by using existing thermodynamic data was confirmed.

The activity coefficients for HSe^- and Se_4^{2-} in NaCl solution were also determined in chapter 3. The ion interaction coefficients by which activity coefficients can be corrected at high ionic strength were obtained as $\varepsilon(HSe^-, Na^+) = -0.01 \pm 0.10$ and $\varepsilon(Se_4^{2-}, Na^+) = -0.03 \pm 0.02$ for HSe^- and Se_4^{2-}, respectively. Thus, the activity coefficients were determined to be

$$\log \gamma_{(HSe^-, Na^+)} = -\frac{0.509\sqrt{I_m}}{1+1.5\sqrt{I_m}} - 0.01\, I_m \quad \text{and} \tag{6-3}$$

$$\log \gamma_{(Se_4^{2-}, Na^+)} = -4 \times \frac{0.509\sqrt{I_m}}{1+1.5\sqrt{I_m}} - 0.03\, I_m . \tag{6-4}$$

Effective diffusion coefficients (D_e) of Se(−II) and Se(IV) species through bentonite/sand mixtures were systematically obtained under the condition of variable bentonite content and porewater salinity, and a diffusion model was developed to understand the diffusion behaviors of Se species in the bentonite porewater in chapter 4. The D_e values of Se(−II) species were within a range of 9.7×10^{-12} - 5.9×10^{-11} $m^2\ s^{-1}$, and decreased with increasing bentonite content and decreasing salinity. The diffusion model was based on the electric double layer theory and the pore diffusion model, assuming that anionic Se species diffuse through only the macro pore. The calculated D_e values of Se species agreed with the experimentally measured ones, which help in the understanding of the diffusion behavior of Se species in the bentonite porewater.

The sorption behaviors of Se(−II) species onto rocks were investigated by batch sorption experiments under reducing conditions in chapter 5. Granodiorite was used to represent crystalline rocks, and sandy mudstone and tuffaceous sandstone were used to represent sedimentary rocks. The sorption behaviors of Se(−II) species onto major constituent minerals and accessory minerals of these rocks were also investigated to identify which minerals were the most sorbent for Se(−II) species and to estimate the sorption mechanism. Obtained sorption distribution coefficients (K_d) were in a range of 2.2×10^{-4} to 4.0×10^{-3} $m^3\ kg^{-1}$ for granodiorite, 3.3×10^{-2} to 5.6×10^{-2} $m^3\ kg^{-1}$ for sandy mudstone and 2.9×10^{-2} to 8.2×10^{-2} $m^3\ kg^{-1}$ for tuffaceous sandstone at pHs 8.5 to 11.5. The values and pH dependence of K_d for Se(−II) species on granodiorite agree with those for Se(IV) species. Experimental results suggest that biotite dominates the sorption of Se(−II) species onto granodiorite at neutral-alkaline pH, and the

sorption mechanism is surface complexation with ≡AlOH sites and ≡FeOH sites. The K_d values for Se(−II) species on sandy mudstone and tuffaceous sandstone were about 1 order of magnitude higher than those for Se(IV) species. Experimental results suggest that pyrite is the dominant sorbent mineral for Se(−II) species in the sandy mudstone and tuffaceous sandstone at neutral-alkaline pH. The higher K_d values for Se(−II) species are likely to be due to the strong sorption of Se(−II) species onto pyrite in sandy mudstone and tuffaceous sandstone. The sorption mechanism of Se(−II) species onto pyrite is estimated to be a local redox reaction with sulfur at the surface.

6.2. Contribution to the Safety Assessment of HLW Disposal System

This study was carried out to improve reliability of the safety assessment of HLW disposal system. The geochemical information on the migration of Se obtained in this study contributes to the safety assessment of HLW disposal system as follows. The key migration parameters determined in this study are summarized in **Table 6-1** for the comparison with the previous ones.[1)] The compositions of the two types of model groundwaters and porewaters,[1)] fresh and saline type, used in the parameter determinations are summarized in **Table 6-2**.

The solubility of Se in the disposal environments was expected to be limited to less than 10^{-8} mol dm^{-3} by $FeSe_2$ in the previous evaluations.[1)] However, the solubility limiting of Se by Fe-Se compounds had not been observed in laboratory experiments. Therefore, there was a possibility of an underestimation and a large uncertainty in the previous solubility evaluations. In this study, it was clarified that the solubility of Se was limited by Se(cr) rather than Fe-Se compounds from the dissolution experiments. The solubility of Se was estimated to be several orders of magnitude higher than the previous evaluation.

The equilibrium constants for dissolution reactions of Se were estimated by thermodynamic calculations with existing thermodynamic data in the previous evaluations.[1)] However, the validity of the equilibrium constants have not been confirmed in aqueous systems. In this study, the equilibrium constants of dissolution reactions of Se were obtained by dissolution experiments. The obtained values consisted with the values calculated from the existing thermodynamic data. From the results, the validity of the equilibrium constants were confirmed and the scientific reliability of the solubility evaluations were improved.

The activity coefficients of HSe^- species were calculated by the Davies equation (Eq. 1-10) in the previous solubility evaluations.[1)] However, the Davies equation is not valid when the ionic strength is more than 0.1 mol kg^{-1}. The ionic strength of the porewater relevant to saline

groundwater is approximately 0.6 mol kg^{-1}, the Davies equation overestimates the activity coefficient at such high ionic strength. In this study, the activity coefficients of HSe^- and Se_4^{2-} species were determined by SIT for high ionic strength. The activity coefficient of HSe^- in saline type porewater calculated from SIT is lower than that from the Davies equation. It enables us to evaluate the solubility of Se under the saline groundwater conditions in coastal repositories more properly. The solubility of Se reevaluated from the results of this study was indicated to be 2 to 4 orders of magnitude higher than the previous estimation (**Table 6-1**).

The diffusivity of HSe^- in the bentonite buffer material was evaluated from diffusion data of I^- considering the charge of the species in the previous safety assessments, due to the lack of diffusion data of HSe^-. Besides, the diffusion characteristics of Se species had not been clarified. In this study, systematic diffusion data of Se species were obtained under variable bentonite content and porewater salinity, and diffusion behaviors of Se species in the bentonite porewater were modeled based on the electric double layer theory and the pore diffusion model. The effective diffusion coefficients of HSe^- in the porewater (D_{mp}; summarized in **Table 4-4**) was estimated to be 7×10^{-11} to 2×10^{-10} m^2 s^{-1} at 25°C. The repository temperature is conservatively assumed to be 60°C, the temperature correction was based on the activation energy for diffusion (E; 15.05 kJ mol^{-1}).[1)] The diffusion coefficients at 60°C (D_p) were calculated by the Arrhenius equation[2)]

$$D_p = A \exp\left(\frac{-E}{RT}\right) \tag{6-5}$$

where A is pre-exponential factor, R is gas constant and T is temperature. The D_p values under the unaltered bentonite conditions agree with the previous evaluated ones, but that under the altered bentonite condition is about a quarter of the previous evaluated one (**Table 6-1**). The previous evaluation was likely to be excessively conservative. From the results of this study, it became possible to evaluate the variation in diffusivity caused by the change in the disposal environments on scientific grounds.

The sorption distribution coefficients of HSe^- on rocks were evaluated from extremely limited sorption data of HSe^- to be 0.01 or 0.001 m^3 kg^{-1} in the previous evaluations.[1)] The validity of the evaluations has not been confirmed, due to the lack of sorption data and understanding of the sorption mechanisms of HSe^-. In this study, systematic sorption data of HSe^- were obtained for crystalline and sedimentary rocks under variable pH. The obtained K_d for sandy mudstone and tuffaceous sandstone were higher than the previous evaluated ones. On the other hand, the obtained K_d for granodiorite were lower than the previous evaluated ones (**Table**

6-1). The most sorbent mineral and the sorption mechanisms of HSe^- were identified from the sorption data for the major constituent minerals and accessory minerals of rocks. The correlation of K_d between rocks and the sorbent minerals, and the sorption mechanisms were clarified. The results of this study give a scientific basis to the evaluation of K_d for HSe^-.

In this way, the geochemical information on the migration of Se obtained in this study contributes to the improvement of the reliability of the safety assessment of HLW disposal system. Further investigations are necessary for the porewater chemistry in bentonite buffer materials which affects solubility and diffusivity, and thermodynamic modeling for quantitative understanding of sorption behavior.

References

1) Japan Nuclear Cycle Development Institute (JNC), *H12: Project to establish the scientific and technical basis for HLW disposal in Japan - Second progress report on research and development for the geological disposal of HLW in Japan*, JNC TN 1410 2000-001, JNC (2000).

2) W. Stumm, J. J. Morgan, *Aquatic Chemistry, 3rd edition*, John Wiley & Sons, Inc., New York (1996).

Table 6-1 Key migration parameters of Se for the safety assessment calculations

		Previous evaluation [1)]	This study
Solubility limiting solid		$FeSe_2$	Se(cr)
Aqueous species		HSe^-	same as on the left
Dissolution reaction		$FeSe_2 + 2H^+ + 2e^- = Fe^{2+} + 2HSe^-$	$Se(cr) + H^+ + 2e^- = HSe^-$
		$\log K^0 = -18.8$	$\log K^0 = -7.62 \pm 0.06$
Activity coefficient	Model	Davies	SIT
	Fresh water	0.87	0.87
	Saline water	0.71	0.65
Solubility (mol dm^{-3})	Fresh water	3×10^{-9}	2×10^{-7}
	Saline water	6×10^{-9}	2×10^{-5}
Diffusion coefficient at 60°C (m^2 s^{-1})	Unaltered, fresh water	2×10^{-10}	2×10^{-10}
	Unaltered, saline water	3×10^{-10}	2×10^{-10}
	Altered	2×10^{-9}	5×10^{-10}
Distribution coefficient (m^3 kg^{-1})	Granite	0.01	0.001 - 0.01 (dependent on biotite content and pH)
	Mudstone	0.01	0.01 - 0.1 (dependent on pyrite content)
	Sandstone	0.001	0.001 - 0.1 (dependent on pyrite content)

Table 6-2 Compositions of model groundwaters and porewaters in Ref. 1)

		Groundwater		Porewater	
		Fresh	Saline	Fresh	Saline
pH		8.5	8.0	8.4	7.8
pe		–4.7	–5.1	–4.7	–5.2
Ionic strength (mol kg^{-1})		0.004	0.6	0.02	0.6
Composition (mol dm^{-3})	Na	3.6×10^{-3}	6.2×10^{-1}	2.8×10^{-2}	5.7×10^{-1}
	K	6.2×10^{-5}	1.1×10^{-2}	1.2×10^{-4}	3.4×10^{-3}
	Mg	5.0×10^{-5}	2.5×10^{-4}	4.2×10^{-6}	1.5×10^{-3}
	Ca	1.1×10^{-4}	3.3×10^{-4}	5.3×10^{-5}	1.4×10^{-2}
	Al	3.4×10^{-7}	3.2×10^{-9}	3.4×10^{-7}	3.2×10^{-9}
	Si	3.4×10^{-4}	3.0×10^{-4}	3.4×10^{-4}	2.7×10^{-4}
	Fe	9.7×10^{-10}	3.9×10^{-8}	2.0×10^{-9}	2.2×10^{-7}
	F	5.4×10^{-5}	1.0×10^{-4}	5.4×10^{-5}	1.0×10^{-4}
	Cl	1.5×10^{-5}	5.9×10^{-1}	1.5×10^{-5}	5.9×10^{-1}
	C	3.5×10^{-3}	3.5×10^{-2}	1.6×10^{-2}	2.2×10^{-2}
	S	1.1×10^{-4}	3.0×10^{-2}	1.1×10^{-4}	7.2×10^{-9}
	B	2.9×10^{-4}	1.7×10^{-3}	2.9×10^{-4}	1.7×10^{-3}
	P	2.9×10^{-6}	2.6×10^{-7}	2.9×10^{-6}	2.6×10^{-7}
	N	2.3×10^{-5}	5.2×10^{-3}	2.3×10^{-5}	5.1×10^{-3}
	Br	–	5.3×10^{-4}	–	5.3×10^{-4}
	I	–	2.0×10^{-4}	–	2.0×10^{-4}

Acknowledgement

I acknowledge Professor H. Moriyama of Kyoto University for supervising this study. I am greatly indebted to Professor I. Takagi and Associate Professor T. Sasaki of Kyoto University for helpful comments on the manuscripts.

I am sincerely grateful to Dr. S Nakayama, Dr. T. Tanaka and Dr. T. Yamaguchi of Japan Atomic Energy Agency (JAEA) for close collaboration throughout this study. Dr. A. Kitamura and Dr. Y. Sakamoto of JAEA, and Ms. T. Nakajima are acknowledged for discussions and collaboration for chapter 2 and 3. Dr. Y. Tachi of JAEA and Mr. H. Kato of Mitsubishi Materials Corporation are acknowledged for fruitful discussions for chapter 4. I would like to express my thanks to Dr. T. Ohnuki of JAEA for generous supports on this work. I am indebted to colleagues in JAEA for their significant contribution to this study. I hereby acknowledge that this study was performed as a part of nuclear safety research program of JAEA.

List of Publications

The content of each chapter has been published as follows;

Chapter 2

Y. Iida, T. Yamaguchi, T. Tanaka, A. Kitamura, S. Nakayama, "Determination of the solubility limiting solid of selenium in the presence of iron under anoxic conditions," *Proc. Mobile Fission and Activation Products in Nuclear Waste Disposal*, La Baule, January 16-19, 2007, 135–145 (2009).

Chapter 3

Y. Iida, T. Yamaguchi, T. Tanaka, S. Nakayama, T. Nakajima, Y. Sakamoto, "The solubility of metallic selenium under anoxic conditions," *Mater. Res. Soc. Symp. Proc.*, **663**, 1143–1150 (2001).

Y. Iida, T. Yamaguchi, T. Tanaka, S. Nakayama, "Solubility of selenium at high ionic strength under anoxic conditions," *J. Nucl. Sci. Technol*., **47**[5], 431-438 (2010).

Chapter 4

Y. Iida, T. Yamaguchi, T. Tanaka, "Experimental and modeling study on diffusion of selenium under variable bentonite content and porewater salinity," *J. Nucl. Sci. Technol*., **48**[8], 1170–1183 (2011).

Chapter 5

Y. Iida, T. Tanaka, T. Yamaguchi, S. Nakayama, "Sorption behavior of selenium(-II) on rocks under reducing conditions," *J. Nucl. Sci. Technol.*, **48**[2], 279–291(2011).